Do Roots Bind Soil? Comparing the Physical and Biological Role of Plant Roots in Streambank Fluvial Erosion

Daniel Jeremy Smith

Dissertation submitted to the faculty of the Virginia Polytechnic Institute and State University in partial fulfillment of the requirements for the degree of

Doctor of Philosophy
In
Biological Systems Engineering

Theresa M. Thompson, Chair
Mark A. Williams
Mark A. Stremler
W. Cully Hession
John R. Seiler

August 25, 2022
Blacksburg, Virginia

Keywords: streambank fluvial erosion; soil microorganisms; extracellular polymeric substances; labile organic matter; plant roots; aggregate stability; stream hydrodynamics; turbulence; recirculating flume; mini jet test device

Do Roots Bind Soil? Comparing the Physical and Biological Role of Plant Roots in Fluvial Streambank Erosion

Daniel Jeremy Smith

ABSTRACT

This study is the first to consider how the combination of root physical effects, microbial production of EPS, and root effects on the hydrodynamic boundary layer could influence streambank soil erodibility. Specifically, the goal of this research was to quantify the physical and biological effects of roots on streambank fluvial erosion. A series of laboratory-scale erosion tests were conducted using a mini jet erosion testing device and a recirculating flume channel to address this goal. Several soil and vegetation factors that influence fluvial entrainment, like extracellular polymeric substances (EPS), soil aggregate stability and root length density, were measured following erosion testing. For flume experiments, three streambank boundary conditions were constructed to simulate unvegetated streambanks, as well as streambanks with herbaceous and woody roots. Soil treatments were also created to represent unamended and organic matter (OM) amended soil either without roots (bare soil), with synthetic roots, or with living roots (*Panicum virgatum*).

Median soil erosion rates along the simulated rooted boundaries were two to ten times higher compared to the unvegetated boundary due to protruding root impacts on the boundary layer. In flume experiments, median erosion rates were 30% to 72% lower for unamended soils containing compacted synthetic root fibers as compared to bare soil samples. Adding both OM and fibers to the soil had a greater effect; the median erosion rate reductions of live rooted treatments (95% to 100%) and synthetic rooted + OM treatments (86% to 100%) were similar and statistically lower than bare soil controls. Stimulated microbial production of EPS proteins were significantly correlated with increased erosion resistance in OM-amended treatments while OM treatments had significantly lower EPS carbohydrates compared to unamended treatments. In summary, while sparsely spaced roots exposed on streambanks may increase soil erosion rates due to

impacts on the hydrodynamic boundary layer, overall results highlight how the synergistic relationship between root fibers and soil microbes can significantly reduce streambank soil erodibility due to fiber reinforcement and EPS production.

Do Roots Bind Soil? Comparing the Physical and Biological Role of Plant Roots in Fluvial Streambank Erosion

Daniel Jeremy Smith

GENERAL AUDIENCE ABSTRACT

Plant roots are known to protect streambank soils from erosion by water; however, exactly how roots provide this protection has remained unclear. Among other things, roots can influence streambank soil erosion by holding soil together through a thick root network, interacting with soil microorganisms to stimulate the release of "sticky" organic compounds called extracellular polymeric substances (EPS), and altering the force of the water against the streambank. This research aimed to quantify and compare the relative importance of these three mechanisms on streambank soil erosion using a mini jet erosion testing device and an indoor recirculating flume channel. To do this in the flume, three walls were constructed to simulate unvegetated streambanks, as well as streambanks with herbaceous and woody roots. In greenhouse settings, soil treatments were also created to represent unamended and organic matter (OM) amended soil either without roots (bare soil), with artificial roots, or with living roots (*Panicum virgatum*). While roots protruding out of streambanks appeared to increase median soil erosion rates due to the impact of roots on near-bank flow, artificial roots in the soil and OM amended soils reduced soil erosion rates. Specifically, OM amendments stimulated the production of EPS proteins, leading to improved soil stability and increased soil resistance to erosion by water. Overall results highlight how the synergistic relationship between root fibers (living roots and artificial roots) and soil microbes can significantly reduce streambank soil erodibility due to root binding and microbial production of EPS. While plant roots naturally provide both fibers and EPS to soils, these materials could be incorporated into fill soils during construction to rapidly increase soil erosion resistance following levee construction and stream restoration projects.

Grant Information

Funds for this research were provided by the National Science Foundation Graduate Research Fellowship Program under Grant No. 1650114; the Virginia Tech Cunningham Doctoral Assistantship; and Virginia Tech's Graduate Research Development Program. Any opinions, findings, and conclusions or recommendations expressed in this material are those of the author(s) and do not necessarily reflect the views of the National Science Foundation or other funding institutions.

Dedication

I dedicate this work to my mom, Donna Grey Dixon-Smith. Without her, none of this work would have been possible. She will forever be loved and missed.

Acknowledgements

First, thanks must be given to my major advisor, Tess Thompson, for all her guidance, encouragement, and advice throughout my PhD program. It is difficult for me to imagine how far I would have progressed without her dedicated support. Second, I would like to thank the advice and research support given by my committee members, Cully Hession, John Seiler, Mark Williams, and Mark Stremler. Thank you for participating in my yearly research update presentations and helping me shape an exciting interdisciplinary project. Third, many thanks to current and retired BSE technical staff members Kelly Peeler, Laura Lehmann, Dumitru Branisteanu, Allen Yoder, and Cora Chen. Thank you for providing lab space, safety training, and taking my sometimes scatter-brain ideas and helping me shape them into physical tools/models that I have used throughout my dissertation. Fourth, I would like to thank all the Virginia Tech faculty and staff members who provided additional research/academic advice, financial support, or recommendation letters for various opportunities, including Kyle Strom, Dwyane Edwards, Ling Li, Matthew Bright, Erin Ling, Laura Eanes, Liza Spradlin, and Teresa Smith. Last, but certainly not least, I would like to thank "Tess' Tots", the awesome research group that has helped me laugh and keep my research running smoothly over the years. Thank you, Samuel Withers, Rex Gamble, Coral Hendrix, Ava Veith, Brian Wilson, Michael Snead, Kiara Macdonald, Suraye Solis, and Akinrotimi Akinola. Many of you suffered through hot greenhouse days, pipe cutting, and helped me cut, glue, and stress over thousands of string pieces; I'm forever grateful.

Special thanks to my family as well; my mom Donna Grey Dixon-Smith, my brothers Andrew Smith, Ronald Smith, and Brian Smith, and my fiancé Trerese Roberts. Thank you for the consistent support and reminder that life continues once graduate school is over.

TABLE OF CONTENTS

List of Tables

List of Figures

Chapter 1. Introduction

1.1 Background

The morphology and migration of stream channels has been a topic of interest for decades in the earth science community. Prior research has shown that while the transport of coarse bed sediment controls the channel profile, the resistance of the streambanks to erosion significantly impacts channel morphology and the rate of meander migration (Bogoni et al., 2017; Fernandez et al., 2021). It has long been recognized that streambank erosion resistance is influenced by riparian vegetation via belowground biomass growth (Pollen-Bankhead & Simon, 2010; Simon & Collison, 2002; Wynn & Mostaghimi, 2006) and effects on stream hydrodynamics (Curran & Hession, 2013). However, the significance of these mechanisms, particularly the role of plant roots and soil microbial interactions, is not fully understood. Specifically, a need exists to understand the linkages between roots, soil microorganisms, and fluvial erosion rates in a streambank setting. Along the Etchemin River in Québec, Canada, Matte et al. (2021) found evidence to suggest that an invasive riparian plant, Japanese knotweed (*Reynoutria japonica* Houtt.), increased streambank erosion rates compared to streambanks dominated by native vegetation. One potential mechanism described as a main cause for the observed increased erosion is associated with the knotweed rhizome structure (Colleran et al., 2020). The rhizome has an outer layer of bark and, therefore, lacks root hairs that could "bond" soil aggregates to root surfaces. Additionally, Japanese knotweed roots are relatively large, with diameters ranging from 5 to 100 mm (Child & Wade, 2000) and so the roots are less likely to have smaller roots (< 2 mm in diameter) that could bind the soil together. While quantitative data supporting these studies are limited, this work underscores the need to quantify the impact of different root mechanisms on streambank fluvial erosion.

Plant root effects on soil resistance to fluvial erosion have received considerable attention over the last century (Burylo et al., 2012; De Baets et al., 2007; De Baets et al., 2020; Kramer & Weaver, 1936; Li et al., 2017; Wang et al., 2014, 2015; Weaver & Noll, 1935), initially in response to rapid soil loss in agricultural lands (e.g., Kramer & Weaver, 1936; Weaver & Noll, 1935). Plant roots were recognized as "binders" of soil and effective at preventing excessive loss of soil particles due to wind or water erosion. Early written descriptions of root effects on streambank soils can be dated back to the late 1800s, when Shaler (1892) observed that: "No sooner do the waters recede

than certain plants of swift growth, which find their appropriate conditions on the verge of the river, extend their roots through it…and thus bind the…land firmly together" (pp. 290-291). By the 1930s, research on roots binding and protecting soil from erosion intensified, specifically in the agricultural sciences (Kramer and Weaver, 1936; Weaver and Noll, 1935). Weaver and Noll (1935, p. 21) observed “roots of great tensile strength entwine soil particles and anchor them firmly”, helping prevent soil erosion by flowing water or gravity. While Shaler and most other soil erosion researchers that followed focused on roots physically “binding” soil particles together to prevent soil loss, today it is known that roots protect soil from fluvial forces through multiple mechanisms.

Roots physically binding soil is defined here as the mixing of root fibers and soil to create a composite soil mass that is both strong in tension and compression, increasing the soil shear strength and apparent cohesion (Coppin & Richards, 1990; Gray & Leiser, 1982). Through interactions with soil microorganisms and by providing a carbon source to the soil environment (e.g., root exudation, root decomposition, etc.), living roots/root hairs can stimulate the production of microbial organic compounds that can have a cementing effect on soil particles or bond soil aggregates firmly to root surfaces (Annabi et al., 2007; Gerbersdorf & Wieprecht, 2015; Redmile-Gordon et al., 2020; Tang et al., 2011; Tengbeh, 1993). On a streambank, roots can also extend out of the streambank face, impacting the hydrodynamic boundary layer and altering the applied forces acting on the streambank surface (Thorne, 1990). In summary, plant roots are known to affect streambank fluvial entrainment through multiple mechanisms, including: 1) physically binding soil aggregates, 2) biochemically bonding soil aggregates to root surfaces and cementing soil aggregates together through the release of sticky organic compounds of root and/or microbial origin called extracellular polymeric substances (EPS), and 3) altering the hydrodynamic boundary layer. Recent research has started to explore the relative contributions of root binding vs. root exudate effects (Li et al., 2017; Wang et al., 2014, 2015), root hairs (De Baets et al., 2020), and stimulating microbial activity through organic matter inputs (Li et al., 2021), on soil resistance to fluvial erosion. However, the relative importance of each mechanism and the interaction among the mechanisms are still unclear.

Specifically, research has explored the effects of EPS type, composition, and production on sediment stability and cohesive soil erodibility (Droppo et al., 2001; Gerbersdorf & Wieprecht, 2015; Grabowski et al., 2011; Stal, 2003; Sutherland et al., 1998; Teasdale et al., 2018; Thom et

al., 2015; Underwood & Paterson, 2003; Van De Lageweg et al., 2018) over the last three decades. Wang et al. (2014, 2015) also explored root physical vs. root biological mechanisms on soil erosion by separating root binding and root exudation effects; their results suggested that the impact of root biological effects on soil erosion increased over time as vegetation matured. Nevertheless, evidence illuminating microbial EPS production effects vs. root physical effects on cohesive streambank soil erosion is not currently available.

Additionally, vegetation can have a significant effect on stream near-surface velocity and turbulence (Hopkinson & Wynn, 2009; McBride et al., 2007; Thorne & Furbish, 1995). For example, low density meadows within fully submerged channels have been shown to diminish sediment deposition and increase sediment erosion when compared to bare soil counterparts (Lawson et al., 2012; van Katwijk et al., 2010; Zhang et al., 2020). Plant roots have mostly been excluded from these studies on hydrodynamics. Given that roots will extend out of a streambank face, particularly on the outside of a meander bend, research is needed to clarify the relationship between root density, root diameter, near-bank hydrodynamics, and soil erosion rates.

Lastly, the effect of root diameter/thickness on fluvial erosion rates has received mixed results depending on the erosion testing device used (e.g., Burylo et al., 2012; De Baets et al., 2007; Khanal & Fox, 2017; Li et al., 1991; Wynn & Mostaghimi, 2006). Therefore, how changes in root size and rigidity (e.g., herbaceous vs. woody vegetation) influence soil erosion rates are still unclear.

1.2 Goals and Objectives

This research sought to understand how plant roots and soil microbial production of EPS impacted streambank hydrodynamics and soil resistance to fluvial entrainment. The overall goal of this research was to highlight the effectiveness of different microbial and root mechanisms in influencing streambank erosion rates. Specific objectives included:

1. Measure the impact of synthetic fibers on critical shear stress and the soil erodibility coefficient compared to bare soil and live rooted soil samples (Ch. 3).
2. Quantify the effects of flexible and rigid roots extending out of the streambank face on near-bank velocity and turbulent stress (Ch. 4).
3. Determine the influence of microbial production of EPS on soil aggregate stability and soil resistance to fluvial erosion (Ch. 5).

4. Quantify the relative impact of soil microorganisms, plant roots, and the interaction between the two on soil erodibility (Ch. 6).

1.3 Dissertation Organization

In Chapter 3, a mini-JET device was used to quantify the impact of inert fibers and living roots on soil resistance to fluvial erosion. While the mini-JET study described in Chapter 3 found some interesting relationships between inert fibers, plant roots, and soil erosion rates, constraints imposed by the JET device limited the scalability of the results. For example, insertion of the JET device base ring into the soil initially disturbs the soil, possibly dislodging/loosing soil aggregates prior to erosion testing. The impinging jet of water also does not naturally mimic streambank fluvial processes. Additionally, using sterilized vs. unsterilized soil samples in a greenhouse setting did not influence microbial activity or production of extracellular polymeric substances, making conclusions about microbial impacts on fluvial erosion impossible. As a result, to further study the influence of plant roots and soil microorganisms on streambank fluvial erosion, all later studies were conducted in a flume channel reconfigured for testing erosion in a streambank setting and organic matter inputs were used to stimulate soil microorganisms above existing conditions.

The experiments described in Chapters 4 – 6 simulated unvegetated and vegetated streambank erosion. To do this, artificial walls were built in a flume channel (described in Chapter 4), simulating a vertical streambank. A different artificial wall was constructed to create each of the three boundary conditions for all the experiments (sand/no root boundary, herbaceous/flexible root boundary, and woody/rigid root boundary). All boundaries were used in Chapters 4 and 6, while only the sand wall boundary condition was used in Chapter 5. Additionally, organic matter was used to stimulate soil microbial activity for erosion tests described in Chapters 5 and 6. More details regarding the methodology/flume construction for each of the studies is presented in the separate chapters.

Chapter 2. Review of Soil and Vegetation Factors Affecting Cohesive Soil Resistance to Fluvial Erosion

2.1 Streambank Erosion Processes

Streambank erosion is dynamic process and occurs due to a combination of: 1) subaerial processes; 2) fluvial entrainment (fluvial erosion); and, 3) mass wasting (Lawler, 1995; Lawler, 1992). Freeze-thaw cycling and soil desiccation are examples of subaerial processes. They reduce soil strength and are primarily controlled by climatic conditions (Wynn, 2006). Weakened soil leaves banks more susceptible to fluvial entrainment, or the direct detachment of individual soil particles/aggregates from streambanks by hydraulic forces (Lawler et al., 1997). Mass wasting is the complete physical collapse of a streambank "block" due to geotechnical instabilities (Lawler et al., 1997; Lawler, 1995). While subaerial processes, fluvial erosion, and mass wasting work together to produce bank retreat (Wynn, 2006), these processes are distinct and fluvial erosion is the primarily considered in this review. The following sections describe current knowledge on soil and plant properties that affect soil resistance/susceptibility fluvial erosion

2.2 Definitions and Clarification

To provide clarity for the following discussion, soil erosion by water is categorized into five distinct processes: 1) raindrop splash erosion, 2) sheet erosion, 3) rill erosion, 4) gully erosion, and 5) channel erosion. Splash erosion is defined as soil particles displaced from the soil surface due to raindrop impact, which creates a relatively uniform crust on the soil surface. Sheet erosion, or overland flow erosion, occurs when water flows over the surface as a thin sheet, but not in defined channels. During rill erosion, temporary concentrated flow paths are created, creating a sediment source and delivery system. Depending on the environmental conditions, water can flow into narrow channels that eventually create gullies depending on the flow intensity. Lastly, channel fluvial erosion involves the direct detachment of individual particles/aggregates from stream bed or banks by hydraulic forces. Each process described is a type of water erosion; however, this review will specifically refer to each erosion type by name for clarity.

Adopting the terminology proposed by Lawler et al. (1997), the terms “fluvial erosion” and “fluvial entrainment” are used to describe the detachment, entrainment, and removal of individual soil particles or aggregates from the streambank face by the hydraulic forces occurring during

flood events. The phrases “bank failure” or "mass wasting" denote the physical collapse of all or part of the stream bank due to geotechnical instabilities. In addition, the “fluvial boundary layer” is a thin layer of water adjacent to the wetted perimeter of a streambank where the effects of friction between the water and streambank surface dominate.

2.3 Erosion of Cohesive Soils

Soil entrainment by fluvial erosion occurs when the hydraulic shear stress (τ, the applied force) is greater than the resisting forces of the streambank (Thorne et al., 1997). While the applied forced is related to environmental factors (e.g., rainfall intensity), the resisting forces of streambanks depend on the soil physical, chemical, and biological properties. Soil resisting forces are generally a function of: 1) grain size distribution, shape, and density (Heinzen, 1976; Partheniades, 2009; Wynn et al., 2004); 2) the amount of sand, silt, and clay present in the soil and the type of clay (Akinola et al., 2019; Wynn et al., 2004); 3) the chemical composition of the pore fluid (e.g., water temperature and pH) (Hoomehr et al., 2018); 4) the presence of organic matter or other biological cementing agents (H. Li et al., 2021); 5) the thixotropy and stress history of the soil matrix or streambank (Akinola et al., 2018; Zreik et al., 1998); and, 6) the soil temperature and moisture content (Akinola et al., 2019; Grabowski et al., 2011). The complex interactions between all the factors listed above make fluvial entrainment of streambank soils difficult to model, particularly when the soil behavior is dominated by clay particles (defined here as cohesive soils). The presence of plant roots further complicates these interactions due to roots binding/bonding soil particles, addition of organic cementing agents into the soil matrix, and the effect of roots on soil moisture content and wetting/drying cycles.

2.4 Review of Streambank Fluvial Erosion Models and the Jet Erosion Test Device

2.4.1 Modeling Streambank Fluvial Erosion

A general model of cohesive soil erosion predicts the erosion rate as a function of the soil erodibility coefficient and a measure of flow energy (Moody et al., 2005):

$$\varepsilon_r = k_d X \tag{2-1}$$

where ε_r is the erosion rate (m s^{-1}); k_d is the soil erodibility coefficient (m^3 N^{-1} s^{-1}); and X is a measure of flow energy. K_d is considered a constant soil property and reflects the overall resistance of the soil to fluvial forces. The flow energy parameter has been quantified using a variety of

different methods for both cohesive and noncohesive soils, including kinetic energy per unit area (Poesen & Savat, 1981); the difference between near-bank velocity and average stream velocity (Ikeda et al., 1981; Pizzuto & Meckelnburg, 1989); near-bank velocity (Pizzuto, 2009); near bank water depth (Odgaard, 1989); unit stream power (Rose et al., 1983); boundary shear stress (Flanagan & Nearing, 1995); and the "excess shear stress", which is the difference between the applied shear stress (τ_a) and a critical boundary shear stress at which erosion starts (τ_c) (Hanson & Cook, 1997; Osman & Thorne, 1988; Partheniades, 1965). The excess shear stress equation representation of flow energy is the most common form of the general erosion model.

Partheniades (1965) proposed the excess shear stress model when studying the erodibility of cohesive soils. A rectangular flume was used to test beds that contained approximately 60% clay, 40% silt, and small amounts of fine sand. Partheniades conducted 32 runs within the flume, separating them into three series to investigate the influence of shear stress, suspended cohesive sediment concentration, and bed shear strength on erosion rates. To his surprise, erodibility of the cohesive sediments only depended strongly on the applied shear stress, increasing rapidly after surpassing a critical shear stress value. The excess shear stress equation incorporates this concept: particle movement or entrainment will not occur unless the applied shear stress is greater than the critical shear stress. Following EQ. 1, soil erosion rates depend on τ_c and increase by a factor of k_d.

2.4.2 Mini-JET Device

Since Partheniades, different erosion testing devices have been developed to measure and predict τ_c and k_d. Some commonly used devices include an open flume channel (e.g., Akinrotimi et al., 2018; Hanson, 1990a); a jet erosion testing (JET) device (Hanson, 1990b; Wynn & Mostaghimi, 2006); and a cohesive strength meter (CSM; Rinaldi & Darby, 2007).

In 1990, Dr. Greg Hanson designed the first iteration of submerged, vertical jet erosion test (JET) device to indirectly determine the soil erodibility coefficient and critical shear stress *in situ*. This JET design could only be used on horizontal beds. At the request of the National Sedimentation Laboratory, Greg Hanson designed a "multiangle" JET device that could be used on vertical surfaces (i.e., streambanks) (Hanson & Cook, 1997). The jet test device is comprised of multiple components – most notably a jet tube, nozzle, point gage, adjustable head tank, and jet submergence tank (Hanson & Cook, 2004). Water initially fills the submergence tank through the

connector line from the adjustable head tank prior to impinging on the soil. After filling the tank, the deflector plate is moved out of the way and a jet of water impacts the soil surface, initiating the test. The point gage is used to measure the depth change due to scour after each time segment. Dunn (1959), Hollick (1976) and Moore & Masch (1962) used similar variations of the JET device for erodibility measurements in the lab. Increasingly, JETs have become a popular method for determining soil erodibility in situ (Hanson, 1990b, 1991; Khanal & Fox, 2017; Mahalder et al., 2018; McNichol et al., 2017; Wynn & Mostaghimi, 2006).

Concepts derived from the excess shear stress equation have been used extensively to model erosion processes under various conditions (Hanson et al., 2002; Stein et al., 1993). For example, Stein et al. (1993) developed an excess stress relationship for a free overfall jet based on jet diffusion principles and the predicted mean peak stress in the impingement zone. Using six soil types, Stein & Nett (1997) later validated this model. Using a similar approach, Hanson et al. (2002) developed an excess shear relationship for the submerged circular jet device.

The scour surface within the impinging jet zone erodes away from the jet nozzle as the erosion test progresses (Hanson & Cook, 2004). Eventually, an equilibrium depth is reached. Based on the equilibrium depth, the critical shear stress, τ_c, can be determined using the model developed by Hanson et al. (2002). However, the length of time required to reach equilibrium can be large and difficult to determine (Blaisdell et al., 1981). For example, Blaisdell et al. (1981) observed that scour in cohesionless sands continued to progress after 14 months at pipe outlets. Therefore, the analysis of the JET device test results predicts the equilibrium depth using a logarithmic-hyperbolic function developed by Blaisdell et al. (1981) which assumes the time to reach equilibrium is infinite. Hanson & Cook (1997, 2004) and Hanson et al. (2002) describe this approach, called Blaisdell's solution (BL), in detail. Over time, other JET analysis methods have been developed to calculate τ_c and k_d, including the iterative solution method (Hanson & Cook, 1997) and the scour depth solution method (Daly et al., 2013)

In 2008, at another request of the National Sedimentation Laboratory, Greg Hanson developed a miniature version of the submerged jet erosion test device (Simon et al., 2010). Termed the "mini-JET", the instrument was designed for easier use in lab and field settings. Simon et al. (2010) compared the "multi-angle" and mini-JETs by conducting side-by-side, in situ tests at 35 sites in the Tualatin River Basin, OR. This comparison indicated the two devices produced nearly identical τ_c distributions. However, the measurements of k_d show parallel but distinctly

different distributions. The measured k_d values using the multi-angle jet device are higher compared to the mini-jet. Simon et al. (2010) hypothesized that the different k_d distributions arise from how the two jet devices diffuse and interact within their respective tanks.

To account for possible in-situ heterogeneity in field measurements, Al-Madhhachi et al. (2013) compared the multi-angle and mini JETs in a controlled lab using silty sand (72% sand and 15% clay) and clayey sand (57% sand and 25% clay). Thirty-six tests were conducted for each device and soil type at various water contents. Measurements of k_d were nearly identical for both devices and soil types. Conversely, Al-Madhhachi et al. (2013) found significant differences in τ_c between the multi-angle and mini JET devices. The mini-JET measured lower τ_c values for each soil type. Al-Madhhachi et al. (2013) speculated these variations occurred because of 1) the method of sample preparation and the methodology used to determine critical shear stress or 2) scaling differences of the nozzles and submergence tanks for the two devices. Because of this, Al-Madhhachi et al. (2013) developed an adjustment coefficient based on the equilibrium depth of the mini-JET tests relative to the original JET results. This adjustment leads to reduced differences in τ_c between the devices.

2.5 Soil Biofilms and Extracellular Polymeric Substances

2.5.1 Definition and Properties

Depending on current environmental conditions, biotic factors can have significant effects on sediment erosion (Black et al., 2002; Underwood & Paterson, 2003). Today, geomorphologist and hydraulic engineers recognize that an understanding in sediment biology and extracellular polymeric substances (EPS) dynamics (i.e., biological processes) are necessary to determine and predict cohesive sediment transport (Black et al., 2002; Gerbersdorf & Wieprecht, 2015; Graham J C Underwood & Paterson, 2003). Thus, researchers have taken the opportunity to explore EPS and its sediment stabilizing properties.

For decades researchers have recognized that microorganisms, in both constructed and natural environments, live and grow in aggregated forms, called biofilms (Wingender et al., 1999). In most biofilms, referred to as the "city of microbes" by Watnick & Kolter (2000), microorganisms typically account for a small percentage of the total dry weight (~10%) compared to the biofilm matrix (~90%). This matrix is composed of extracellular polymeric substances (EPS) which is mostly produced by the microbes inhabiting the biofilm. Representing the "house of the

biofilm cells" (Flemming et al., 2007), EPS are considered responsible for the structural integrity of biofilms and are key components in determining the overall physicochemical and biological properties of biofilms (Wingender et al., 1999). EPS provides the adhesion properties of biofilms to surfaces; protection of cells against harmful environmental influences; water retention; sorption of organic/inorganic compounds; enzymatic activities; and more (Flemming & Wingender, 2010).

As defined by Flemming & Wingender (2010), EPS are hydrated biopolymers secreted by biofilm cells to encase and immobilize microbial aggregates. EPS can be further separated into capsular (C-EPS), slime (S-EPS), loosely bound (LB-EPS), and tightly bound (TB-EPS) depending on their association with cells (More et al., 2014). They are responsible for the cohesion of cells and particulate materials in biofilms, and the adhesion of this substratum to surfaces (Characklis & Wilderer, 1989). For example, microbial attachment to substrate (i.e., soil or sediment) surfaces occurs in three steps: 1) bridging the gap between cells and surfaces via London forces; 2) using fimbriae and/or flagellas to overcome electrostatic repulsion between the cell and the substrate surface; and, 3) using secreted EPS and other polar forces to irreversibly bind to the substrate (Busscher & Weerkamp, 1987; More et al., 2014). Once attached, bacterial cells multiply, producing more EPS and further building the biofilm matrix (Flemming & Wingender, 2010). Evidence also suggests that attached microbes communicate with each other once attached, "recruiting" further settlement into the biofilm matrix by the same species or different taxa (More et al., 2014).

While EPS composition can vary significantly, they are commonly composed of water, carbohydrates, proteins, nucleic acids, phospholipids, and other polymeric compounds (Flemming & Wingender, 2010). EPS proteins, among other things, play an important role in the formation and stabilization of the polysaccharide matrix. This in turn enhances some of the functions provided by biofilms and aids in linking cell surfaces to the extracellular EPS matrix (Flemming & Wingender, 2010). Various organisms can produce EPS, including bacteria, green and red microalgae, diatoms, fungi, and archaea (Costa et al., 2018; Flemming & Wingender, 2010; Xiao & Zheng, 2016). The type and composition of the secreted EPS, and functions they have, will change significantly depending on the environmental conditions and the organism producing it.

2.5.2 Stabilization of Soils and Sediments

Holland et al. (1974) were the first to quantify the effects of EPS secretions (termed mucilage) on both cohesive and non-cohesive sediment stability by benthic microalgae diatoms under laboratory conditions. Microalgae cultures that created large amounts of mucilage were shown to significantly reduce sediment erosion. Holland et al. (1974) showed that EPS secreted in cohesive sediments (100% clays and silts or 90% sand+10% clays and silts) significantly increased sediment stability. In addition, the authors found that different diatom species have varied effects on erosional processes due to the type and amount of EPS produced. Coles (1979) later supported the idea of diatom stabilization presented by Holland et al. (1974). Coles (1979) showed that muddy sediments were stabilized by diatom biofilms through a successional process, leading to the development of saltmarsh systems from tidal flats.

The effects of microorganisms on sediment stability has also been studied in the field by inhibiting their activity. De Boer (1981) conducted an experiment to study the effects of surficial stabilization of intertidal, sandy (non-cohesive) sediments by algae. During low tide, a solution of copper sulfate and seawater was poured along a 1m strip over a sandy megaripple to eliminate all biological activity. After two high tide periods, the treated parts of the megaripple had completely eroded (see Fig 2 in De Boer 1981). Massive and sudden sediment loss on this scale had not been seen before, so De Boer (1981) concluded that the elimination of biological activity, specifically the destruction of the organic matter layer, was the cause. While not directly measured, the destruction and reduced production of EPS could have had a significant impact on sediment stability as well.

Dade et al. (1990) conducted flume experiments to correlate adhesive bacterial exopolymer concentration, measured in terms of uronic acid (carbohydrate) components, with the boundary shear stress required to initiate fine sand transport in marine environments. Shear velocities required to initiate erosion of sand, sand + media (EPS extracted from *Alteromonas atlantica*), and sand + media + incubation with *Alteromonas atlantica* were measured. Sand incubated with the bacterium had statistically significantly higher critical shear stresses compared to the other two treatments. Dade et al. (1990) correlated increases in uronic acids (a component of EPS) to increases in critical shear stress. Additionally, the concentration of uronic acids increased with the growth of *Alteromonas atlantica* in fine sands. In a separate study, Dade et al. (1996) determined a 60% increase in critical shear stress over control sediments for microbially bound marine clays,

supporting the 1990 study results. Dade et al. (1990) also suggested that long-chain sugar exopolymers released adjacent to the sediment-water interface may result in thickened viscous-dominated regions in the hydrodynamic boundary layer and subsequently, drag reduction.

Early studies on the effects of EPS composition and production on sediment stability centered around marine and intertidal environments (Stal, 2003; Underwood & Paterson, 2003). Droppo et al. (2001) was one of the first studies to consider the influence of biological processes on the stabilization of bed sediments in riverine systems. In an annular flume, kaolinite clay (D_{50} = 5 μm) and coal tar contaminated sediment from the Hamilton Harbor, Ontario (<63 μm) were used as the test bed. The critical shear stress of sediment eroded without biofilm development was 0.024 Pa. However, the critical shear stress increased more than 10-fold to 3.25 Pa when biofilms were allowed to develop for five days. Droppo et al. (2001) showed and argued that the biostabilization effects of microorganisms in riverine systems should be considered seriously in sediment transport models because of this finding.

Following Droppo et al. (2001), Gerbersdorf et al. (2005, 2008, 2009) conducted a series of studies on biostabilization in natural riverine systems. The three studies by Gerbersdorf and colleagues spanned ten freshwater sites, six reservoirs and four groyne fields, throughout Germany and the Czech Republic in the Rivers Neckar, Rhine, and Elbe. Sediment samples were collected near-bank at each location to a depth of 50 – 70 cm. Colloidal carbohydrates measured in both reservoirs and groyne fields were comparable with previous studies in intertidal areas (Gerbersdorf et al., 2009). For example, the colloidal EPS in all four groyne fields ranged from 0.4 – 3.40 mg g^{-1} dry weight (DW) while colloidal carbohydrates in intertidal areas have ranged from 0.01 – 4.00 mg g^{-1} DW. Bound carbohydrates and proteins are harder to compare across studies due to the differences in extraction methods. Nevertheless, results suggest that biostabilization is important in riverine systems, but the mechanisms driving stabilization may be different compared to marine/tidal environments.

Sediment depth considerably impacted EPS components in riverine systems as well. The ratio of bound to colloidal EPS increased with depth, indicating fresh production of polymeric substances (colloidal) in the upper sediment layers and mainly accumulation of refractory (bound) material in the lower layers (Gerbersdorf et al., 2008, 2009). At sediment depths below 5 cm, Gerbersdorf et al. (2008, 2005) found colloidal and bound EPS fractions (both carbohydrates and proteins) to have a significantly positive impact on critical shear stress. The same significant trend

was not found in the top sediment layers. In summary. Gerbersdorf et al. (2008, 2009) state that networks of EPS can probably permeate void spaces and promote inter-particle linkages, thus enhancing sediment stability over depth.

These results indicate that EPS in riverine sediments could have a significant impact on erosion resistance. However, in the Lauffen reservoir on River Neckar, Gerbersdorf et al. (2005) found colloidal carbohydrates in the top 4 cm of sediment to significantly increase critical shear stress only during spring months (March – May). The authors concluded that the physiological status and taxonomic composition of the EPS producer, which is impacted by outside environmental factors (i.e., temperature) influences the stabilizing potential of the EPS produced. In a 2009 study, Droppo made a similar argument when comparing the relative stability of five contrasting freshwater sediments and how the present biological communities impact the erosion process. The sediment types used included a stormwater pond, aquaculture waste, industrial grade kaolin, contaminated lacustrine, and fluvial (South Nation River near Ottawa, Ontario). While sediment critical shear stress increased as biofilms developed (2-14 days) in each sediment type, the degree of increase varied. Natural sediments (fluvial, stormwater, and lacustrine) significantly increased resistance to shear at a greater degree compared to kaolin and aquaculture sediments. Droppo (2009) showed that differences in sedimentological and biogeochemical properties of sediments (e.g., kaolin sediment had no initial organic content) has the potential to impact the EPS produced and, as a result, the impact of biofilm development on sediment resistance to erosion.

2.5.3 Incorporating Biological Processes into Sediment Transport Equations and Models

The role of EPS and biofilms in the transport of freshwater sediments, particularly in riverine environments, has received considerable attention over the last two decades. Researchers are becoming increasingly aware that the biological adhesion of sediment particles can have a significant impact on how sediment moves. As a result, some are arguing to include biological components in sediment transport equations/models to improve their accuracy. For example, Droppo et al. (2001) and Garcia-Aragon et al. (2011) argue that there is a strong need to consider biological influences on sediment in sediment transport models. Garcia-Aragon et al. (2011) studied the effects of biostabilization on cohesive sediments in the Athabasca River in Canada. Sediment was allowed to settle for 1, 3, or 7-day periods to consolidate/biostabilize. The critical shear stress measured by flume testing following the 1, 3, and 7-day settling periods was 0.21,

0.26, 0.32 Pa, respectively. Total erosion rates also decreased as settling time increased. Garcia-Aragon et al. (2011) attributed these results to the biostabilization of the sediment rather than consolidation and concluded that sediment transport models focused on the Athabasca River needed to include biological components to avoid making erroneous river management decisions.

Researchers focused on sediment transport in non-cohesive sediment beds have also called for increased attention to the impact of biological processes. Malarkey et al. (2015) studied the impact of small amounts of EPS on bedform development in fine, well-sorted sand using a flume. While most practical predictions of sediment transport are based almost exclusively on non-cohesive sand with no biological components considered, Malarkey et al. (2015) found that even small amounts of EPS (0.016 – 1% of total sediment weight) significantly changed bedform development. Sediment transport rates and the size of post-test ripples decreased with increasing EPS. Thus, they argue that equations based on non-cohesive sand do not fully capture what is happening in natural settings, so future models would need to incorporate biological processes to get the full picture of sediment motion.

Modified sediment transport equations and models have been developed. Fang et al. (2014) measured the effects of biofilm development on incipient motion in cohesive and non-cohesive sediment. After 8 weeks of biofilm growth, the incipient velocity in both cohesive and non-cohesive sediments increased 40-70%, indicating an increased resistance to erosion in the sediment. Using the experimental results, they developed equations for incipient velocity of sliding and rolling that included particle cohesive and biofilm adhesion properties. Based on the developed equations, biofilm adhesion of sediment played a dominate role in sediment transport when particle diameter was less than 0.2 mm (fine sand) but greater than 0.01 mm (fine silt). To compare results with the modified Shields curve (based on non-cohesive sediment motion), Fang et al. (2014) transformed their data in terms of Shields number and particle Reynolds number (Re_*). They concluded that the adhesion effect of biofilms is important for the region of $0.2 < Re_* < 1.0$.

Hongwei Fang's research group at Tsinghua University has done considerable work on the impact of biofilms on sediment physicochemical properties and transport characteristic. They have proposed methods for computing size gradation, density, settling velocity, and critical erosion velocity for biosediment (Fang et al., 2014; Shang et al., 2014) and studied the bed form dynamics and transport characteristics for biosediment through flume experiments (Fang et al., 2017a; Fang et al., 2016; Fang et al., 2015). Using this information, Fang et al. (2017b) developed and proposed

a three-dimensional (3-D) model of hydrodynamics and biosediment transport. Biofilms were allowed to develop for 0 (clean sediment), 10, and 20 days for coarse (d_{50} = 0.061 mm) and fine (d_{50} = 0.01 mm) sediments. Comparison of velocity profiles between the 0-, 10-, and 20-day biofilm-developed sediment showed significant discrepancies with respect to particle size (e.g., a greater flow velocity was needed to erode 20-day sediment compared to clean sediment). Model simulations showed considerable agreement between experimental results when accounting for biofilm development. While the lab conditions used were relatively simple and more research is needed to model complex field conditions, Fang et al.'s (2017b) model is the first attempt at integrating traditional sediment transport and biological properties. The paper provides further insight into how biostabilized sediment is eroded/transported differently compared to clean sediment and makes a case for why more work needs to be done in incorporating biological effects into sediment transport models.

2.5.4 EPS Extraction Methods

The literature contains considerable variations in EPS extraction methods (see More et al., 2014, Table 4). Because the extraction method used can have considerable impact on the measured EPS composition (Jost Wingender et al., 1999), researchers have sought to define an effective method that can be used under any situation. However, results vary. Underwood et al. (1995) compared EPS extraction from intertidal mudflat sediments using a saline solution or a combination of EDTA + saline (Na_2EDTA). Mixing sediments for 10 minutes at 20°C with 100 mM Na_2EDTA and 25% saline extracted the most carbohydrate EPS (0.295 mg/dry weight [DW] sediment). To the author's knowledge, this is the only paper that compares two or more extraction methods on sediment samples.

Due to the importance of EPS production in biotechnology (Vu et al., 2009) and wastewater treatment (Liu & Fang, 2003), EPS extraction methods have been studied almost exclusively on activated sludge samples or granular filter media. When comparing cation exchange resin (CER), sodium hydroxide, and heating (80°C) extraction methods in wastewater activated sludge samples, Frolund et al. (1996) found sludge mixed with CER for 17 hours at 900 rpm extracted the most EPS (48 and 243 mg/g-volatile solids [VS] carbohydrates and proteins, respectively). CER is partly chemical (removal of divalent cations such as Ca^{2+}) and partly mechanical due to the applied shear

(Frolund et al., 1996). Combined with a long extraction time and a high stirring intensity, Frolund et al. (1996) showed that CER is a viable method for extracting EPS from activated sludge samples.

Table 2-1 presents some of the extraction methods commonly used and/or compared. Using infra-red (IR) spectrometry on extracted EPS samples, Comte et al. (2006b) and D'Abzac et al. (2010) sought to determine if the physical and chemical extraction methods changed the chemical structure of EPS. In both cases, no notable differences in IR bands appeared between physical and control EPS extractions. However, the authors found particular bands in chemical extractions which did not appear in control or physical extractions used, indicating a contamination of EPS. The formation of EDTA-EPS complexes are known to form when using EDTA as an extraction method. These complexes are not completely removed from solution during centrifugation, thus adding to the extract contamination. Additionally, D'Abzac et al. (2010) measured EPS extraction yields that exceeded 100% in both EDTA and formaldehyde + NaOH extractions. This further indicates a bias in EPS measurements due to the contamination of EPS extract solutions. Lastly, Comte et al. (2006a) found that chemical extractions and heating significantly modified the complexation properties of EPS between two heavy metals (Pb^{2+} and Cd^{2+}). As a result, Comte et al. (2006a) suggest using physical extraction methods over chemical extractions since complexation modifications may lead to other physico-chemical changes in EPS not measured in the study. The results of these studies have lead authors to generally accept the CER extraction method as the best alternative for EPS extraction. It consistently has the highest yield among all physical extraction methods and has a low degree of cell lysis/extract contamination (Redmile-Gordon et al., 2014; Sheng et al., 2010).

Table 2-1: Different EPS extraction methods used in comparison studies (Comte et al., 2006b; Comte et al., 2006a; D'Abzac et al., 2010; Liu & Fang, 2002). Each method includes the typical extraction concentration, temperature, stirring speed, and time if applicable). Modified from More et al. (2014)

Methods		Mechanism
Physical:	Centrifugation	EPS separates from cell surface and dissolves to solution under the centrifugal force.
	Heating (80°C, 1 hour)	The molecular movement is enhanced that accelerates the EPS dissolution.
	Sonication (40W, 2 minutes)	Disintegrates flocs/aggregates that aids in the release of enzymes.
	CER (4°C, 600 rpm, 1 hour)	Divalent cations are very important for the cross-linking of charged compounds in the EPS matrix; CER removes the divalent cations, thus causing the EPS to fall apart.
Chemical:	2% EDTA (4°C, 3 hours)	Chelating agent. EDTA also removes divalent cations, causing the EPS matrix to fall apart.
	36.5% Formaldehyde (4°C, 1 hour) with 1M NaOH (4°C, 3 hours	NaOH increases the pH, resulting in the dissociatoin of acidic groups in EPS and the repulsion between the negative-charged EPS. The addition of formaldehyde reduces the cell lysis that is caused by the addition of NaOH.
	10% Glutaraldehyde (4°C, 12 hours)	As glutaraldehyde has the ability to fix cells and denatures EPS, it can also be used to extract EPS.

2.6 Organic Matter and Soil Aggregate Stability

The erosion of cohesive soils is usually in aggregates (Utley & Wynn, 2008; Mirtskhulava, 1966), so aggregate formation and stability are important processes to understand. Martin et al., (1955) defined soil aggregates as "naturally occurring clusters or groups of soil particles in which the forces holding the particles together are much stronger than the forces between adjacent aggregates" (pp. 3). Particulate organic matter can act as the "center" of newly formed micro- or macroaggregates (Six et al., 2004); the formation of these aggregates is influenced by five factors: 1) soil fauna, 2) soil microorganisms, 3) roots, 4) inorganic binding agents, and 5) environmental variables (Six et al., 2004). According to the aggregate hierarchy theory proposed by Tisdall & Oades (1982), microaggregates (20-250 μm) and macroaggregates (> 250 μm) form within the soil, with microaggregates potentially developing within macroaggregates as well (Oades, 1984).

Macroaggregates are temporary structures stabilized by plant roots, hyphae, and other binding agents like root exudates while microaggregates are permanent structures stabilized by smaller inorganic and organic substances (Kay, 1990; Tisdall & Oades, 1982).

In riparian zones, plants commonly incorporate organic matter/organic carbon into soils via root exudates, root turnover, aboveground biomass decomposition, microbial biomass, and mycorrhizae/hyphae inputs (Cotrufo & Lavallee, 2022). The dominant vegetation type plays a role in the type and amount of SOC incorporated into the soil environment. Prior studies have measured significantly higher total SOC content in woody plant-dominated riparian areas/upland environments compared to areas dominated by herbaceous vegetation (de Rebello et al., 2019; Paul et al., 2008). On the other hand, Paul et al. (2008) found that higher root densities in grass-dominated environments may lead to greater fractions of SOC that are directly associated with initial aggregate formation/stabilization.

While plant roots generally improve soil aggregation and increase soil aggregate stability compared to bare soil (Graf & Frei, 2013; Gyssels et al., 2005; Haynes & Beare, 1997; Reid & Goss, 1981), the impact of live roots is species specific. Reid & Goss (1981) found that maize and tomato roots can decrease soil aggregate stability by chelating iron and aluminum, thus destroying chemical bonds with organic matter. Another factor impacting root impact on soil aggregate stability may be related to the aggregate destruction hypothesis. The hypothesis states that plant roots can promote the destruction of soil aggregates more than their formation, thereby exposing the physically protected labile soil organic matter (SOM) to microbial attack that can result in increased SOM decomposition (Cheng & Kuzyakov, 2005). Lu et al. (2019) investigated the effects of three non-woody perennials (*Stipa grandis*, *Leymus chinensis*, and *Medicago sativa*) on soil aggregate stability for 476 days. By the end of the experiment, the total weight of macroaggregates (> 0.25 mm) was significantly lower in *M. sativa* treatments compared to the bare clay loam soil control ($p < 0.05$). *S. grandis and L. chinensis* also had lower macroaggregates compared to the control, though not significant at $\alpha = 0.05$. Additionally, at most time points, Lu et al. (2019) measured smaller aggregate stability values in planted treatments compared to bare clay loam soil treatments. In particular, *M. sativa* significantly decreased soil aggregate stability compared to unplanted soil at each sampling time used. These results provided evidence for the aggregate destruction hypothesis, where plant roots promoted the destruction of stable soil macroaggregates more than their formation.

When broken down into its elementary mechanisms, soil aggregate breakdown can be caused by 1) soil slaking, the rapid disintegration of an aggregate due to the compression of trapped air during aggregate wetting; 2) differential swelling that cause microcracking in clayey soils; and 3) mechanical breakdown due to impact forces (e.g., raindrop impacts) (Le Bissonnais, 1996). Organic matter can influence soil aggregate stability by 1) increasing interparticle cohesion and 2) increasing soil hydrophobicity (Abiven et al., 2009). Interparticle cohesion can increase soil resistance to breakdown to all mechanisms described above, while increasing aggregate hydrophobicity influences aggregate wetting rates, thus increasing soil resistance to slaking and differential swelling.

In a laboratory incubation experiment, Annabi et al. (2007) studied the influence of three urban compost at two maturity levels on soil aggregate stability. Samples were incubated in triplicate for 0, 3, 7, 14, 28, 56, 112, 164, and 336 days at 28°C in complete darkness. Following incubation period, samples were analyzed for hot water extractable polysaccharides, microbial and fungal biomass, water drop penetration time (measure of hydrophobicity), and aggregate stability. Aggregate stability was measured using the fast wetting, slow wetting, and mechanical breakdown procedures outlined by Le Bissonnais (1996). An increase in soil resistance to slaking was correlated with labile organic matter inputs and subsequent increases in microbial/fungal biomass and soil hydrophobicity. On the other hand, only mature compost (lower labile organic carbon content) consistently improved soil resistance to mechanical breakdown. Neither microbial biomass, fungal biomass, nor hydrophobicity were positively correlated with mechanical breakdown (Annabi et al., 2007); thus, the authors suggested that increased interparticle cohesion probably occurred due to the diffusion of organic substances into the aggregates from mature composts.

In a 9-year field study, Annabi et al. (2011) found similar results. Soils amended with municipal solid waste compost (MSW), farmyard manure (FYW), biowaste compost (BW) and green waste and sewage sludge compost (GWS) were compared to an unamended control. The MSW amendment provided the most labile organic carbon to the soil environment and was found to have the greatest improvement on soil resistance to slaking. Biowaste compost had the lowest carbon mineralization rate but the highest improvement on soil resistance to mechanical breakdown compared to the control. The biodegradability of the organic matter (OM) amendment also influenced total organic carbon (TOC) contents over the course of the experiment; TOC

increased by 3.5, 2.7, 2.6, and 0.5% yr^{-1} in the GWS, FYM, BW and MSW treatments, respectively, compared to the control.

Recent work has also described significant relationships between bound EPS, labile OM inputs, and soil aggregate stability. In the 2020 field study conducted by Redmile-Gordon et al. at Rothamsted Research, UK, the authors investigated the effect of land use and agricultural management changes on soil EPS and soil aggregate stability. Treatment plots included established grassland, fertilized arable, and fallow sites (> 50 years) and recently converted sites (e.g., a grassland converted to a arable field, 2.5 years). The authors found that recent land use changes had a greater impact on soil EPS and aggregate stability (fast wetting method) compared to larger accumulations of "old" soil organic matter, with high C input from perennial grassland contributing the greatest EPS and stability. Redmile-Gordon et al. (2020) also found both EPS proteins and carbohydrates were significantly correlated with soil MWD, but EPS proteins had the higher R^2 (0.30 vs 0.15).

Some studies suggest the increase in macroaggregate stability with increasing organic matter is driven by soil fungi populations (Lucas et al., 2014; Tang et al., 2011). Every five days for 40 days in total, Tang et al. (2011) measured water stable soil aggregates, EPS carbohydrates, fungal and bacterial biomass, and fungal hypha length in soil amended with 1% maize leaves and compared the results to unamended soil samples. The authors found that stable large macroaggregates in amended treatments increased significantly compared to the control at every measurement time. However, when fungicide was applied to the soil samples, maize leaves had no effect on macroaggregate formation. While the application of bactericide also impacted final macroaggregate stability, the effect was not as dramatic as fungicide, indicating that fungi played a more dominant role in macroaggregate formation compared to bacteria. Lucas et al. (2014) found similar results to Tang and colleagues when considering how different soil amendments (vetch clippings, vegetable compost, and dairy manure) impact large macroaggregate weight. Over the 82-day incubation period, Lucas et al. found vetch clippings and manure amendments significantly increased soil macroaggregate mass compared to the unamended control. This significant increase was attributed to the higher fungal:bacterial ratios measured in the vetch and manure treatments due to their relatively high levels of bioavailable organic carbon, as compared to the compost amendment and the control.

Barto et al. (2010) used structural equation models to explore how biotic and abiotic factors impacted soil aggregate stability. Experiments were in the German Biodiversity Exploratories, with sites in Schorfheide Chorin, Hainich Dün, and the Schwäbische Alb. From the 27 50 m x 50 m grassland sites selected, five 200 g soil samples (0 – 10 cm depth) were randomly collected. Biotic factors measured included arbuscular mycorrhizal fungi (AMF), root length (0-0.2 mm and 0.2-1 mm), and intraradical AMF structures (e.g., hyphae and vesicles that grow inside plant roots). Abiotic factors measured included soil hydrophobicity, aggregate stability, total N and C, and plant available P. When considering biotic factors alone, extraradical AMF length was the only parameter to have a significant positive effect on aggregate stability. However, when considering abiotic and biotic factors together, extraradical AMF (e.g., AMF structures that grow outside plant roots) length was no longer a significant predictor of aggregate stability. In contrast, only abiotic factors (sand and carbonate-C concentrations) developed significant and negative correlations with aggregate stability. While testing biotic and abiotic factors together explained the most variation within the structural model, unexplained variation ranged between 57-85%, strongly suggesting that there are additional factors they did not measure that also influenced soil aggregate stability. Nevertheless, Barto et al. (2010) attributed their aggregate stability results to the high total abundance of water stable aggregates initially found at their sites (92 +/- 7.2%). In such highly aggregated systems, they explained that the effects of biotic factors that increase aggregation may be less apparent than effects of abiotic factors that decrease aggregation.

Soil aggregates and labile OM inputs are directly linked to the resistance of soil to erosional processes, specifically water erosion (Barthès & Roose, 2002; Le Bissonnais, 1996). Li et al. (2021) conducted simulated rainfall experiments on loess soil samples with increasing soil organic carbon (SOC) content (7.54 to 21.69 g kg^{-1}). The authors found that SOC and light fraction organic carbon, which represents the labile portion of organic matter contents, played key roles in increasing soil aggregate stability and reducing aggregate disintegration during splash erosion events. Barthès & Roose (2002) studied the susceptibility of soil to water erosion in the field and related it to topsoil aggregate stability. In study areas were intense rainfall is frequent, Barthès & Roose (2002) found that runoff rates and soil loss were negatively correlated with topsoil aggregate stability, especially stable macroaggregate contents. The stability of soil aggregates has been shown to increase with plant roots (Reid & Goss, 1980, 1981) due to the release of organic exudates within the rhizosphere, further reducing soil erodibility. Increases in stable aggregates

have been measured in newly cleared fields as well (Turkelboom et al., 1997). A reduction in soil loss was correlated with this increase in stable aggregates, but soil loss increased overtime as the roots decayed and aggregates broke down.

2.7 Plant Root Mechanisms

Vegetation and the associated roots significantly influence the erodibility and migration of streambanks (Ielpi et al., 2022; Miller et al., 2014; Purvis & Fox, 2016; Smith, 1976; Wynn & Mostaghimi, 2006). In 1976, Derald Smith conducted an experiment on well-vegetated vs. unvegetated anastomosed channels in Banff Park, Alberta. Using bank pins and an instream erosion box, Smith concluded that areas with 16%-18% root reinforcement were 600 times more resistant to erosion compared to unvegetated sections. When root riprap was also added to the vegetated banks, these sediments were 20,000 times more resistant to erosion than bare sediments. The potential root mechanisms that drive this increased resistance are explored in the following sections.

2.7.1 Mechanical Effects of Root Reinforcement

In 1966, Henri Vidal (Vidal, 1966, 1969) introduced the theory of earth reinforcement. Initially, the theory referred to creating a composite material containing earth (soil or rocks) and linear reinforcement (strip, bars, fibers, etc.) with high shear and tensile strength (Shukla et al., 2009). This concept quickly expanded to plant roots (strong in tension, weak in compression) and soil (weak in tension, strong in compression). Like Weaver & Noll's (1935) description, root reinforcement is analogous to the use of fibers in the reinforced earth theory: tensile resistance in the roots is mobilized by soil shear stresses, increasing the soil shear strength and apparent cohesion (Coppin & Richards, 1990; Gray & Leiser, 1982). Because of this increase in soil shear strength, root reinforcement using vegetation has been shown to stabilize slopes, preventing soil loss due to landslides and erosion (Gray, 1973; Rice et al., 1969).

Root reinforcement of streambanks increases the mechanical shear resistance of soil (Docker & Hubble, 2008; Thorne, 1990). Quantification of this increased soil strength was measured in-situ on four common Australian riparian trees by Docker & Hubble (2008) using field shear-boxes. The magnitude of shear strength increased linearly with increasing root area ratio (RAR), defined at the shear plane, as well as root tensile strength and orientation in the soil.

Abernethy & Rutherfurd (2001) noted that root distribution also plays an important role in streambank stability. In their field and lab studies on two Australian riparian trees (*Eucalyptus camaldulensis*-river red gum and *Melaleuca ericifolia*-swamp paperbark), Abernethy & Rutherfurd (2001) found that bank root reinforcement decreased exponentially with depth and distance away from the trees.

2.7.2 Hydrological Effects

Interception of rainfall by plant canopies and the extraction, or evapotranspiration (ET), of water by roots for aboveground plant use (Dingman, 2001) constitute the hydrologic effects of vegetation (Pollen et al., 2004; Simon & Collison, 2002) on streambank soils. Drier soil leads to reduced positive pore-water pressure and enhances the development of matric suction, leading to increased shear strength and, consequently, increased bank stability (Simon & Collison, 2002). For example, Pollen et al. (2004) measured a 1-3 kPa increase in the apparent cohesion due to increases in matric suction by ET by young trees. Due to negligible ET in winter and spring months, root reinforcement due to hydrologic effects is generally greatest in the summer (Pollen-Bankhead & Simon, 2010; Simon & Collison, 2002).

Simon & Collison (2002) measured how the hydrologic effects of four riparian tree species and two erosion-control grasses impacted bank stability. They conducted in-situ shear tests and characterization of root parameters (i.e., tensile strength) along with measurements of bank pore-water pressures at varying depths. Using the ARS bank stability model, Simon & Collison (2002) found that the mechanical and hydrologic effects of vegetation on bank stability vary with species and time. Mechanical effects increased bank stability in summer and spring months for both species while hydrologic effects decreased bank stability in the spring. Pollen-Bankhead & Simon (2010) reported similar results; the hydrological reinforcement of riparian tree and switchgrass species, measured through increases in apparent cohesion, was estimated as 1.0-3.1 kPa in spring and as high as 5.0 kPa in summer.

2.7.3 Root Biochemical Effects

While washing root cores, Tengbeh (1993) noticed adhesion of soil particles onto root surfaces. The process to remove clay soil particles from the roots was more difficult than removing sandy clay loam particles. Because the grasses used were known to exude organic exudates,

Tengbeh (1993) suggested that this process bound soil particles to root surfaces, increasing soil strength. Some recent research has focused on the role these biochemical root processes play in protecting soil from concentrated flow erosion.

Wang et al. (2014) investigated the effects of near surface soil characteristics on overland flow in a 7-yr old natural succession grassland located in the Loess Plateau, northeast China. The experiment consisted of five treatments controlling for root physical and chemical effects (dead vs. live roots), plant litter, and biological soil crusts (BSCs). Flume study results indicated a 98.9% reduction in soil detachment capacity due to near surface soil characteristics, with 30.3%, 14.9%, and 53.7% contributed by plant litter, BSCs, and total roots (combined chemical and physical), respectively. Further breakdown explained that 39% and 14.7% of the total root effects were due to the physical (root-binding) and biochemical (root-bonding) effects of plant roots, respectively.

Wang et al. (2015) and Li et al. (2017) found similar results. Wang et al. (2015) looked at the resistance to overland flow in 1-yr and 24-yr old natural succession grasslands. Experimental treatments controlled for the same variables described by Wang et al. (2014). Over 60% and 62% of the variance in the soil erosion resistance was explained by total root effects for the 1-yr and 24-yr grasslands, respectively. Root chemical bonding explained 7% of the total root effects in the 1-yr grassland and 14% in the 24-yr old grassland. Combined with results presented by Wang et al. (2014), this suggests that root chemical bonding effects increase in significance over time as vegetation matures, up until a threshold value. In Li et al. (2017), biochemistry effects of plant roots were determined using four treatment types: 1) purple alfalfa root-penetrated soil, 2) loess soil sampled below rooting depth, 3) soil sampled < 25 cm and sieved (biochemical effects), and 4) root-texture cotton thread penetrated soil (physical effects). Soil detachment rates due to concentrated flow showed biochemistry effects contributed 20% of the overall root-reinforcement. Additionally, as root density increased, the physical binding effect of roots increased while the biochemistry effects decreased.

2.7.4 Effect of Root Density and Root Volume

In response to the severe agricultural damage caused by dust storms that occurred in the drought-stricken Southern Plains region of the United States in the 1930s (i.e., the Dust Bowl), research around the 1930s saw increased investigations into understanding how vegetation reduced soil erosion and runoff (e.g., Kramer & Weaver, 1936). Kramer & Weaver (1936) were the first to

examine the role plant tops (foliage) and bottoms (roots) played in protecting soil from concentrated flow erosion. Rectangular (1 m long, 0.5 m wide and 10 cm deep) samples of multiple field crops, pasture crops, weeds, and native plants were collected and placed on a slope in a greenhouse. Water was applied to the sloped samples and the time required for an entire soil sample to be washed away was monitored; treatments included bare soil, plant roots alone, and the combination of plant roots and foliage. While the combination of aboveground foliage and roots had the greatest impact on reducing the erosion time, roots alone significantly influenced the erosion time as well. For example, bare soil took 16-18 minutes to erode, with roots of sunflowers, millet, or Sudan grass, erosion time increased to 2-4 hours, and with foliage added on, about 35%+ of soil remained after 9-12 hours.

While much of the early work on vegetation and soil erosion focused on aboveground biomass, research within the last two decades has expanded on how plant roots protect soil from erosion by water. Gyssels & Poesen's (2003) field experiment measured the erosion rates of previously formed rills and gullies flowing within fallow soil or soil planted with winter cereal crops (barley, wheat, triticale) or grasses. The grasses and cereal crops were members of the family Gramineae or Poaceae. Their results showed rill/gully cross-sectional areas decreasing exponentially as root and shoot density increased. Because both below- and aboveground biomasses explained the exponential decrease in soil detachment rates (SDR), Gyssels & Poesen (2003) emphasized the importance of vegetation density measurements for all plant components.

Additional studies have reported exponential decreases in SDRs as root density (RD), defined as the dry root mass per unit volume of soil, increases (De Baets et al., 2006; De Baets et al., 2007; Zhang et al., 2013). However, results from a flume study conducted by Gyssels et al. (2006) on single- and double-drilled field crops (barley, winter wheat, spring wheat) were inconclusive. For this project, samples were grown in the field and taken at various stages of growth for flume experiments. Using the Hill curve (Hill, 1910) empirical equation (EQ. 2.2), Gyssels et al. (2006) predicted a 50%-60% decrease in soil detachment. However, RD had no significant impact on SDR during flume experiments. Aging effects, or changes in root effects and soil properties over time, were described as potential causes of this deviation. Gyssels et al. (2006) found that their roots only affected soil erosion significantly when cracks or irregularities were present in the soil surface. De Baets et al. (2006), De Baets et al. (2007), and Zhang et al. (2013) conducted experiments using a similar procedure; however, in each case all samples were collected

at the same time. Because of variations in vegetation, soil type, growth environments, and flume characteristics, comparisons between articles are challenging.

$$D_{rr} = \frac{RD^{-0.85}}{5.32+RD^{-0.85}} \quad (2\text{-}2)$$

where D_{rr} = the soil detachment rate; and RD = root density (kg m^{-3}).

Root length density (RLD), defined as the root length per unit volume of soil, is another common measurement found when studying the impacts of root properties on erosion by concentrated flow. Mamo & Bubenzer (2001a) conducted a flume study using pipes packed with bare or ryegrass-rooted soil to study the effects of roots on rill erosion. Erosion tests were conducted at three different time periods at various flow rates: 1) 8, 12, and 16 weeks after initial planting (experiment I) and 2) 6, 8, 10, 12, 14, and 16 weeks after initial planting (experiment II). Mean soil detachment rates for rooted samples decreased by 64% and 27% in experiments I and II, respectively, compared to fallow soil. SDR and rill erodibility decreased exponentially as RLD increased as well. A companion field study (Mamo & Bubenzer, 2001b) and a flume experiment setup by De Baets et al. (2006) found similar exponential decreases in SDR as RLD increased.

Burylo et al. (2012) expanded on the idea presented by Gyssels & Poesen (2003) and measured ten different plant traits to assess their impact on concentrated flow erosion, including RD, RLD, root diameter, percent fine roots (%FR), specific root length (SRL) [the ratio of root length to dry mass of fine roots], and external root surface (RSA). Flume experiments used two tree species (*Pinus nigra austriaca* and *Robinia pseudo acacia*) and one grass species (*Achnatherum calamagrostis*) after four weeks of growth. *Robinia pseudo acacia* roots reduced SDR the most, followed closely by *Achnatherum calamagrostis*. The two tree species had tap roots whereas the grass had a fibrous root system; however, *Robinia pseudo acacia* was characterized by small diameter roots and high values of %FR, SRL, RLD and RSA (opposite for *Pinus nigra austriaca's* roots). Burylo et al. (2012) results suggest that RLD, SRL, and RSA, in combination with root diameter and %FR are better indicators of soil detachment rates than RD (found no direct relationship between RD and SDR). Tap rooted plants have been shown to be less efficient at protecting soil from concentrated flow events (De Baets et al., 2007; Li et al., 1991). However, Burylo et al. (2012) found significant correlations between SDRs and other plant functional traits, implying that root diameter alone may not explain the differences in detachment rates between fibrous and tap rooted plants.

2.7.4.1 Large Diameter vs. Small Diameter Roots

The impact of plant type on fluvial erosion is an ongoing debate. Some studies have found vegetation with a greater percentage of fine roots has lower soil detachment rates compared to tap (large) rooted systems (Burylo et al., 2012; De Baets et al., 2007). Narrower stream channels have been associated with grassland riparian areas, suggesting that grasses better resist bank erosion compared to forested riparian areas (Davies-Colley, 1997). In contrast, field measurements of fluvial erosion on streambank soils showed an inverse relationship between root diameter and soil erosion (Wynn & Mostaghimi, 2006). Observations and measurements of channel migration after major flood events illustrated that stream reaches with forested riparian areas eroded less than their grassy counterparts (Rood et al., 2015). Anderson et al. (2004) sought to provide some clarity on these contradictory results by examining datasets for factors affecting widths of streams and rivers. The authors found that the effect of riparian vegetation on channel size was scale-dependent. Channels with thick woody vegetation were narrower than grass lined or unforested banks when catchments were greater than 10–100 km^2; the opposite relationship was found for smaller catchments.

The erosion testing method used appears to contribute to this uncertainty. Wynn & Mostaghimi (2006) conducted submerged jet tests on streambank soils near Blacksburg, VA USA to study the effects of root density, subaerial processes, and soil type and chemistry on the erodibility and critical shear stress of streambanks. Both the upper (within 45 cm of top of bank) and lower (within 1 m of base flow water level) banks were tested at 25 sites along six different streams. When conducting in-situ submerged jet tests on streambank soils near Blacksburg, VA USA, Wynn & Mostaghimi (2006) found that increases in the root volume ratio of 2 to 20 mm diameter roots had a significant inverse effect on soil erodibility. Similarly, Khanal & Fox (2017) measured a negative, nonlinear relationship between soil erodibility and root diameter (as root diameter increased, k_d decreased exponentially) on greenhouse grown root samples. These findings contradict previous concentrated flow/flume studies that have found finer roots (<2 mm) decrease soil erodibility compared to larger diameter roots (Burylo et al., 2012; De Baets et al., 2007; Li et al., 1991).

2.8 Impact of Vegetation on Stream Hydrodynamics and Erosion Potential

2.8.1 Channel Beds

Over the last three decades, the impact of vegetation on stream hydrodynamics has received increased attention. In channel beds, fully submerged seagrass meadows have been shown to enhance or diminish sediment deposition depending on the meadow density (a function of shoot diameter and average spacing between shoots) (Lawson et al., 2012; Nepf, 2012a; van Katwijk et al., 2010; J. Zhang et al., 2020). At various intertidal field sites within the Netherlands, van Katwijk et al. (2010) found that meadows with high vegetation cover (≥ 160 shoots m^{-2}) at relatively sandy sites showed clear increases in fine sediment/organic matter (OM) deposits as opposed to adjacent unvegetated sediment sites. In contrast, at relatively muddy sites with low vegetation cover (< 120 shoots m^{-2}), the authors measured a significant decrease (increased erosion) of fine sediments/OM compared to nearby unvegetated sites. Similarly, using seagrass microcosms, Lawson et al. (2012) measured increasing sediment suspension into the water column at shoot densities between 76 to 239 shoots m^{-2} compared to the bare soil control. However, at the highest shoot density used in the study (558 shoots m^{-2}) suspended sediment in the water column was zero (sediment erosion was eliminated).

The reduction of particle retention in sparse meadows has been linked to sediment resuspension through stem-scale turbulence (Zhang et al., 2020). At low shoot densities, individual shoots may generate additional turbulence because channel velocity was not significantly diminished relative to bare soil (see Figure 2 in Nepf, 2012a). Zhang et al. (2020) demonstrated this link between sediment resuspension and stem-scale turbulence in their flume study. Using rigid circular rods representing seagrass canopies, Zhang et al. (2020) found that particle retention in meadows is enhanced or diminished compared to adjacent bare soil depending on the meadow density and channel velocity. When using a relatively sparse meadow (260 shoots m^{-2}) and a flume velocity of 0.16 m s^{-1}, the authors measured identical net depositions and near-bed turbulences within the meadow ($[3.8\pm0.8]\times10^{-4}$ m^2 s^{-2}) and over bare soil in an open channel ($[3.6\pm0.7]\times10^{-4}$ m^2 s^{-2}). However, when the flow rate was increased to 0.22 m s^{-1} using the same meadow density, net sediment deposition decreased and near-bed turbulence increased within the meadow compared to the bare soil ($[7.4\pm1.4]\times10^{-4}$ vs. $[5.1\pm1.0]\times10^{-4}$ m^2 s^{-2} for meadow and bare soil, respectively).

2.8.2 Riparian Floodplains

One of the early written descriptions of the impact of floodplain vegetation on stream flow dates back to 1892. Shaler (1892) observed that: "No sooner do the waters recede than certain plants of swift growth, which find their appropriate conditions on the verge of the river, extend their roots through it and cover it with their thick-set stems, and thus bind the new-made land firmly together" (pp. 290-291). With the newly grown vegetation, Shaler (1892) described a slackening of water discharge as the water flowed over the streambanks. This slackening, Shaler explains, led to an increase in the rate of vertical sediment accretion on floodplains.

Since Shaler's observation, more in depth experiments have been conducted investigating near-bank velocity and turbulence under the presence of vegetated floodplains. Using a Froude-scaled hydraulic model of a northeastern Vermont stream, McBride et al. (2007) conducted a flume experiment to compare the near-bank turbulence between forested and non-forested floodplain vegetation. Synthetic grass and wooden dowels were used to represent non-forested and forested floodplains, respectively. An acoustic doppler velocimeter (ADV) measured three-dimensional velocities to characterize velocity distribution and turbulence within the floodplain vegetation, near the streambank, and within the main channel. The mean near-bank streamwise velocity for the non-forested floodplain (39.8 cm s^{-1}) was significantly higher ($p < 0.0001$) than the near-bank velocity of the forested floodplain (36.9 cm s^{-1}). However, near-bank turbulent kinetic energy for the forested floodplain was roughly double the non-forested condition, indicating that forested floodplains have a potential for higher streambank erosion.

Hopkinson & Wynn (2009) explored the influence of unvegetated and vegetated (grass, shrub, and tree) sloping streambanks on near-bank and main channel velocity and turbulence. A second order prototype stream, simulating Tom's Creek in Blacksburg, VA, USA, was created in a flume channel. Trees and shrubs were simulated using 1.5 to 6.4 cm and 0.3 cm wooden dowels, respectively. Woven grass mats with widths of 0.6 cm and lengths of 20.5 cm were used to represent grass banks; shrub and grass stem densities were 1296 stems m^{-2} and 4150 stems m^{-2}, respectively. Hopkinson & Wynn found near-bank streamwise velocities to decrease for all vegetation types when compared to the unvegetated condition. TKE increased near the streambank, particularly at the streambank toe, for the shrub treatment compared to all other bank conditions. On the other hand, turbulence was lower near the bank for the grass treatment, potentially due to the folding of the vegetation during flume testing.

Similar to Hopkinson & Wynn's study, Liu et al. (2017) and Valyrakis et al. (2021) conducted a series of flow and turbulence flume experiments using a simulated sloping streambank. Vegetation elements, represented by 0.6 cm diameter acrylic dowels, were placed at varying densities along the sloping bank during each flume run. The total number of streambank rods for each flume run and the vegetation density ranged from 30 stems m^{-1} to 540 stems m^{-1} and 0.06 stems m^{-1} to 1.88 stems m^{-1}, respectively. Using an ADV to measure velocity and turbulence distributions, Liu et al. (2017) found turbulence intensities to initially increase at the streambank toe for sparsely spaced vegetation densities (0.06 stems m^{-1} to 0.23 stems m^{-1}) compared to the unvegetated streambank model. However, as vegetation density increased (0.47 stems m^{-1} to 1.88 stems m^{-1}), turbulence intensities were lowered by a maximum of ~20% compared to the unvegetated streambank. On the other hand, for the same flume configurations, Valyrakis et al. (2021) showed that boundary shear stress (i.e., erosion potential) nearly doubled in the main channel for dense vegetation configurations (0.94 stems m^{-1} to 1.88 stems m^{-1}) compared to unvegetated configurations.

2.9 Summary

Broadly, climate change and land use changes may impact streambank erosion and channel migration in part due to changes in water and soil temperature (Hoomehr et al., 2018; Nelson & Palmer, 2007) storm frequency/intensity (Ross et al., 2019), and invasive species encroachment like Japanese knotweed. Bank erodibility can have significant impacts on channel morphology, including meander morphology (Bogoni et al., 2017) and channel form (Fernandez et al., 2021). Therefore, effectively mitigating and adapting to changing environmental conditions and the consequential impacts on channel migration is not possible without first understanding the components (e.g., organic matter and vegetation) and/or processes (e.g., exudate production) that are important to soil stability.

Prior experiments have shown that erosion rates and sediment transport are influenced by soil microorganisms and the production of extracellular substances (Gerbersdorf & Wieprecht, 2015; Parsons et al., 2016), labile organic matter inputs (Li et al., 2021), plant roots and root length density (Burylo et al., 2012; De Baets et al., 2007; De Baets et al., 2020), and vegetation impacts on stream hydrodynamics (Lawson et al., 2012; van Katwijk et al., 2010; J. Zhang et al., 2020). However, these mechanisms have typically been considered individually in streambed or upland

soil environments. As a result, many questions remain regarding the relative influence of these mechanisms on the soil erosion rates of a vertical streambank, where the forces of gravity are working against soil resistance. For example, while (Wang et al., 2014, 2015) found results to suggest that root biological effects on soil erosion increased over time as vegetation matured, evidence illuminating microbial vs. root effects on streambank soil erosion is not currently available. Additionally, vegetation in sparsely spaced meadows within fully submerged channels have also been shown to increase sediment erosion when compared to bare soil counterparts (Zhang et al., 2020). Given that roots input organic matter into the soil environment and will extend out of a streambank face as erosion occurs, more research is needed to clarify the relationship between roots along a streambank, stream hydrodynamics, soil microorganisms, and soil erosion rates. Therefore, this research sought to answer the following questions:

1. How does soil microbial production of EPS, stimulated through labile organic matter inputs, impact soil properties such as aggregate stability and soil resistance to fluvial erosion?
2. How do fibers that extend out of a vertical streambank face impact near-bank velocities, turbulence, and soil erosion rates within the fully develop region?
3. Does the density and type (flexible vs. rigid) of synthetic fibers, representing root binding effects, influence soil resistance to fluvial erosion?
4. How does the combination of synthetic fibers, microbial production of EPS, and changes in the boundary layer influence overall soil erodibility?

Chapter 3. Do Roots Bind Soil? A Mini-JET Study

Plant roots are known to affect streambank fluvial entrainment through 1) physically binding soil aggregates, 2) biochemically bonding soil aggregates to root surfaces, 3) cementing soil aggregates together through the release of organic root/microbial exudates, and 4) altering near-bank flow and turbulence. Limited work had been done to access the relative impact of each of these root mechanisms on soil resistance to streambank erosion. Therefore, the first study described here sought to study root and soil microbial impacts on streambank soil erosion using a mini-Jet Erosion Testing (JET) device. The following hypotheses were addressed: (1) the fiber matrix created by artificial roots increases soil resistance to fluvial erosion; (2) the soil microbial community enhances streambank erosion resistance through the production of extracellular polymeric substances (EPS); and (3) the fiber matrix of live roots provides the most resistance to fluvial erosion.

3.1 Methods

To compare the physical and biological effects of plant roots on five treatments (12 replicates per treatment) were created (Table 3-1): (1) no roots, sterile soil (NR-S); (2) synthetic roots, sterile soil (SR-S); (3) no roots, inoculated soil (NR-I); (4) synthetic roots, inoculated soil (SR-I); and (5) live roots, inoculated soil (LR). Following mini-JET testing, soil erosion was quantified by measuring the final volume of soil loss and calculating critical shear stress (τ_c) and soil erodibility (k_d). Potential explanatory soil and root properties, including percent water stable aggregates (%WSA), root length density (RLD), and extracellular polymeric substances (EPS), were also measured.

Table 3-1: Experimental treatments and the hypotheses addressed

	No Roots (NR)	**Synthetic Roots (SR)**	**Live Roots (LR)**
Sterile Soil (S)	Control	Fibers important?	-
Inoculated Soil (I)	Soil microbes important?	Fibers + soil microbes important?	Living roots + soil microbes important?

3.1.1 Vegetation, Soil, and Container Preparation

Herbaceous (switchgrass, *Panicum virgatum*, 'Alamo') plants were harvested from the Virginia Tech Price's Fork Research Center in Blacksburg, VA and stored at 4°C in moist soil until planting. For synthetic roots, four different sizes of 100% polyester sewing thread and filler cords were selected in three different diameter classes: (1) 0.2 mm and 0.3 mm very fine thread (Coats and Clark Dual Duty XP®, Charlotte, NC); (2) 1.0 mm fine cords (PandaHall, ShenZhen, China); and (3) 2.0 mm small cords (Bohemian Findings, Prince Edward Island, Canada). The root length density used for the very fine (0.78 cm cm^{-3}), fine (0.10 cm cm^{-3}), and small diameter (0.012 cm cm^{-3}) classes were determined in a preliminary study where switchgrass plants were grown and RLD was measured after growth.

Silt loam (16% clay, 4% sand, and 80% silt) soil was collected from the New River floodplain near Whitethorne, VA (37.192616°, -80.573133°). After passing the soil through a 1 mm sieve, ~500 kg of soil was placed in multiple 19-L buckets and steam sterilized for two hours at 100°C. After cooling for two hours, the sterilized soil was stored in three 210-L covered bins until use.

Plastic containers (20 x 20 x 20 cm, U.S. Plastic Corp., Lima, OH) with lids were modified to allow air interaction with one side of each container to simulate a streambank. Prior to any soil placement, each container was prepared by removing one side and replacing it with nursery fabric to provide stability once the soil was placed in the container. In addition, it enabled any root systems to grow in a semi natural state simulating a streambank, as the mesh allowed both air and water to pass through. Four drainage holes were drilled in the bottom of each container. Before planting and/or soil placement, the inside of each container was sprayed with SpinOut® (SePRO Corp., Carmel, IN), a root-growth regulator that prevented roots from growing along and pushing on the bucket sides. SpinOut® was not sprayed on the container bottom or over the nursery fabric, allowing the roots to grow down and out through the mesh. Finally, for the NR-S and NR-I treatments, soil was placed in each container and compacted to achieve a dry bulk density of 1.0 g cm^{-3} in a 4900 cm^3 volume.

Figure 3-1: "Planting" of synthetic roots in soil container. Roots were randomly distributed in container before soil was compacted inside. The dimensions of the container were 20 x 20 x 20 cm.

Synthetic roots used in SR-S and SR-I treatments were created by tying the desired amount of polyester thread at each diameter using tape. To arrange the synthetic roots, four cable ties were place over the soil containers, creating nine different rectangular sections (Figure 3-1). For SR-S, the tied synthetic roots were rinsed with bleach for two minutes to clean the surfaces, then rinsed thoroughly for 10 min with tap water. After drying, the synthetic roots were separated and placed randomly into each rectangle. Lastly, soil was placed inside and compacted around the roots to the desired bulk density of 1.0 g cm^{-3}. Excluding the bleach and rinsing step, the same method was utilized to "plant" synthetic roots for SR-I. Before planting, switchgrass plants were removed from the cooler and rinsed thoroughly with water to remove excess field soil. Sterile soil was compacted into containers and the rhizomes were planted by removing the topsoil layer, placing the plug, and then replacing the soil. All brown shoots were removed, and each sample was left with one green shoot (any extra green shoots were removed as well). For all inoculated treatments, a broth was created by mixing 1 kg of dry nonsterile soil, collected from the New River floodplain at Kentland

Farm (Blacksburg, VA), with 19 L of dechlorinated water. After settling, 1 L of the supernatant was used to inoculate the non-sterile treatments (NR-I, SR-I, LR). Sterile treatments (NR-S, SR-S) were watered with 1 L of dechlorinated water.

After all treatments were set up, the soil containers were placed in 8.5-cm deep aluminum trays and allowed to mature in a greenhouse. The containers were arranged in blocks, with one container for each treatment randomly placed within each block. Watering by capillary action was done to reduce the effect of soil wetting/drying cycles on measured soil erosion, particularly in the live rooted samples. Therefore, sample trays were filled frequently, about every 1-2 d, to keep the soil consistently moist. Although some sample trays did dry out during the first- and second weeks following sample placement, when both the soil and vegetation were taking large amounts of water overnight, sample trays were rarely empty of water for the remainder of the experiment.

3.1.2 Erosion Resistance Measurements

A commonly used fluvial erosion model is the excess shear stress equation:

$$\varepsilon_r = k_d(\tau - \tau_c)^a \quad (3\text{-}1)$$

In this equation, ε_r = the erosion rate in a volume of soil per unit time and unit area ($cm^3\ h^{-1}\ cm^{-2}$), k_d = the erodibility coefficient ($cm\ h^{-1}\ Pa^{-1}$), τ = the applied shear stress (Pa), τ_c = the critical shear stress (Pa), and a = an exponent typically assumed to equal one. Based on the excess shear stress equation, soil erosion rates depend on τ_c, the shear stress at which the soil will start eroding, and k_d, the volume of soil eroded per unit time and per unit of applied force (Hanson et al., 2002; Hanson and Simon, 2001).

Hanson (1990) designed the submerged, vertical jet device to measure the soil erodibility coefficient and critical shear stress in situ. Hanson and Cook (1999; 2004) modified the initial JET apparatus for increased flexibility in field testing and provided a detailed description of the "multi-angle" jet along with the data analysis methods. In 2008, a miniature version of the JET device was developed for easier lab and field use (Simon et al., 2010). A version of the mini-JET device was used for this study. JET calibration was done following the instructions provided in the JET Spreadsheet Tool version 2.1 (Daly et al., 2013).

Erosion testing was conducted for an entire block when the roots of the vegetated sample within that block were visible through the drainage holes or nursery fabric at the bottom of the container. This happened within 5 – 8 weeks of planting for all blocks. The day before jet testing,

samples were allowed to wet via capillary rise; the volumetric moisture content (VWC) of each sample was measured immediately prior to testing using a HydroSense^{TM} Soil Water Measurement System (Campbell Scientific, Australia). However, VWC of the first eight samples tested with the mini-JET was not measured. Aboveground biomass was cut at the soil surface for vegetated samples and the container was placed in a horizontal position prior to removing the nursery fabric. Care was taken not to disturb roots growing at the "bank" face.

JET testing was conducted similarly to the methods described in Khanal et al. (2016). First, the mini-JET metal foundation ring was inserted into the exposed soil face until flush with the soil surface. Next, the mini-JET tank was attached and filled with water until the nozzle was completely submerged; a constant water head was maintained using a head tank. After the JET nozzle was submerged for two minutes, a jet of water was applied perpendicularly to the soil surface. Each run was conducted at the same head setting of 43 cm. Scour depth measurements were taken every 15 s until the depth reading remained constant for three consecutive point gage readings. The time between scour depth readings was increased to 30, 45, 60, and 300 s sequentially following three constant depth readings at each setting. Using this testing procedure, the erosion testing run time (RT) varied for each sample. To account for this variation, RT was considered a dependent variable in all regression analyses.

Mini-JET erosion test data can be analyzed using three possible solution techniques: (1) Blaisdell's solution, (2) the Scour Depth solution, and (3) the Iterative solution (Daly et al., 2013). Although Blaisdell's solution (Blaisdell et al., 1981) has been commonly used for calculating τ_c and k_d, recent work has shown that the scour depth method provided more stable solutions to the excess shear stress equation compared to Blaisdell's solution (Daly et al., 2013). Thus, the scour depth solution method was used in this study along with the excel spreadsheet analysis tool developed by Daly et al. (2013) to calculate τ_c and k_d. Plots of observed and predicted scour depth vs time provided were inspected to determine model fit. For all samples, the scour depth solution method fit the observed scour data better than both the Blaisdell and Iterative solution methods.

Preliminary erosion testing using the mini-JET on rooted and bare soil samples revealed that the scour holes formed by the jet were not always uniform between treatments (Figure 3-2). Wider and shallower scour holes generally formed in no rooted (Figure 3-2a-b) and synthetic rooted (Figure 3-2c-d) samples compared to live rooted samples (Figure 3-2e). This variation in scour hole shape can influence jet diffusion and impact the resulting τ_c and k_d. Additionally, τ_c and

k_d are sensitive to the solution method used for data analysis (Khanal et al., 2016). Because no standard solution method exists and different values are obtained depending on the solution technique, data interpretation is difficult. As a result, immediately following mini-JET testing, the volume of the developed scour hole was also measured to determine the actual volume of soil loss. Any roots that withstood the jet of water were removed from the scour hole before measurement and preserved in a small mason jar filled with 50% ethanol. The scour hole volume (SHV) was measured by placing a thin sheet of plastic over the scour hole and measuring the volume of water required to fill the hole.

Figure 3-2: Typical scour hole shapes for (a) no roots, sterilized; (b) no roots, inoculated; (c) synthetic roots, sterilized; (d) synthetic roots, inoculated; and (e) live roots, inoculated treatments in this experiment. Note narrower scour hole in live rooted sample compared to the other treatments. The inner diameter of the black ring surrounding each soil sample was 10 cm.

3.1.3 Plant, Soil, and Microbial Parameters

Following mini-JET testing, two 12-g samples of soil were collected from each soil box (2 g of soil from six locations inside the scour hole) and stored in Nalgene® bottles. These soil samples were frozen at -18°C for later use in EPS analysis. Next, loose soil particles caused by running the mini-JET were removed and then 200-g of soil was collected from around the scour hole. Following air drying, the 200-g samples were transferred to brown paper bags and stored at room temperature for later percent water stable aggregate (%WSA) analysis. %WSA was initially measured following the wet sieve procedure outlined in Kemper and Rosenau (1986). Air dry soil samples were rapidly wet for one minute prior to stability testing. Follow-up testing was done using the same Kemper and Rosenau (1986) procedure, but the samples were prewet slowly through capillary rise for 10 min prior to stability testing. Samples that were rapidly prewet were not significantly correlated with any regression result, so only slow prewet data (herein referred to as %WSA) were considered.

To quantify the amount of vegetation in each container, both aboveground and belowground biomass was measured. Aboveground biomass trimmed from soil containers before JET testing was stored at 4°C and dried at 60°C until constant weight. Plant roots were washed from the remaining soil and then placed in 1000-ml glass jars filled with 50% ethanol. Root diameter and RLD were measured using the 2015 WinRhizo™ Tron and 2003 WinRhizo™ Pro systems (Regent Instruments Inc., Québec, Canada). Root diameter classes included: very fine (< 0.5 mm), fine (0.5-2.0 mm), small (2-5 mm), and medium (5-10 mm).

EPS, composed mainly of polysaccharides and proteins, have been measured to quantify the impacts of soil microorganisms on soil stability (Gerbersdorf and Wieprecht, 2015). Frozen soil samples were thawed overnight at 4°C and bottle contents were mixed thoroughly before extraction. For this study, potassium sulfate (K_2SO_4) was used as the extractant (modified from Chang et al., 2007). Seven grams (wet weight) of composite soil were weighed and placed into 50-mL tubes. An additional 7 g of soil was weighed into a metal pan for dry weight analysis. A total of 7 mL of 0.05 M K_2SO_4 was added to each tube. The mixture was vortexed at 300 rpm for 10 min and then centrifuged at 5000 rpm at 4°C with the supernatant saved. Another 7 ml of 0.05 M potassium sulfate solution was added to the soil sample, mixed and vortexed vigorously for 1 min, and incubated at 100°C for 20 min. During incubation, samples were vortexed once every five minutes. Samples were then centrifuged as above, and the pooled supernatant was filtered through

a 0.45-µm syringe filter. To the collected supernatant, 30 ml of ethanol was added, and the sample was precipitated overnight at 4°C before centrifuging the following day. Lastly, the precipitate was dissolved in 6 mL of Milli-Q water. This extraction produced clear to slightly yellow supernatants, with yellow colors corresponding to higher polysaccharide content. Following EPS extraction, EPS was measured as polysaccharides using the phenol–sulfuric acid method (Dubois et al., 1956). The polysaccharide concentration measured (µg) was normalized by the soil dry weight (g).

3.1.4 Data Analysis

EPS results suggested that sterile conditions were not fully achieved as no significant difference in EPS was observed between sterilized and inoculated treatments. Therefore, inoculated and sterilized results were combined for no root (NR, n = 24) and synthetic root (SR, n = 24) treatments.

Following the procedure outlined in Wynn (2004), histograms were developed for each parameter to determine distribution symmetry. Next, the data were tested visually and statistically for normality and equal variance. All variables met the assumption of homoscedasticity; however, %WSA, SHV, and τ_c, did not follow a normal distribution. As a result, the nonparametric pairwise Wilcoxon rank-sum test was used to identify significant differences between treatments.

Because multiple erosion response variables (τ_c, k_d, and SHV) were measured/calculated, Kendall's correlation coefficient was calculated for each pairwise combination to determine if the erosion parameters were correlated. Next, the data were separated into two groups: all data and live root data. Theil-Sen nonparametric linear regression (Sen, 1968; Siegel, 1982; Theil, 1992) was then performed for all erosion response variables to evaluate the individual relationship between each independent variable and the dependent variables within the live root data group. Independent variables included %WSA, EPS, RLD, VWC, and RT. Theil-Sen regression is not as sensitive to outliers as standard least squares regression and can be a more robust procedure for environmental data.

Multiple linear regression was conducted to evaluate which soil, microbial, and vegetation parameters had the greatest influence on the erosion response variables across all treatments. To do this, the parameters were first standardized to the control (NR) so the magnitudes of the regression coefficients could be compared directly to determine the relative influence of each

explanatory variable. With NR acting as the baseline, the presence of live (LR) and synthetic (SR) fibers were treated as categorial variables. Categorical variables allow the regression mean (the intercept) to shift by taking on a value of zero or one. An alpha of 0.05 was used for statistical significance. For multiple linear regression, the residuals of each significant regression relationship were visually assessed for independence, normality, and constant variance. To improve all data regression diagnostics, τ_c/k_d and SHV were transformed using natural-log and squared transformations, respectively.

3.2 Results

3.2.1 JET Run Time and Soil Water Content

Erosion testing run times and soil volumetric water contents varied between treatments depending on root type (Table 3-2); however, the mean values of RT and VWC were not significantly different between treatments. RT and VWC were not significant predictors of any erosion parameter for the live root treatment, as determined using the Theil-Sen regression method. Additionally, VWC was not significantly correlated with any erosion parameters, as determined using multiple linear regression. Because VWC was statistically equal for all samples, and VWC was not correlated with any of the erosion parameters, VWC was not included in further analyses.

Table 3-2: Mini-JET average erosion testing run times (RT) and average soil volumetric water content (VWC) for experimental treatment groupings. Median values are shown in prentices.

	No Roots (n = 24)	**Synthetic Roots (n = 24)**	**Live Roots (n = 12)**
RT (minutes)	54 ± 9.4 (51)	51 ± 5.8 (49)	50 ± 5.1 (48)
VWC (%)	69 ± 6.6 (68)	73 ± 12 (72)	68 ± 6.1 (67)

3.2.2 Root Length Density and Aboveground Biomass

Panicum virgatum aboveground biomass dry weight and total RLD ranges were 635 – 4960 kg ha^{-1} and 0.67 – 4.11 cm cm^{-3} in this study, respectively (Table 3-3). Except for the fine root diameter class, all synthetic rooted RLDs (very fine and small) fell within the range of the live rooted samples.

Table 3-3: Root length density quantities for *Panicum virgatum* (live root) and synthetic root treatments in each diameter class.

Vegetation Type and Measurement		Diameter Class (mm)			Total
		Very Fine (0-0.5)	Fine (0.5-2.0)	Small (2.0-5.0)	
Live Roots (cm cm^{-3})	**Average**	1.62	0.24	0.06	1.92
	Median	1.28	0.23	0.065	1.57
	Range	0.51 – 3.67	0.13 – 0.40	0.0021 – 0.11	0.67 – 4.11
Synthetic Roots (cm cm^{-3})	**Total**	0.78	0.1	0.012	0.89

3.2.3 Extracellular Polymeric Substances and Aggregate Stability

As defined by Flemming and Wingender (2010), EPS are hydrated biopolymers secreted by biofilm cells to encase and immobilize microbial aggregates; they are commonly composed of water, polysaccharides, proteins, nucleic acids, (phosphor)lipids, DNA, and other polymeric compounds. This study measured EPS as polysaccharides and found median EPS values of 31.5 µg g^{-1}, 32.6 µg g^{-1}, and 38.3 µg g^{-1} for NR, SR, and LR treatments, respectively. LR had significantly higher EPS compared to all other treatments (Figure 3-3a). Median %WSA measured were 91%, 90%, and 83% for NR, SR, and LR treatments, respectively. %WSA was significantly lower in LR compared to NR and SR (Figure 3-3b). Neither EPS or %WSA were correlated with RLD, aboveground biomass, or with each other.

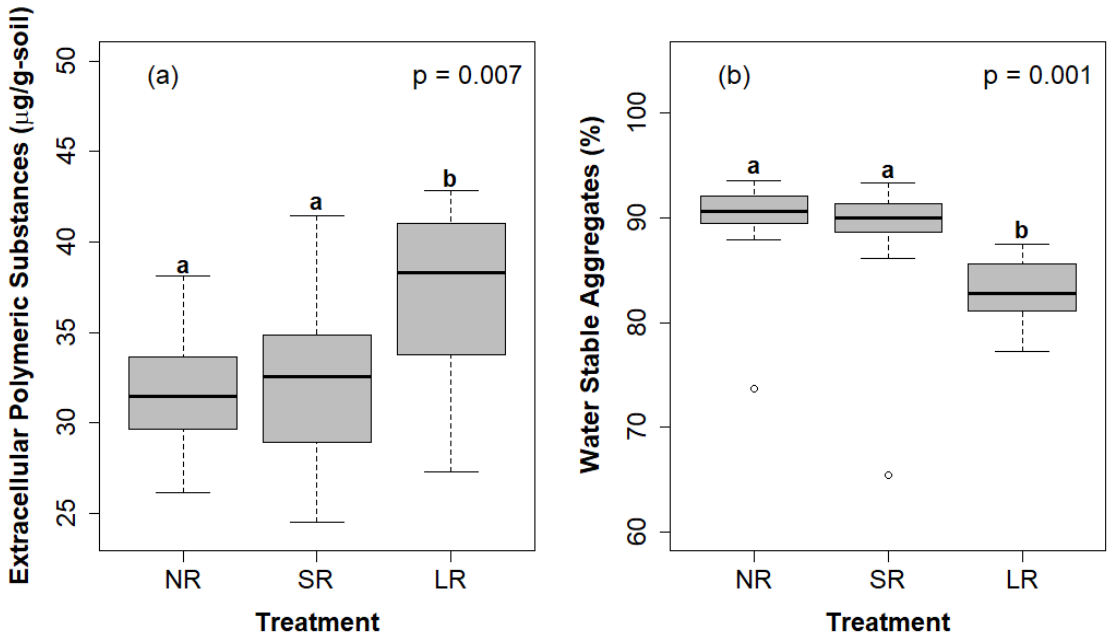

Figure 3-3: a) Extracellular polymeric substances and b) percent water stable aggregates measured following mini-JET testing for each treatment. Letters denote statistically significant differences between each treatment pair, and the p-value on the top right denotes the Kruskal-Wallis p-value. NR = No Roots; SR = Synthetic Roots; and LR = Live Roots (*Panicum virgatum*).

3.2.4 Critical Shear Stress, Soil Erodibility, and Scour Hole Volume

Critical shear stress ranges were 0.90 – 2.91 Pa, 1.24 – 3.02 Pa, and 1.32 – 4.41 Pa for NR, SR, and LR treatments, respectively. The median τ_c and k_d of LR were 1.94 Pa and 69.3 $cm^3\ N^{-1}\ s^{-1}$, respectively. For NR and SR, the median τ_c were 1.62 Pa and 1.60 Pa, while the median k_d were 48.0 $cm^3\ N^{-1}\ s^{-1}$ and 100.3 $cm^3\ N^{-1}\ s^{-1}$, respectively. The τ_c of LR was significantly higher compared to both the NR and SR treatments (Figure 3-4a). Additionally, in this study, there was no observed relationship between RLD and τ_c. On the other hand, %WSA was positively correlated with τ_c within the LR treatment (Figure 3-4b: $p = 0.007$, $n = 11$). This general relationship between τ_c and %WSA was not present for NR or SR in this study. In fact, Figure 3-4b shows that even though the median %WSA in NR and SR were 3 – 15% higher compared to each LR sample, the median τ_c of these two treatments was generally lower.

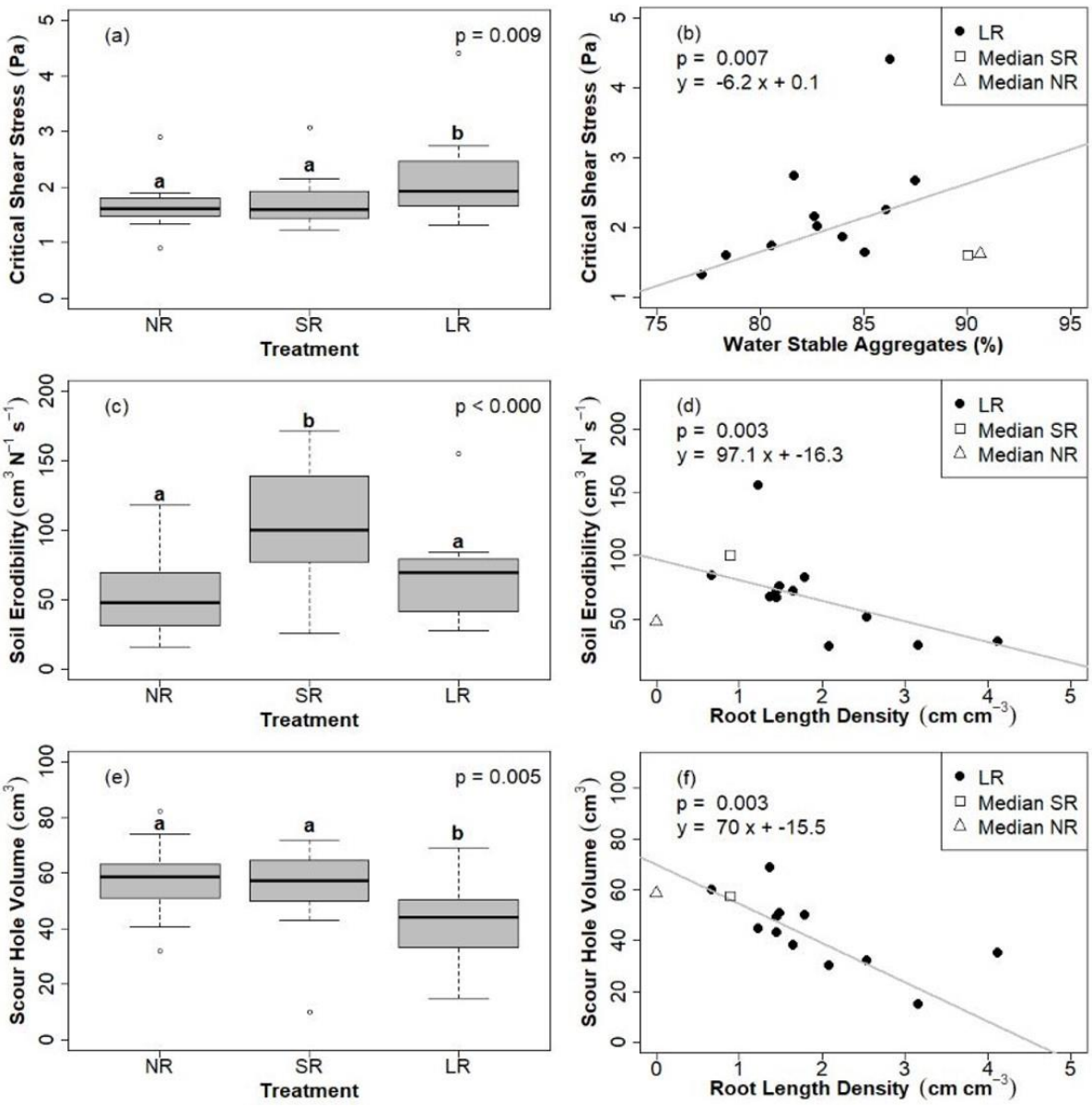

Figure 3-4: (a, c, e) Critical shear stress, soil erodibility, and scour hole volume boxplots and (b, d, f) significant Kendall Theil-Sen nonparametric linear regressions between erosion and predictor variables for live root data group. Bold letters above boxplots denote statistically significant differences between each treatment pair, and the p-value in all plots denote the Kruskal-Wallis p-value. The median no root and synthetic root values are plotted on scatter plots for comparison. NR = No Roots; SR = Synthetic Roots; and LR = Live Roots (*Panicum virgatum*).

Soil erodibility ranged from 16.2 to 118.1 $cm^3\ N^{-1}\ s^{-1}$, 25.4 to 171.8 $cm^3\ N^{-1}\ s^{-1}$, and 28.0 to 155.4 $cm^3\ N^{-1}\ s^{-1}$ for NR, SR, and LR treatments, respectively. Soils with synthetic fibers had significantly higher k_d compared to NR treatments (Figure 3-4c). Soil erodibility was also slightly higher in LR compared to NR, but this was not statistically significant. Another interesting note is that SR had the largest range of k_d values, initially suggesting that the presence of fibers produces more variation in results. However, excluding the outlier, LR had the lowest variation in k_d compared to both SR and NR.

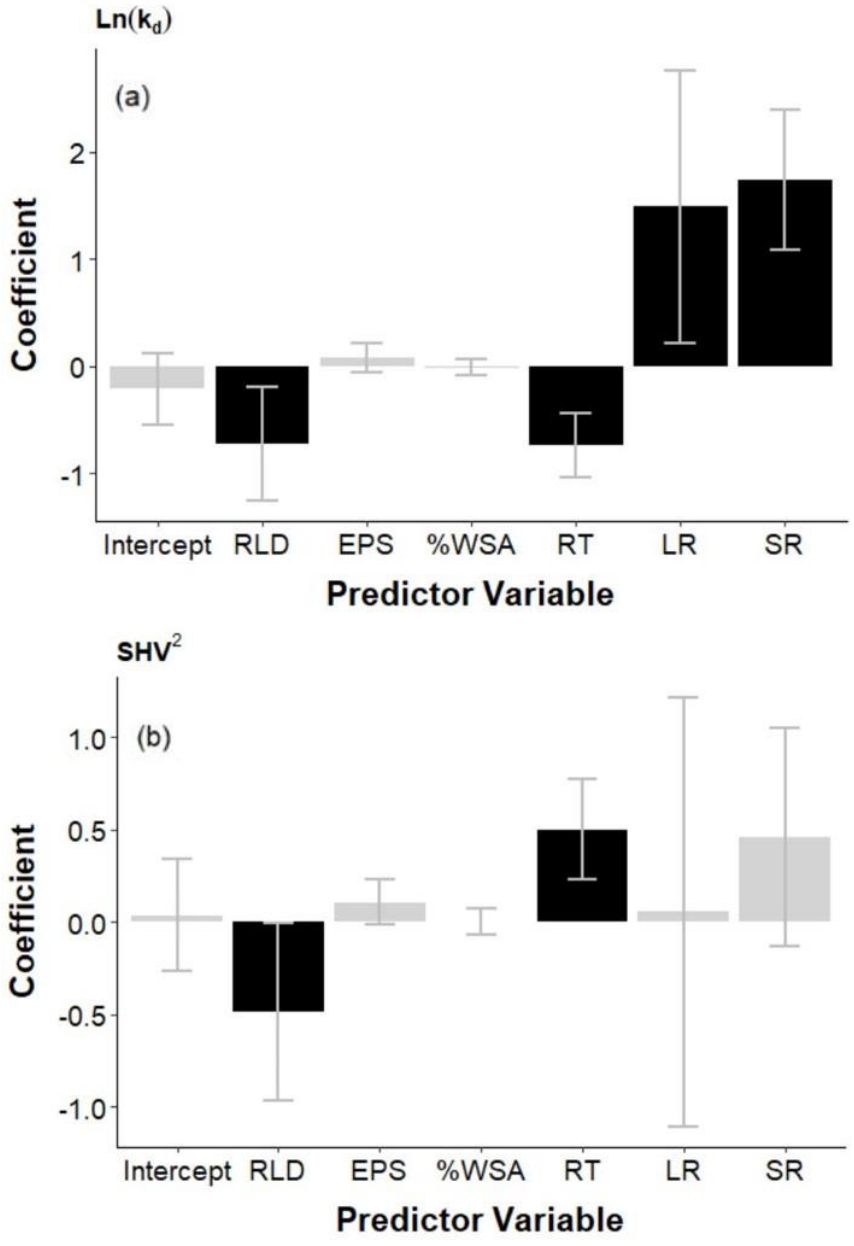

Figure 3-5: (a) Ln(k_d) and (b) SHV^2 multiple linear regressions. Significant correlations ($p < 0.05$) are highlighted in black. Error bars represent the sample confidence interval. SHV = scour hole volume, k_d = soil erodibility, RLD = root length density, % WSA = percent water stable aggregates, EPS = extracellular polymeric substances, RT = jet runtime, LR = live roots, and SR = synthetic roots. LR and SR represent categorical variables within the multiple linear regression.

Although increasing RLD was associated with lower k_d in this study, the presence of root fibers (both alive and synthetic) at a low RLD were correlated with a higher initial k_d (Figure 3-4d: $p = 0.003$, $n = 12$). This finding was further supported by the multiple linear regression conducted on k_d, which revealed that RLD and RT were negatively correlated with $\ln(k_d)$ whereas the categorical variables, LR and SR, were positively correlated (Figure 3-5a: $R^2 = 0.525$, $p < 0.001$). At "planted" RLDs of 0.89 cm cm^{-3}, the median k_d measured in SR was significantly higher compared to NR (Figure 3-4c). At RLDs < 2 cm cm^{-3}, the soil erodibility measured in LR samples was higher than the median NR k_d as well. However, visual inspection of Figure 3-4d shows the k_d of LR samples with RLDs > 2 cm cm^{-3} were lower than the median NR k_d. Consequently, the higher k_d measured in SR treatments appears to be a result of the low RLD used.

Following mini-JET testing, the total volume of soil loss was 32 – 82 cm^3, 10 – 72 cm^3, and 15 – 69 cm^3 for NR, SR, and LR, respectively. The median scour hole volume for LR was 44 cm^3, which was significantly lower when compared to NR (59 cm^3), and SR (58 cm^3) (Figure 3-4e). SHV was not significantly correlated with τ_c or k_d in this study, indicating it is an independent measure of soil erosion resistance. Theil-Sen linear regression revealed RLD (Figure 3-4f: $p = 0.003$) to be negatively correlated with SHV for live root data. Multiple linear regression showed a similar result; RLD was negatively correlated with SHV^2 (Figure 3-5b: $R^2 = 0.367$, $p < 0.001$).

3.3 Discussion

As stated in Section 2.4, no significant difference in EPS was observed between sterilized and inoculated treatments, despite soil steam sterilization. Multiple explanations exist for this finding, including: (1) rapid recolonization of sterilized soils by microbes, which has been documented previously (Marschner and Rumberger, 2004; Wertz et al., 2007); and (2) this study did not account for the unknown amount of EPS that was likely already present in the soil prior to greenhouse growth. Thus, no conclusions can be drawn regarding the impact of microbially derived EPS on soil resistance to fluvial erosion. In other words, the influence of microbes alone (NR-S vs NR-I) or with fibers (SR-S vs SR-I) cannot be determined. The presence of synthetic fibers had little impact on EPS production as well (NR vs SR), which is unsurprising considering the fiber material was inert and provided relatively little additional surface area, as compared to the NR treatment. Study results showed that EPS was significantly higher in the LR treatments, as

compared to the NR and SR treatments. However, because plant roots can release 5% to 21% of their photosynthetically fixed carbon as soluble sugars, amino acids, or secondary metabolites (Badri and Vivanco, 2009; Badri et al., 2013; Chaparro et al., 2013) and because the EPS extraction method did not differentiate between microbial and plant-derived polysaccharides, the higher measured EPS in LR may not be exclusively from microbial components.

In addition, EPS was not correlated with %WSA, RLD, or any measure of soil erosion resistance. Prior research has shown EPS, macroaggregate formation, and microbial biomass increase in soil with plant residues (Tang et al., 2011). Thus, to assess the impact of EPS on fluvial erosion, future research could consider comparisons between a soil control and soil with increased organic matter content (e.g., plant residues) to encourage microbial growth.

This study also found no evidence that the presence of artificial fibers increased soil resistance to erosion, as the τ_c and SHV of SR and NR were equivalent, and both treatments had statistically lower τ_c compared to LR. Streambank field experiments have shown aggregate stability to be positively correlated with τ_c and negatively correlated with k_d (Wynn and Mostaghimi 2006). Additionally, under simulated rainfall experiments, Barthès and Roose (2002) found overall soil loss was negatively correlated with aggregate stability. Although there was a positive relationship between τ_c and %WSA for the live roots in this study (Figure 3-4b), a similar relationship was not determined for the NR and SR treatments, despite the statistically higher %WSA for both of these treatments.

However, the data suggests that synthetic roots affect the applied hydrodynamic forces. Although k_d was significantly higher in SR compared to both NR and LR (Figure 3-4c), this finding is likely attributable to the relatively low RLD of the synthetic roots. In fact, unless RLD was greater than 2 cm cm^{-3}, treatments with fibers (either live or synthetic) had higher k_d compared to NR (Figure 3-4d). Given that the SR and LR fibers/roots used in this study were relatively flexible, the fibers may have waved around in the jet, increasing turbulence, and disturbing the soil structure, leading to a greater volume of soil loss once erosion started. This process may have been exacerbated in samples with low RLDs. For submerged vegetation within open channels, Nepf (2012) describes increased near-bed turbulence in regions of small diameter or sparsely spaced vegetation, which causes increased erosion of fine bed particles. At higher densities, the spacing between vegetal elements and the velocity near the sediment bed/soil surface is reduced. At low RLDs, fibers are generally spaced farther apart compared to high RLD samples. As a result, low

RLDs may have initially caused greater soil loss, regardless of treatment type (i.e., SR vs. LR), as indicated by the inverse relationship between fiber density and SHV (Figure 3-4f) and fiber density and k_d (Figure 3-4d).

To further explore the role of fibers on the applied hydrodynamic force, future experiments should vary the RLD of planted synthetic roots to capture the full range of possible comparisons between live and synthetic roots. Additionally, the *Panicum virgatum* and corresponding synthetic roots used in this study had relatively small diameters (mostly very fine to fine) and were flexible. Thicker, more rigid roots may have greater effects on the applied hydraulic forces; Wynn and Mostaghimi (2006) found that roots with diameters of 2 to 20 mm were correlated with reduced k_d. Thus, future work should also consider herbaceous and woody (both live and synthetic) fibers to get a complete picture of how the physical and biological properties of roots impact fluvial streambank erosion processes.

This study did provide evidence to support the final hypothesis that live roots provide soil the most protection against fluvial erosion; however, the relative importance of the possible reinforcement mechanisms (e.g., soil binding by roots, increased EPS concentrations, bonding of soil aggregates to root surfaces, and/or hydrodynamic effects) is still unclear. Both k_d and SHV significantly decreased with increasing RLD and the SR data fit the inverse relationships between live RLD and both soil erodibility and scour hole volume well (Figure 3-4d and Figure 3-4f), suggesting roots affect the hydrodynamic boundary layer differently as root density increases.

For live rooted samples, %WSA was positively correlated with τ_c (Figure 3-4b), but no correlation was found between RLD and %WSA. In addition, %WSA was significantly lower in LR compared to NR and SR (Fig. 3b). Mamo and Bubenzer (2001a) had a similar result when comparing aggregate stability of ryegrass pot grown soil to that of bare soil treatments. The %WSA of the bare soil after 8, 12, and 16 weeks of growth was always 24%, whereas %WSA for the ryegrass planted soil was 19%, 23%, and 32%, respectively. As a result, although the significantly lower aggregate stability measured in LR compared to NR and SR was surprising, it may have been a product of the experiment conditions. Piotrowski et al. (2004) noted that test duration and high root biomass growth in confined spaces (e.g., pot studies) can have negative effects on %WSA formation. In this study, vegetation was grown in relatively small containers (20 x 20 x 20 cm). After only 5 – 8 weeks of growth, median RLDs were 1.57 cm cm^{-3}, indicating rapid plant growth over a short time. Given these results, one would expect the τ_c of NR and SR treatments to be

higher than LR because both treatment types had higher %WSA compared to LR. However, τ_c was significantly higher in LR and no relationship between τ_c and %WSA was found for NR or SR. Multiple interpretations exist for this result, including that τ_c is impacted by the bonding of soil aggregates to live root surfaces by plant exudates (Tengbeh, 1993), regardless of the overall soil aggregate stability. Alternatively, a parameter not measured in this study (e.g., soil organic matter content) could affect τ_c and be strongly correlated with %WSA. Through their experiment, Piotrowski et al. (2004) noted that mechanisms other than root biomass/density and hyphae length were potentially correlated with soil aggregate stabilization.

τ_c, k_d, and SHV results in this study were consistent with previous JET experiments. First, Khanal and Fox (2017) and McNichol et al. (2017) measured statistically higher τ_c values in root-permeated soils compared to bare soil samples while statistically equal k_d values were measured between the two treatment types. However, k_d tended to be lower in root-permeated treatments in those studies. For example, the median k_d of root-permeated and bare soil were 62.2 $cm^3\ N^{-1}\ s^{-1}$ and 70.4 $cm^3\ N^{-1}\ s^{-1}$, respectively ($p = 0.44$), in Khanal and Fox's 2017 study. Secondly, Khanal and Fox (2017), Wynn and Mostaghimi (2006), and Mamo and Bubenzer (2001) also found no significant correlation between root density characteristics and τ_c. On the other hand, when conducting submerged JET testing on vegetated streambanks, Wynn and Mostaghimi (2006) did find a positive correlation between %WSA in nonplastic soils and τ_c, similar to the results found in this study. Lastly, several field and greenhouse studies have shown inverse power relationships between soil erodibility and root length density (De Baets et al., 2006; De Baets et al., 2007; Mamo and Bubenzer, 2001a), the erodibility coefficient and root diameter (Khanal and Fox, 2017), and between scour hole volume and root length density (Pollen-Bankhead & Simon, 2010). Khanal and Fox's 2017 study is of particular interest. After plant maturity, the authors measured RLDs that ranged from 0.1 to 1.89 cm cm^{-3}. Although RLD was not correlated with k_d in Khanal and Fox's study, k_d was correlated with root diameter. At small root diameters (~ 0.4 to 0.8 mm), the measured k_d in root-permeated soil was generally higher compared to the median bare soil k_d value. This result is comparable to what is shown in Figure 3-4c and Figure 3-4d, where k_d was higher in rooted soil with RLDs less than 2 cm cm^{-3} when compared to the median k_d value for NR. As described above, the higher k_d in samples with low RLDs (widely spaced fibers) or relatively small root diameters may be attributed to increased stem-scale turbulence (Heidi M. Nepf, 2012a).

3.4 Conclusions

Since the mid-1900s, a large body of research has shown plant roots contribute significantly to reducing soil loss by fluvial processes. This relationship is particularly evident on a streambank, where plant roots are known to affect fluvial entrainment through multiple processes, including: (1) physically binding soil aggregates, (2) biochemically bonding soil aggregates to root surfaces, (3) cementing soil aggregates together through the release of organic exudates, and (4) altering the applied hydrodynamic forces. This research sought to determine the relative importance of these mechanisms by quantifying the effect of no rooted, synthetic rooted, and live rooted soil on streambank fluvial erosion. It was hypothesized that: (1) the fibers of artificial roots would increase soil resistance to fluvial erosion; (2) the soil microbial community would enhance streambank erosion resistance through the production of EPS; and (3) the fiber matrix of live roots and the associated microbial community would provide the most resistance to fluvial erosion.

Based on this study, two overall conclusions can be drawn. First, the impact of fibers (both live and synthetic) on k_d indicate that fibers affect the applied hydraulic forces. Samples with relatively low RLDs (below 2 cm cm^{-3}) had a higher k_d compared to the median k_d for no rooted samples, whereas live rooted samples with RLDs above 2 cm cm^{-3} had a lower k_d. This result is attributed to how densely packed the fibers are, with low RLD samples leading to increased stem-scale turbulence and greater soil loss. Second, the impact of live roots on the soil environment provided additional protection by increasing soil resistance to fluvial erosion (higher τ_c); this increased erosion resistance happens even though %WSA is significantly lower in live rooted treatments compared to synthetic and no rooted treatments. Additionally, the presence of roots at densities below 2 cm cm^{-3} did not adversely impact τ_c like they did k_d. These results indicate that root fibers reduce soil loss caused by fluvial erosion through a combined effect on soil aggregate stability and by holding (binding) the soil together through a dense fiber network.

Chapter 4. Impact of Artificial Roots on Near-Bank Flow and Turbulence

In Chapter 4, the experimental goal was to compare the effects of root type (simulated herbaceous roots vs. simulated woody roots) on near-bank velocity and near-bank turbulent stress. The impact of stream bed and floodplain vegetation on stream hydrodynamics is an important topic that has received considerable attention over the last three decades (Hopkinson & Wynn, 2009; Liu et al., 2017; McBride et al., 2007; Valyrakis et al., 2021; Yang et al., 2007). However, natural streambanks can be steep where roots extending out of the streambank face are the only vegetation elements that interact directly with flowing water. Therefore, studying how roots alter near-bank turbulent stress, which has not been explored before, is important to understanding how plant roots may impact geomorphologic processes like streambank erosion. To study this, the velocity and turbulence profiles developed over three distinct streambank boundary conditions [sand wall (SW), flexible rooted wall (FRW), and rigid rooted wall (RRW)] were examined. Based on prior research, it was hypothesized that: 1) lower streamwise velocities would be produced near the bank along the FRW and RRW compared to the SW and 2) turbulent stresses would initially increase more rapidly with distance from the bank surface along the RRW and FRW, compared to the SW.

4.1 Methods

4.1.1 Flume Description

All experiments were performed in an 8 m by 1 m by 1 m recirculating flume (Figure 4-1a; Engineering Laboratory Design Inc., Lake City, MN). A Vectrino II acoustic Doppler profiling velocimeter (ADP; Nortek AS, Vangkroken, Norway) was used to take streamwise, crosswise, and vertical velocity measurements. The flume has a maximum capacity of 5000 L and is equipped with a 2282 Mg m min^{-1} pump which can drive flows of up to 70 L s^{-1} in the flume channel. Because the goal of this experiment was to simulate unvegetated and vegetated streambanks, artificial walls were built in the flume representing a vertical streambank. A different artificial wall was constructed to create each of the three boundary conditions of this experiment (sand only, flexible roots, and rigid roots).

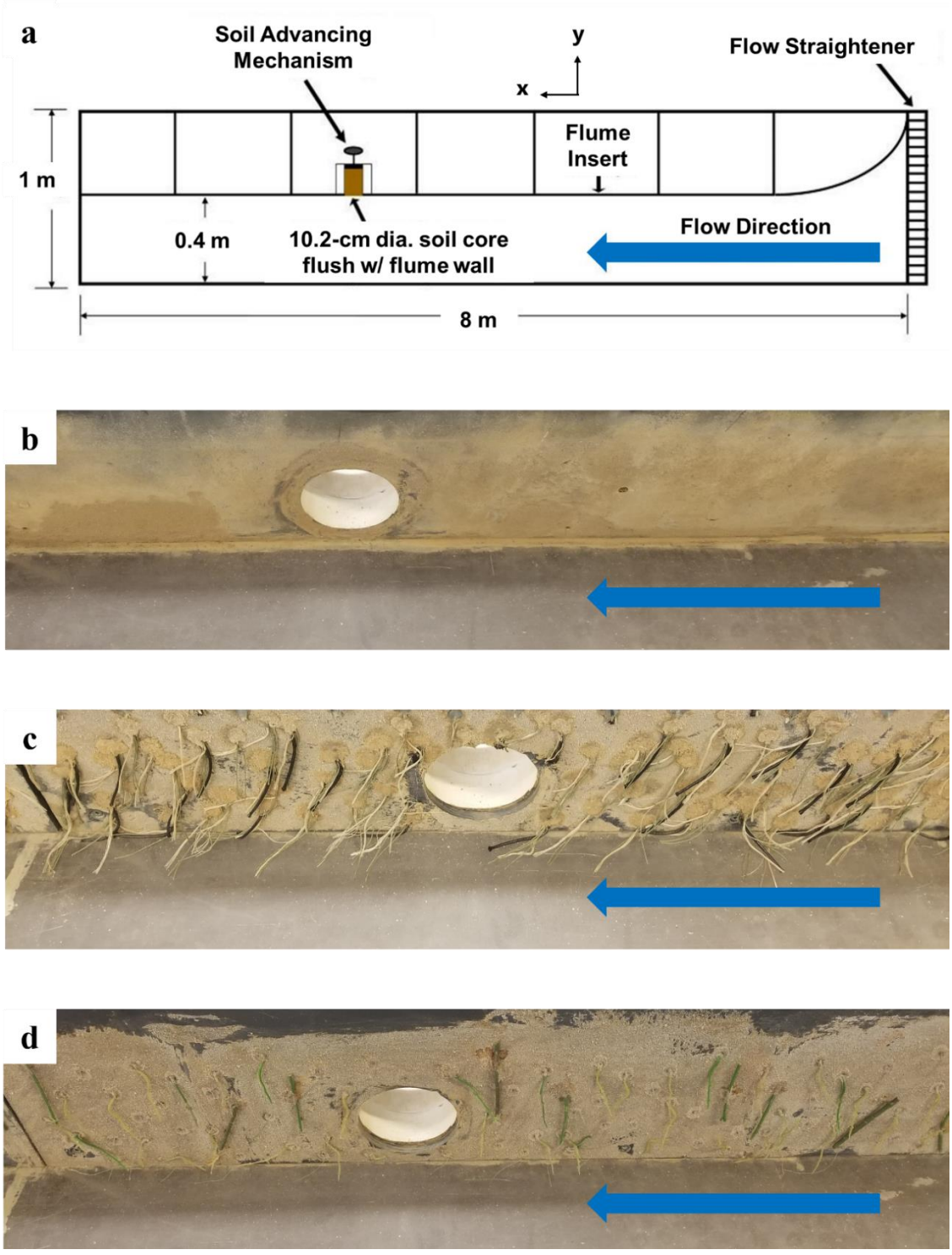

Figure 4-1: a) Plan view of flume setup with axis labels (the z-axis, not shown, represents the vertical direction); b) test section of the PVC insert for the sand wall; c) the test section of the PVC insert for the flexible rooted wall; and d) the test section of the PVC insert for the rigid rooted wall.

The initial sand wall (SW) was used by Parks (2012); a curved wall was created at the upstream end of the channel to gradually transition the width of the flume from 1.0 m to 0.4 m. The artificial wall was constructed of 1.25-cm thick PVC sheets supported with a wooden frame running the entire length of the flume channel (Figure 4-1b). The face of the wall was roughened over the entire length by coating the surface with sand (Premium Play Sand No. 1113, Quickrete, Atlanta, GA; D_{50} = 0.15 mm, D_{84} = 0.3 mm) and a thin film of glue. The upstream end of the channel was equipped with a flow straightener to dissipate turbulence and develop one dimensional flow.

Simon & Collison (2002) provide root area ratios (RARs) for a variety of herbaceous and woody vegetation, including switchgrass, at multiple depths and root diameter classes on selected streambanks in the Goodwin Creek Experimental Watershed (Mississippi, USA). The RARs provided in Simon and Collison's study were used as guides for constructing the two rooted boundary conditions and to highlight differences in root areas occupied by herbaceous and woody roots. Using the total area of the artificial wall sheets (7400 cm^2), the RARs provided by Simon and Collison were used to determine the total area of roots needed to cover the PVC sheet based on fiber diameters. Simon & Collison's switchgrass data were used for the flexible rooted wall (FRW), while an average of all woody plant RARs in their study (Black Willow, Sweetgum, River Birch, and Sycamore) were used for the rigid rooted wall (RRW) (Table 4-1).

Flexible fibers were selected to represent roots of herbaceous vegetation while more rigid fibers represent the roots of woody vegetation (Pallardy & Kozlowski, 2007). Constructing the flexible fiber and rigid fiber wall configurations required thin PVC sheets (0.625 cm thick) that spanned the entire length of the flume. For both the FRW and RRW, the face of the PVC sheet was roughened over the entire length by gluing sand, like the sand wall. Next, 1-cm diameter holes were drilled into the PVC sheeting at predetermined locations along the flume length. Polyester fibers with different diameters (0.3 mm, 1.0 mm, and 2.0 mm) were used to simulate flexible fibers. These fibers were cut into 8 cm lengths, allowing the tips of these fibers (1 cm) to be glued into each hole; the hole was covered with sand again to keep the wall surface consistent. The remaining 7 cm fiber length was allowed to hang below the glued tip to interact directly with the flowing water in the flume (Figure 4-1c). For the RRW, the synthetic fiber material changed. Rigid fibers were simulated by braided fishing line (0.38 mm, Prue Fishing, Inc., Spirit Lake, Iowa) and plastic plant stems with diameters of 1 mm, 2 mm, 3 mm, and 5 mm (Bloom Room, San Francisco, CA).

Like the FRW, 7 cm of fiber length was allowed to hang below the glued tip to interact directly with the flowing water in the flume (Figure 4-1d). Due to the different fiber diameters, the fiber density for the FRW was an order of magnitude greater than for the RRW, but the RAR of the FRW was only two times higher compared to the RAR of the RRW, reflecting typical differences between herbaceous and woody plant root characteristics (Simon & Collison, 2002).

Table 4-1: Root area ratios (RAR) and corresponding stem density used for the flexible rooted wall (FRW) and rigid rooted wall (RRW) boundary conditions.

Flexible rooted wall (FRW)						
Root diameter (mm)	0.3	1	2	3 – 5	5 – 10	Total
Fiber density (cm^{-2})	0.38	0.15	0.02	0	0	0.55
RAR (%)	0.00027	0.0012	0.00074	0	0	0.0022
Rigid rooted wall (RRW)						
Root diameter (mm)	0.37	1	2	3	5	Total
Fiber density (cm^{-2})	0.026	0.027	0.006	0.004	0.003	0.066
RAR (%)	0.00003	0.0002	0.0002	0.0003	0.0006	0.0013

Using a Vectrino II acoustic Doppler profiling velocimeter (ADP; Nortek AS, Vangkroken, Norway; Figure 4-2) at a frequency of 100 Hz and a bin size of 1 mm, 3D velocity profiles were measured down the center of the flume channel and along the wall to confirm flow development prior to experimentation. The ADP is a multi-static acoustic Doppler velocity profiler that allows for simultaneous measurements of three-dimensional velocity profiles and distance to a solid boundary. Velocity measurements can be taken over a 35-mm profiling range, starting 40 mm away from the transmitter, and the bin size (vertical resolution) can be adjusted between 1 to 4 mm (Craig et al., 2011).

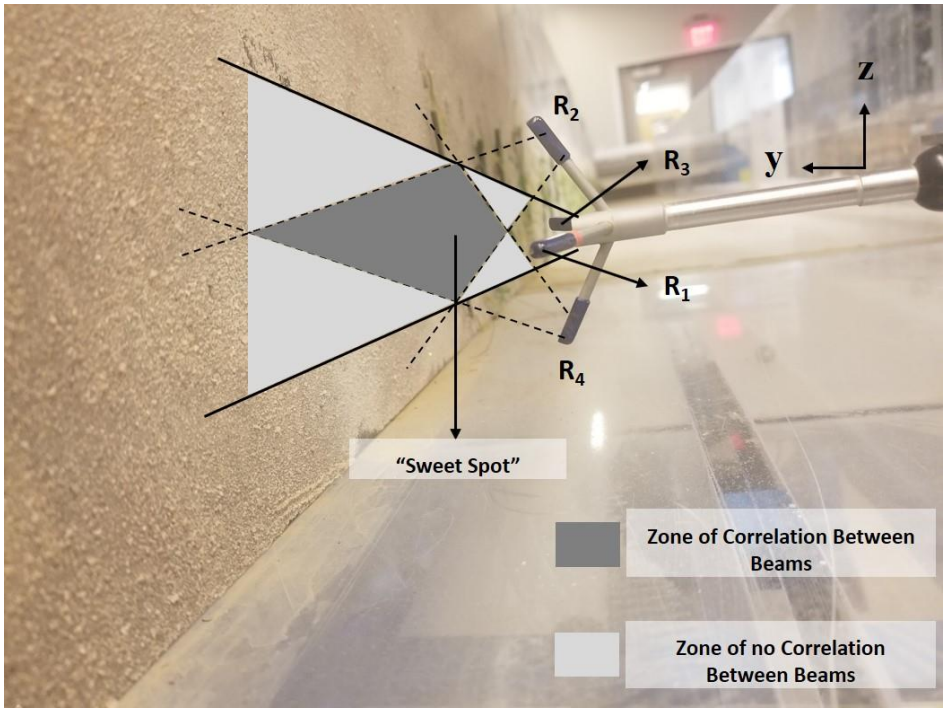

Figure 4-2: Picture taken of Vectrino II acoustic Doppler (ADP) used in the following flume experiments along with illustrations of the measurement zones (redrawn after Brand et al. (2016)). This ADP has four receivers (R_1 – R_4) used to measure three-dimensional velocity profiles. The x, y, and z-axis represent the horizontal (into the page, not shown), lateral, and vertical directions, respectively. Dark grey areas indicate zones where there is an overlap of coverage (correlation) between two beams. Light grey areas indicate zones where there is no overlap of coverage (no correlation) between two beams. Decorrelation of beam signals increases above and below the ADP "sweet spot", the area where signal overlap is the highest.

4.1.2 Experimental Procedure and Statistical Analysis

To determine the effect of each boundary type on velocity and turbulent stress, ADP measurements were taken at 12 locations immediately upstream of the circular sample hole. (Figure 4-3). The 12 measurement locations were determined based on the root locations of the RRW to ensure the effects of different root diameters could be captured. In comparison, the roots along the FRW were so densely packed that each measurement location was near all root diameters, while there were no fibers on the SW. As a result, 12 velocity profiles were taken over each wall at the locations shown in Figure 4-3.

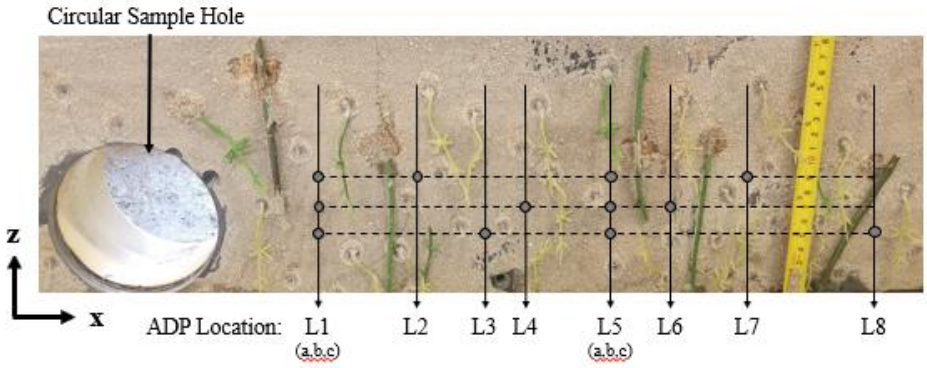

	L1 (a, b, and c)	L2	L3	L4
x (cm)	7	13	18	20.5
z (cm)	9, 7, and 5	9	5	7
	L5 (a, b, and c)	**L6**	**L7**	**L8**
x (cm)	26	30	35.5	44
z (cm)	9, 7, and 5	7	9	5

Figure 4-3: Vectrino II acoustic Doppler profiler (ADP) measurement locations along the rigid rooted wall (grey dots). X refers to the horizontal ADP measurement location in relation to the upstream edge of the circular sample hole. Z refers to the vertical ADP measurement location in relation to the flume bed. For example, L2 was 13 cm away from the testing location upstream edge and 9 cm above the flume bed.

The flume slope was kept constant at 0.1% and three flow rates (19, 29, and 38 L s^{-1}) were used at each measurement location. The flume tailgate height and corresponding flow depth varied depending on the flow rate used to keep the ADP completely submerged during testing (15 cm flow depth for 19 L s^{-1}, and 12 – 13 cm flow depth for 29 and 38 L s^{-1} flow rates). Velocity was sampled for five minutes at 100 Hz with a 1 mm bin size at each location and flow rate. While the ADP has a profiling range of 35 mm, the most accurate velocity measurements close to the boundary have been reported at or near the ADP "sweet spot", a measurement location where signal decorrelation is at a minimum (Figure 4-2; Koca et al., 2017). As a result, velocity measurements were made at 10-mm increments over the range of 10-50 mm from the boundary and 20-mm increments over the range of 50-110 mm. A measurement was also taken at 6-mm

away from the bank, the closest measurement possible. Therefore, velocity and turbulent stress profiles were developed using ADP measurements reported at nine distances from the bank surface: 6, 10, 20, 30, 40, 50, 70, 90, and 110 mm. Throughout the remainder of this chapter, "location" refers to the ADP measurement areas of L1 to L8 shown in Figure 4-3, while "distance" refers to the lateral space between the ADP probe and the streambank surface (6 mm away from the bank up to 110 mm away from the bank).

The velocity time series data from the ADP were processed in R (R Core Team, 2021). ADP data were filtered out if the signal-to noise (SNR) ratio was ≤ 10 dB and the signal correlation (COR) was ≤ 50% (Martin et al., 2002; Strom & Papanicolaou, 2007). If a bin had 30% of its velocity data removed after filtering, that entire bin was removed from further analysis. Following data filtering, all velocity time series were despiked using the phase-space threshold method developed by Goring & Nikora (2002) and modified by Wahl (2002) using Matlab code created by Scott Ikard (2016). Velocity was measured and turbulent stress was calculated at all 12 locations. A median value was calculated using the data collected at each location; the median values were used to construct the velocity and turbulent stress profiles for each streambank boundary condition. However, some locations had datapoints that were filtered out due to low SNR or COR values; datasets with missing datapoints due to filtering are shown in Table 4-2.

.

Table 4-2: ADP measurements for each boundary, flow rate, and distance from the surface that had at least one measurement location filtered out during data processing. SW = sand wall; FRW = flexible rooted wall; RRW = rigid rooted wall; and n = sample size.

Boundary	Flow rate (L s^{-1})	Distance from wall surface (mm)	n
SW	19	110	11
	38	110	11
FRW	29	6	11
	29	10	11
	38	6	9
	38	10	11
RRW	19	90	11
	29	6	11
	38	6	9
	38	10	10

Following data processing, turbulent stress was estimated by calculating the turbulent kinetic energy (TKE) and Reynolds stresses (Hopkinson & Wynn, 2009) at each sample location and distance. TKE is defined as the mean kinetic energy associated with eddies in turbulent flow. The TKE pertaining to each data point was calculated from velocity data using the following relationship:

$$\mathbf{TKE} = \mathbf{0.5} \times [\overline{(\mathbf{u}')^2} + \overline{(\mathbf{v}')^2} + \overline{(\mathbf{w}')^2}] \quad (4.1)$$

where the overbar denotes a mean and the prime terms are the velocity fluctuations associated with the streamwise ($u = \bar{u} + u'$), lateral ($v = \bar{v} + v'$), and vertical ($w = \bar{w} + w'$) velocity components. Reynolds stresses, stresses due to turbulent fluctuations that represent momentum exchange (Hopkinson & Wynn, 2009), were calculated using the following equations:

$$\boldsymbol{\tau}_{yx} = -\overline{(\mathrm{v}'\mathbf{u}')} \quad (4.2)$$

$$\boldsymbol{\tau}_{zx} = -\overline{(\mathrm{w}'\mathbf{u}')} \quad (4.3)$$

$$\boldsymbol{\tau}_{yz} = -\overline{(\mathrm{v}'\mathbf{w}')} \quad (4.4)$$

While the fluctuating velocity components in Reynolds stress and TKE are typically multiplied by water density and reported in units of pascals (N/m^2), water density in this study

remained constant between 997 to 999 kg/m^3. Therefore, for easier comparison with similar experiments, density was not used in equations 4.1 – 4.4; TKE and the Reynolds stresses units are expressed as m^2 s^{-2}. The goal of this experiment was to evaluate the effects of exposed roots on the hydrodynamic boundary layer. To do this, velocity, and turbulent stress profiles of the three distinct streambank boundary types were measured, calculated, and compared. First, the interquartile ranges (IQR) of the streamwise velocity, TKE, and Reynolds stress data were calculated and divided by the respective median value. These nondimensional IQR values were then statistically analyzed using nonparametric Conover's test (Pereira et al., 2015) to determine if root type/density influenced spatial variability within each boundary type at each flow rate. For Conover's test, distance from the bank was treated as a block to account for changes in IQR over the profiling range.

Once the effect of root type/density on spatial variability was determined, the median velocity, TKE, and Reynolds stresses were calculated for each boundary type and distance using all measurement locations. These median values are henceforth called spatial medians for clarity. Spatial medians were compared to evaluate the overall effect of exposed roots on near-bank velocity and turbulent stress, which are important when considering the fluvial entrainment of streambank soil. Additionally, between-boundary comparisons were made using the nonparametric Wilcoxon rank-sum test, which compares medians rather than means. Parametric tests were not used due to violations of the normality assumption within the datasets. Spatial medians were compared between each boundary at each distance from the streambank. Parameters that represent spatial median values were denoted with brackets (e.g., $<\tau_{yx}>$).

4.2 Results and Discussion

4.2.1 Spatial Variability

The interquartile ranges divided by the median values for streamwise velocity, turbulent kinetic energy, and the Reynolds stresses (τ_{yx}, τ_{yz}, and τ_{zx}) are shown for each boundary in Table 4-3. Table 4-3 shows the FRW has a value of 0.05 for streamwise velocity at 6 mm away from the bank when using a 38 L s^{-1} flow rate. The 0.05 value means the IQR of the FRW was only 5% of the respective median value, indicating a relatively low variability.

Table 4-3: Nondimensional interquartile range (IQR divided by the respective median value). The nondimensional IQR for the streamwise velocity, turbulent kinetic energy, and Reynolds stresses are shown at each distance and flow rate.

Distance (mm):	**6**	**10**	**20**	**30**	**40**	**50**	**70**	**90**	**110**
Sand wall: 19 L s^{-1}									
Streamwise Velocity	0.10	0.11	0.12	0.08	0.06	0.04	0.04	0.07	0.06
Turbulent Kinetic Energy	0.08	0.11	0.34	0.67	1.02	1.06	0.68	0.72	0.55
Reynolds stress, τ_{yx}	0.33	0.19	0.23	0.70	19.74	1.20	0.85	1.29	1.38
Reynolds stress, τ_{yz}	5.68	2.51	13.57	4.01	7.74	84.03	1.44	0.44	1.27
Reynolds stress, τ_{zx}	0.26	1.06	0.85	1.24	2.94	2.88	4.10	5.62	16.30
Flexible root wall: 19 L s^{-1}									
Streamwise Velocity	1.02	0.23	0.27	0.24	0.17	0.14	0.11	0.09	0.09
Turbulent Kinetic Energy	0.43	0.18	0.24	0.55	0.64	0.89	1.36	1.47	1.53
Reynolds stress, τ_{yx}	1.28	0.31	0.58	0.86	0.87	1.58	253.09	1.09	1.57
Reynolds stress, τ_{yz}	2.34	2.00	0.58	1.01	1.25	2.63	4.34	2.69	0.88
Reynolds stress, τ_{zx}	485.49	3.41	0.70	0.70	0.83	1.29	2.64	2.23	2.14
Rigid root wall: 19 L s^{-1}									
Streamwise Velocity	0.24	0.15	0.04	0.09	0.07	0.11	0.11	0.09	0.10
Turbulent Kinetic Energy	0.61	0.43	0.50	0.49	0.41	0.32	0.29	0.50	0.62
Reynolds stress, τ_{yx}	1.89	0.33	0.38	0.41	0.29	0.16	0.84	8.81	9.75
Reynolds stress, τ_{yz}	2.15	1.91	1.97	1.40	65.15	0.74	1.03	2.64	292.43
Reynolds stress, τ_{zx}	2.01	15.17	2.76	5.41	31.67	6.55	1.03	3.85	2.75
Sand wall: 29 L s^{-1}									
Streamwise Velocity	0.02	0.03	0.03	0.02	0.01	0.01	0.01	0.02	0.02
Turbulent Kinetic Energy	0.16	0.17	0.16	0.20	0.22	0.28	0.24	0.29	0.28
Reynolds stress, τ_{yx}	0.14	0.09	0.12	0.27	0.90	3.73	4.15	50.24	1.78
Reynolds stress, τ_{yz}	2.28	1.42	4.93	15.80	10.61	4.67	6.46	2.22	0.41
Reynolds stress, τ_{zx}	1.54	0.60	1.17	1.39	0.79	0.97	0.61	0.37	0.97
Flexible root wall: 29 L s^{-1}									
Streamwise Velocity	0.19	0.06	0.09	0.07	0.07	0.07	0.06	0.07	0.09
Turbulent Kinetic Energy	0.53	0.15	0.14	0.06	0.17	0.32	0.60	0.63	0.78
Reynolds stress, τ_{yx}	0.49	0.29	0.21	0.19	0.30	0.60	2.16	6.43	57.58
Reynolds stress, τ_{yz}	2.37	0.56	0.25	0.29	0.85	1.07	1.02	3.26	34.58
Reynolds stress, τ_{zx}	14.91	2.25	7.49	0.52	0.48	0.95	1.17	1.01	1.22

Table 4-3 continued: Nondimensional interquartile range (IQR divided by the respective median value). The nondimensional IQR for the streamwise velocity, turbulent kinetic energy, and Reynolds stresses are shown at each distance and flow rate.

Distance (mm):	**6**	**10**	**20**	**30**	**40**	**50**	**70**	**90**	**110**
Rigid root wall: 29 L s^{-1}									
Streamwise Velocity	0.15	0.16	0.05	0.03	0.01	0.02	0.02	0.04	0.04
Turbulent Kinetic Energy	0.40	0.17	0.16	0.08	0.04	0.05	0.21	0.32	0.74
Reynolds stress, τ_{yx}	2.82	0.20	0.23	0.25	0.12	0.18	0.15	0.96	0.85
Reynolds stress, τ_{yz}	8.11	30.87	11.76	3.72	3.88	3.50	2.22	1.46	2.46
Reynolds stress, τ_{zx}	4.35	5.04	4.28	0.96	0.68	1.11	7.88	14.26	9.32
Sand wall: 38 L s^{-1}									
Streamwise Velocity	0.04	0.03	0.03	0.02	0.03	0.02	0.01	0.01	0.03
Turbulent Kinetic Energy	0.03	0.02	0.10	0.23	0.39	0.20	0.19	0.33	0.51
Reynolds stress, τ_{yx}	0.04	0.11	0.16	0.34	1.17	30.82	1.32	1.68	5.56
Reynolds stress, τ_{yz}	0.86	2.01	4.78	8.39	51.38	12.62	5.34	0.94	1.71
Reynolds stress, τ_{zx}	0.92	0.97	2.38	3.72	7.82	6.60	5.47	4.68	2.65
Flexible root wall: 38 L s^{-1}									
Streamwise Velocity	0.05	0.06	0.05	0.07	0.07	0.08	0.08	0.09	0.11
Turbulent Kinetic Energy	0.19	0.10	0.17	0.16	0.19	0.54	1.06	1.17	1.12
Reynolds stress, τ_{yx}	0.17	0.23	0.29	0.32	0.40	0.66	21.64	11.37	5.46
Reynolds stress, τ_{yz}	0.67	1.09	0.42	0.86	2.26	9.43	2.31	1.36	1.32
Reynolds stress, τ_{zx}	4.34	0.56	11.22	0.78	1.78	2.66	2.60	1.55	1.17
Rigid root wall: 38 L s^{-1}									
Streamwise Velocity	0.06	0.13	0.06	0.04	0.02	0.04	0.04	0.04	0.04
Turbulent Kinetic Energy	0.23	0.10	0.13	0.04	0.06	0.05	0.39	0.80	1.05
Reynolds stress, τ_{yx}	0.67	0.17	0.21	0.12	0.11	0.16	0.20	1.81	1.81
Reynolds stress, τ_{yz}	2.60	8.97	6.45	3.66	3.99	7.32	3.54	139.35	5.20
Reynolds stress, τ_{zx}	1.41	30.22	2.61	1.30	0.23	2.25	14.15	4.51	2.69

For streamwise velocity, the IQR was always smaller than the median value (nondimensional IQR = 0.05 to 1.02) for all boundary conditions and flow rates. Relatively low nondimensional IQRs indicate adequate precision in the velocity data collected with the ADP, regardless of the changes in root density. Nevertheless, both the FRW and RRW had significantly higher IQRs in streamwise velocity compared to the SW at all three flow rates (Table 4-4). This is likely a result of differences in how roots interact with the flow at the different measurement locations, thus making the velocity measurements more variable between the boundaries, even though the actual nondimensional IQRs were relatively low.

Table 4-4: Conover's test p-value results comparing the nondimensional interquartile ranges of the streamwise velocities, turbulent kinetic energies, and Reynolds stresses between each boundary type at each flow rate. Distance from the streambank was treated as a block factor in this analysis. Significant p-values < 0.1 are shown while ns = not significant. SW = sand wall; FRW = flexible rooted wall; and RRW = rigid rooted wall.

Parameter	Flow Rate (L s^{-1})	SW ≠ FRW	SW ≠ RRW	FRW ≠ RRW
Streamwise velocity	19	0.002	0.078	0.078
	29	0.001	0.031	ns
	38	0.005	0.032	ns
Turbulent kinetic energy	19	ns	ns	ns
	29	ns	ns	ns
	38	0.050	ns	ns
Reynolds stress, τ_{yx}	19	ns	ns	ns
	29	ns	ns	ns
	38	ns	ns	0.078
Reynolds stress, τ_{yz}	19	ns	ns	ns
	29	ns	ns	ns
	38	0.031	ns	0.02
Reynolds stress, τ_{zx}	19	ns	ns	0.050
	29	ns	0.050	ns
	38	ns	ns	ns

Like the streamwise velocity, nondimensional IQRs for the calculated turbulent kinetic energy were also relatively low, between 0.1 to 1.53. Only the FRW had significantly higher variability compared to the SW at 38 L s^{-1}, though this was not found for the RRW or for the other flow rates used. It is possible that higher flow rates would continue to increase the variability of the calculated TKE over the rooted boundaries compared to the bare streambank.

On the other hand, the Reynolds stress components τ_{yx}, τ_{yz}, and τ_{zx}, show inconsistent, and sometimes highly variable, results. For example, some interquartile ranges for the Reynolds stress components were five to 400 times larger than the respective median value (Table 4-3). High variability was found for all three flow rates and boundary types, indicating that this was not driven

by specific boundary conditions. Near-surface turbulence statistics calculated using ADPs have been shown to be highly variable when compared to the measured velocity data, though this effect appears to diminish when measurements are made near the ADP "sweet spot" (Koca et al., 2017). Therefore, it is unclear why high variability was measured for the Reynolds stresses and not TKE, even though all measurements in this study were made at the ADP "sweet spot". Nevertheless, these results indicate that when measuring velocity using an ADP, calculating TKE to represent flow turbulence may provide more consistent results if calculated at or near the aforementioned "sweet spot". Given the inconsistent results and highly variable Reynolds stresses, it is difficult to assess the impact of root type/density on the variability of calculated turbulence data in the present study.

4.2.2 Streamwise Velocity

All streamwise velocities appear to follow a turbulent boundary layer profile (Figure 4-4a-c). Similar to the grass and shrub vegetation models used in the Hopkinson & Wynn (2009) study, the roughness added by the flexible roots and rigid roots in the present study led to an overall reduction in streamwise velocity near the bank, as compared to grain roughness only. Regardless of flow rate, streamwise velocity was always significantly lower between 6 mm and 20 mm for the FRW, and between 6 mm and 50 mm for the RRW when compared to the SW (Table 4-5; Figure 4-4a-c). Comparing the FRW and RRW, rigid roots caused the greatest reduction in streamwise velocity closer to the bank, despite the lower stem density. Streamwise velocity ($<V_x>$) over the RRW was generally 10% to 54% and 7% to 37% lower compared to the SW and FRW, respectively, between 6 mm to 50 mm (Figure 4-4a-c). At and beyond 90 mm from the wall, the RRW velocities were significantly higher than along the SW at all flow rates and higher than the FRW at 38 L s^{-1} (Table 4-5). Prior studies using rigid vegetation elements along streambanks also documented higher velocities near the center of the flume/channel (Hopkinson & Wynn, 2009; Thorne & Furbish, 1995; Valyrakis et al., 2021).

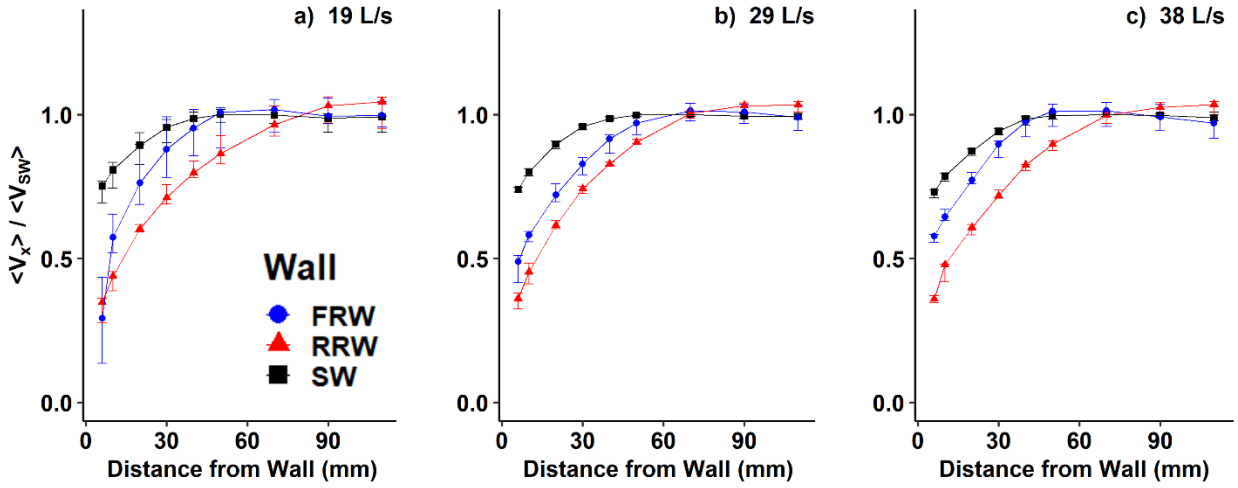

Figure 4-4: Streamwise velocity ($<V_x>$) measured for each boundary type divided by the maximum SW velocity ($<V_{SW}>$) at each flow rate. Error bars represent the interquartile range of spatial medians for all locations that were not filtered out following Acoustic Doppler Profiler data processing. SW = sand wall (black squares); FRW = flexible rooted wall (blue circles); and RRW = rigid rooted wall (red triangles).

Table 4-5: Wilcox rank-sum test p-value results comparing streamwise velocity (<V_x>), turbulent kinetic energy (<TKE>), and Reynolds stresses (<τ_{yx}>, <τ_{zx}>, and <τ_{yz}>) between each boundary type comparison. All flow rates (19 L s^{-1}, 29 L s^{-1}, and 38 L s^{-1}) are presented. The near-bank distance (6 mm), the distance of maximum <τ_{yx}> for the rooted boundaries (20 mm), and the furthest distance measured away from the streambank (110 mm) are represented here. Significant p-values ($p < 0.1$) are shown while ns = not significant. SW = sand wall; FRW = flexible rooted wall; and RRW = rigid rooted wall.

		Distance from Streambank (mm) and Boundary Type								
		6			20			110		
Parameter	Flow Rate (L s^{-1})	SW ≠ FRW	SW ≠ RRW	FRW ≠ RRW	SW ≠ FRW	SW ≠ RRW	FRW ≠ RRW	SW ≠ FRW	SW ≠ RRW	FRW ≠ RRW
<V_x>	19	<0.001	<0.001	ns	0.01	<0.001	<0.001	ns	0.037	ns
	29	<0.001	<0.001	0.007	<0.001	<0.001	<0.001	ns	0.014	ns
	38	<0.001	<0.001	0.002	<0.001	<0.001	<0.001	ns	0.03	0.01
<TKE>	19	<0.001	<0.001	ns	<0.001	<0.001	ns	0.002	<0.001	ns
	29	<0.001	<0.001	ns	<0.001	<0.001	<0.001	<0.001	<0.001	ns
	38	<0.001	<0.001	ns	<0.001	<0.001	<0.001	<0.001	<0.001	ns
<τ_{yx}>	19	ns	ns	ns	<0.001	<0.001	ns	ns	0.009	0.008
	29	ns	ns	ns	<0.001	<0.001	0.001	ns	0.005	ns
	38	<0.001	0.034	ns	<0.001	<0.001	<0.001	ns	<0.001	0.024
<τ_{zx}>	19	0.024	ns	ns	ns	<0.001	<0.001	0.004	0.027	ns
	29	ns	ns	ns	0.024	ns	ns	<0.001	ns	0.017
	38	ns	ns	ns	ns	ns	ns	<0.001	ns	ns
<τ_{yz}>	19	0.003	0.028	ns	<0.001	ns	0.008	ns	ns	0.039
	29	ns	ns	ns	<0.001	ns	<0.001	0.007	<0.001	ns
	38	<0.001	ns	0.022	<0.001	ns	0.001	ns	ns	0.039

4.2.3 Turbulent Kinetic Energy and Reynolds Stress

The high turbulent stress and reduced velocity near the bank along the rooted boundaries (Figure 4-4a-c) is indicative of sparsely spaced vegetation elements (Nepf, 2012; Hopkinson & Wynn, 2009). This region can be seen in Figure 4-5a-f. <TKE> due to sand roughness was significantly lower at every bank distance compared to the FRW and the RRW (Table 4-5; Figure 4-5a,c,e). At all flow rates, the maximum <TKE> was measured at 6 mm from the bank for the SW and FRW. On the other hand, the maximum <TKE> for the RRW occurred at 6 mm or 20 mm, depending on the flow rate. $<\tau_{yx}>$, which represents momentum exchange parallel to the streambank, followed a similar pattern to <TKE> (Figure 4-5b,d,f) with a few minor differences. At 6 mm away from the bank surface, $<\tau_{yx}>$ for the RRW was 35% and 25% lower compared to the SW at 19 L s^{-1} and 29 L s^{-1} flow rates, respectively (Figure 4-5b and Figure 4-5d), though this difference was not statistically significant. In addition, the maximum $<\tau_{yx}>$ distance was identical for both the FRW and RRW (20 mm) while the maximum $<\tau_{yx}>$ distance was 10 mm for the SW (Figure 4-5b,d,f). <TKE> and $<\tau_{yx}>$ along the RRW between 10 mm to 70 mm were significantly higher compared to the FRW at 29 L s^{-1} and 38 L s^{-1} (Table 4-5; Figure 4-5c-f). As shown in prior research, the waving motion of the flexible fibers during flume testing likely contributed to lower momentum transfer in the streamwise direction when compared to the rigid fibers (Hopkinson & Wynn, 2009; Nepf & Ghisalberti, 2008).

Similar to the results presented in this study, sparsely spaced vegetation has been shown to increase near-bank/near-bed turbulent stress compared to unvegetated areas (Liu et al., 2017; McBride et al., 2007; Nepf, 1999; van Katwijk et al., 2010; Zhang et al., 2020). Densely packed fibers decrease velocity and turbulence at the interface between the fibers and the main flow (Liu et al., 2021; Nepf, 2012b), so the higher near-bank <TKE> and $<\tau_{yx}>$ over the FRW compared to the SW was surprising given the relatively high fiber density used (Table 4-1; 0.55 cm^{-2} or 5500 m^{-2}). The orientation of the flexible fibers during flume testing likely explains this result. In simulated and natural stream environments, vegetation density is defined by the vegetation frontal area and the average vegetation height (Nepf, 2012b). While all fibers in the present study were cut to 7-cm lengths, the flexible fibers generally oriented parallel to the bank surface during testing and only extended a few millimeters (~2 mm on average) into the main channel. As a result, the FRW, based on the frontal area (a) and how far the roots extend into the flow (h), can also be considered sparsely spaced due to a low ah value ($ah << 0.1$; Nepf, 2012a). Here the frontal area

is defined as a = nd (Nepf, 1999; Nepf, 2012a), where n is the number of roots per unit area (roots/cm^2) and d is the root diameter (cm). As such, the flexible fibers acted as additional grain roughness, reducing near-bank velocities but increasing near-bank turbulent stress due to element-scale turbulence generated in the wake of the root fibers (Nepf, 2012b). The rigid fibers also remained aligned to the bank surface during testing, though they extended slightly further into the main channel (~4 mm on average) due to the higher root thickness and rigidity.

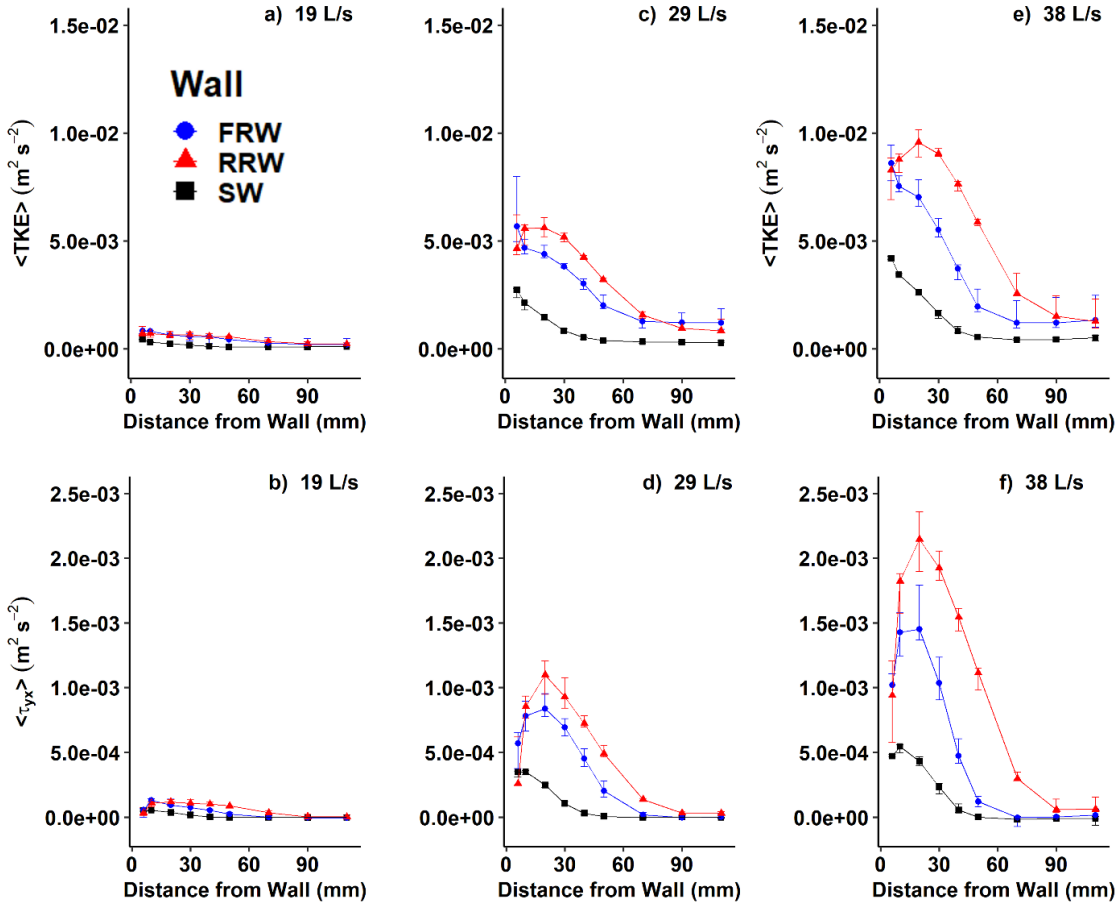

Figure 4-5: Spatial median turbulent kinetic energy (<TKE>) and Reynolds stress <τ_{yx}> measured at each flow rate and boundary type. Error bars represent the interquartile range of spatial medians for all locations that were not filtered out following ADP data processing. SW = sand wall (black squares); FRW = flexible rooted wall (blue circles); and RRW = rigid rooted wall (red triangles).

The Reynolds stresses $<\tau_{zx}>$ and $<\tau_{yz}>$ represent momentum exchange parallel to the flume bed and perpendicular to the streambank, respectively. $<\tau_{yx}>$ was ten times higher on average compared to $<\tau_{zx}>$ and $<\tau_{yz}>$ (Figure 4-6a-f); nevertheless, interesting profile patterns existed for $<\tau_{zx}>$ and $<\tau_{yz}>$ along the rooted boundaries. Over the SW, $<\tau_{zx}>$ and $<\tau_{yz}>$ remained near zero at all distances and flow rates, excluding $<\tau_{zx}>$ at 6 mm and 10 mm from the bank for 29 L s^{-1} and 38 L s^{-1} (Figure 4-6c,e), likely due to the presence of secondary currents. On the other hand, for the RRW, $<\tau_{zx}>$ increased with distance from the bank up to 40 mm for the 29 L s^{-1} and 38 L s^{-1} flow rates. At that point, $<\tau_{zx}>$ decreased with distance from the bank at both flow rates. $<\tau_{zx}>$ for the FRW followed a similar pattern to the RRW; however, $<\tau_{zx}>$ changed from positive to negative closer to the bank (at 20 mm instead of 70 mm), likely due to the roots folding against the banks during testing. While the magnitude of $<\tau_{zx}>$ between the FRW and RRW is similar near the boundary (6 mm to 50 mm; Figure 4-6c,e), the FRW produces sometimes significantly higher τ_{zx} towards the center of the channel (Figure 4-6c,e; Table 4-5).

With respect to $<\tau_{yz}>$, the RRW generally mimicked the SW at all distances and flow rates (Figure 4-6b,d,f). On the other hand, vertical momentum exchange along the streambank due to the flexible fibers is evident. The magnitude of $<\tau_{yz}>$ over the FRW was significantly greater than the SW and RRW between 6 to 50 mm (29 L s^{-1}) and 6 to 40 mm (38 L s^{-1}) (Table 4-5). A maximum $<\tau_{yz}>$ (highest magnitude) was reached at between 6 to 20 mm away from the bank over the FRW. The vertical waving motion of the fibers likely caused this increased momentum transfer along the y-z plane; a phenomenon not observed for the sand grains or rigid fibers.

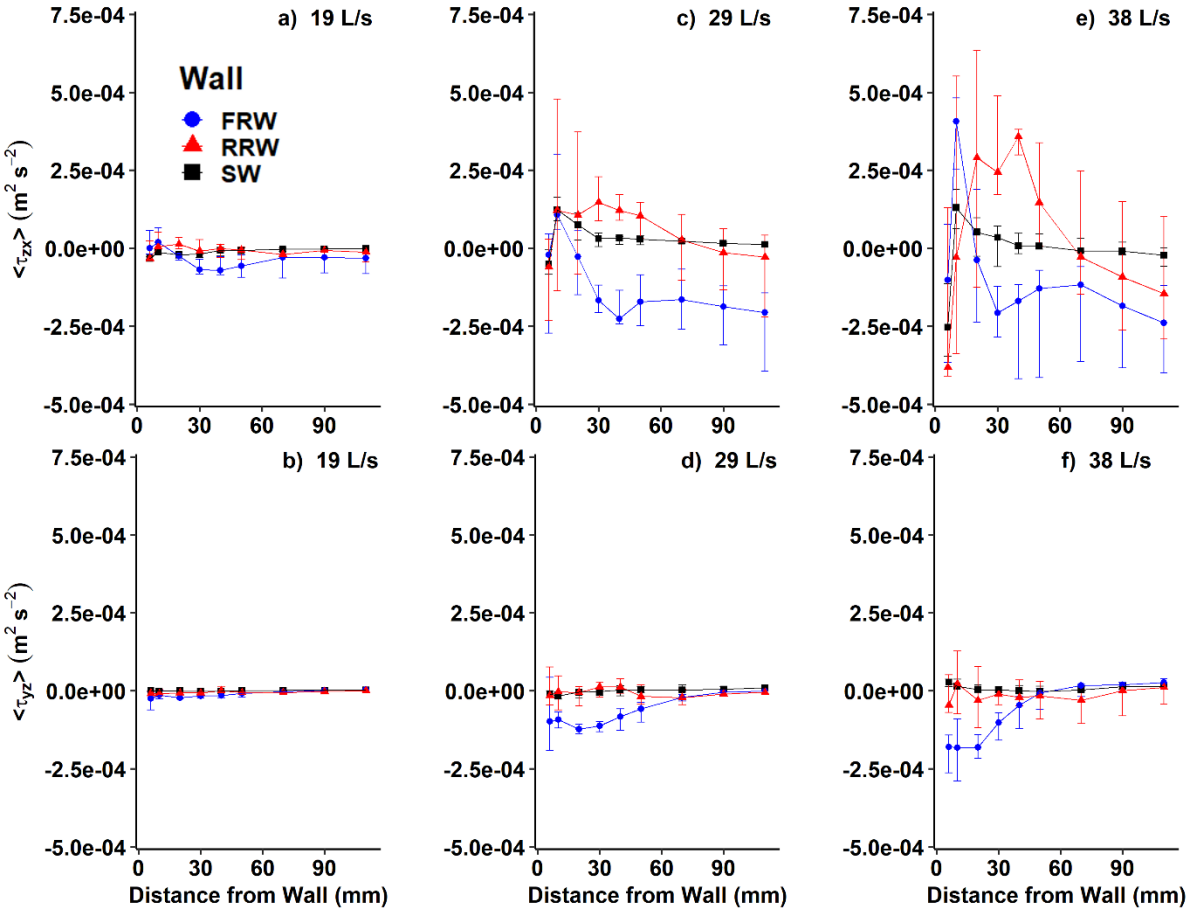

Figure 4-6: Spatial median Reynolds stresses ($<\tau_{zx}>$ and $<\tau_{yz}>$) measured at each flow rate and boundary type. Error bars represent the interquartile range of spatial medians for all locations that were not filtered out following Acoustic Doppler Profiler data processing. SW = sand wall (black squares); FRW = flexible rooted wall (blue circles); and RRW = rigid rooted wall (red triangles).

4.3 Conclusions

This study compared the velocity and turbulence profiles along a vertical bank roughened with sand grains (no roots), sand + flexible fibers, and sand + rigid fibers in a rectangular flume channel. Simulated rooted streambanks were modeled after root area ratios measured in the field at the Goodwin Creek Experimental Watershed in Mississippi, USA (Simon & Collison, 2002). Key findings include the following:

1. Calculated Reynolds stresses were more variable than TKE even though all ADP measurements were taken at the "sweet spot". These results indicate that when measuring velocity using an ADP, calculating TKE to represent flow turbulence may provide more consistent results if calculated at or near the ADP "sweet spot".
2. Rooted boundaries significantly reduced streamwise velocity compared to the no root streambank. Overall, the rigid fiber boundary produced the lowest near-bank velocity, followed by the flexible fiber boundary.
3. <TKE> and $<\tau_{yx}>$ were significantly higher in the rooted boundaries at distances of 6 mm to 50 mm from the bank surface compared to the sand wall boundary. While higher near-bank turbulent stress suggests higher near-bank turbulence, lower near-bank velocities indicate lower wall shear stresses compared to the bare (unvegetated) boundary. Given that both shear stress (e.g., Flanagan & Nearing, 1995; Larsen et al., 2009) and turbulence (e.g., Yang & Nepf, 2018; Zhang et al., 2020) can drive fluvial entrainment, the cumulative impact of exposed roots on streambank erosion rates, using velocity/turbulent stress results alone, is unclear.
4. $<\tau_{yx}>$ was the dominant stress for all boundary types (10x higher than both $<\tau_{zx}>$ and $<\tau_{yz}>$). Nevertheless, rooted boundaries also increased stress parallel to the bed surface ($<\tau_{zx}>$) while only the flexible fibers influenced vertical momentum transfer ($<\tau_{yz}>$) due to the waving motion of the fibers.

Overall, this research highlights the important role exposed plant roots play in the streambank boundary layer, which has implications for the erosion rate of stream channels with vegetated floodplains.

Chapter 5. Labile Organic Matter and Soil Resistance to Fluvial Erosion

Aggregate stability, EPS, and arbuscular mycorrhizal fungi have all been shown to significantly influence soil resistance to fluvial erosion (Barthès & Roose, 2002; Li et al., 2021; Mardhiah et al., 2016; Wynn & Mostaghimi, 2006); however, to the authors' knowledge, no work has been done directly linking the effect of increasing labile OM inputs with increasing soil resistance to fluvial streambank erosion. As a result, the goal of this experiment was to determine if soils amended with OM, in the form of dry and crushed grass clippings, would be more stable and resistant to fluvial erosion via an increase in EPS. The following hypotheses were addressed: 1) EPS concentration (both carbohydrates and proteins) and aggregate stability increase with increasing OM inputs; and 2) OM-amended soils are more resistant to fluvial erosion, due in part to higher EPS production and aggregate stability, as compared to unamended control soils. Detailed descriptions of the flume used (Figure 4-1a), the sand wall boundary used (Figure 4-1b), and how fully developed flow was confirmed can be found in Chapter 4, section 4.1.1.

5.1 Methods

5.1.1 Experimental Treatments and Setup

Silt loam soil (16% clay, 27% sand, and 57% silt) was collected from the New River floodplain near Whitethorne, VA (37.192616°, -80.573133°). The soil was passed through a 2-mm sieve, steam sterilized for two hours at 100°C, and then stored in covered 210-L bins. The day before experiment setup, steam sterilization was repeated to ensure limited microbial community colonization of the soil. For this experiment, 24.8 cm long and 10.2 cm diameter PVC pipes were used as growth containers. On the "top" side of the pipe, a slot was cut using a 3.8-cm diameter hole saw. Both ends of the pipe were covered in nursery fabric mesh. To quantify the impact of OM inputs on soil aggregate stability, EPS, and streambank fluvial erosion rates, increasing amounts of dried and crushed (< 1 mm) cool season grass clippings were mixed at rates of 0, 1, and 4 g of clippings per 100 g of sieved soil. Treatments were named T0, T1, and T4, respectively. Based on the carbon content of the grass clippings (40.6%) and surface area of the growth containers, T0, T1, and T4 corresponded to 0, 96 g C/m^2, and 384 g C/m^2, respectively. For comparison, a review conducted by Cotrufo & Lavallee (2022) collated prior research and reported that carbon inputs from plant roots (root exudates and root turnover) have been measured as 3 to

400 g/m^2/year for grasslands and 120 to 960 g C/m^2/year for forests. A total of eight samples were created per treatment (24 samples in total). Following mixing of soil and OM inputs, soil samples were compacted in the growth containers to a bulk density of 0.95 g/cm^3 and allowed to mature in a closed greenhouse for 50 days prior to erosion testing and soil sampling. To maintain consistent soil moisture content via capillary action, the growth containers were placed in shallow aluminum trays filled with tap water. To prevent wetting/drying cycles, water levels were maintained in the trays to keep the soil samples at field capacity.

A randomized complete block design was used for this experiment, with one treatment randomly placed within each block (Figure 5-1). The blocking was done to control for spatial variation in the greenhouse conditions, such as sunlight and temperature. Placement of each block in the greenhouse was done separately over a three-week timeframe starting in March 2021; therefore, the block design was also used to account for temporal effects. One to two days was required per block for erosion testing, so block separating each block placement by two – three days was done to ensure each sample matured in the greenhouse for 50 days total. Over the course of the experiment, temperatures in the greenhouse ranged from 31 to 46°C during the day and 17 to 23°C throughout the night. Following the 50-day maturation period, samples were moved to a temperature-controlled lab and allowed to sit in trays full of water overnight. This ensured that all soil samples were at field capacity prior to being tested in the flume.

Figure 5-1: Greenhouse setup and growth containers. A randomized complete block design was used for this study with one treatment per block.

5.1.2 Erosion Testing Procedure

A general model of cohesive soil erosion predicts the erosion rate as a function of the soil erodibility coefficient and a measure of flow energy (Moody et al., 2005):

$$\varepsilon_r = k_d X \quad (5\text{-}1)$$

where ε_r is the erosion rate (m s^{-1}); k_d is the soil erodibility coefficient (m^3 N^{-1} s^{-1}); and X is a measure of flow energy. K_d is considered a soil property and reflects the overall resistance of the soil to fluvial forces. A variety of methods have been used to quantify flow energy in the model (Moody et al., 2005); however, X is commonly quantified using "excess shear stress", which is the difference between the applied shear stress (τ_a) and a critical boundary shear stress at which erosion starts (τ_c), which is also considered a soil property. To calculate k_d and τ_c, immediately prior to erosion testing, each sample was cut into three subsamples. Each subsample was tested using a different flow rate: 17.5, 28.5, and 48.8 L s^{-1}. These flow rates corresponded to average applied shear stresses of 0.06 ± 0.01 Pa, 0.31 ± 0.03 Pa, and 0.95 ± 0.08 Pa, respectively. Finally, linear regression was conducted on the measured erosion rates vs. the respective applied shear stress to calculate k_d and τ_c for each sample, where k_d was the slope of the regression line and τ_c was the intercept. However, for treatments T0 and T1, the intercept was frequently negative due to relatively high soil loss at the lower applied shear stresses. It is common procedure to assume τ_c equals zero and to calculate only k_d (Al-Madhhachi et al., 2013; Hanson, 1990). Ultimately, assuming a zero intercept provided the best linear fit for the measured erosion data.

The flume tank was filled with tap water from the Blacksburg-Christiansburg VPI Water Authority; this water was kept at a constant temperature of 25°C using three 1000-W aquarium heaters (True Temp T-1000, Transworld Aquatic Ent., Inglewood, CA, USA). Digital heaters (50-W, Nova pet supplies, Guangdong China) were used to keep soil temperature (ST) constant at 25°C as well (Akinola et al., 2019); however, soil temperatures actually varied between 18.7°C to 20.7°C. Volumetric water content (VWC), water temperature (WT), and ST were measured for each subsample; the average value was reported for each sample. A total of 21 VWC and ST measurements were taken; these data were unfortunately not recorded for the first block of samples (three data points are missing). WT was measured directly by the ADP.

To simulate the geometry of soil-water interactions along an eroding streambank, the soil sample was introduced into the flume channel through a circular hole in the vertical PVC wall (Figure 4-1a). The sample distance from the channel inlet, approximately 6 m, was selected to be

where the boundary layer was fully developed, and secondary flows/tailgate effects were minimized. The flume bed slope was held constant at 0.1%. The sample was covered before running the flume to prevent the application of hydraulic shear on the soil surface as the flow developed in the channel. Testing started once the flow became fully developed (about 90 seconds). The ADP was set to a recording frequency of 100 Hz. Erosion testing lasted for 10 minutes, or until all the soil had been eroded away, whichever came first. The ADP probe was 60 mm away from the soil surface for each sample. The distance of the ADP probe head to the soil surface was monitored via the Vectrino software, and the soil core was advanced back to the initial position, flush with the wall, after every millimeter of erosion (Akinola et al., 2019). This process was repeated for all three soil subsamples using a different flowrate for each subsample. The erosion testing time was reduced to 5 minutes for the T0 and T1 subsamples at 48.8 L s^{-1} due to the high amount of erosion that occurred. This was done so some soil would be left over for additional analyses following erosion testing.

The velocity time series data from the ADP was processed in R. ADP data were filtered out if the signal-to noise (SNR) ratio was ≤ 10 dB and the signal correlation (COR) was ≤ 50% (V. Martin et al., 2002; Strom & Papanicolaou, 2007). If a bin had 30% of its velocity data removed after filtering, that entire bin was removed from further analysis. Following data filtering, all velocity time series were despiked using the phase-space threshold method developed by Goring & Nikora (2002) and modified by Wahl (2002) using Matlab code created by Ikard Scott (2016).

Following data processing for each flume run, turbulent stress was determined from the three-dimensional velocity data 13 mm away from the sample surface using the Reynolds stress calculation (τ_{yx}):

$$\boldsymbol{\tau_{yx}} = -\boldsymbol{\rho_w} * \overline{(\mathbf{v_1'u'})} \quad (5\text{-}2)$$

where ρ_w is the density of water, and the prime terms are the velocity fluctuations associated with the longitudinal (u) and transversal (v) velocity components. The water density, which changes with temperature, was estimated from the following equation (Jones & Harris, 1992):

$$\boldsymbol{\rho_w} = \mathbf{999.85} + [\mathbf{0.063}(\boldsymbol{T}) + \mathbf{0.0085}(\boldsymbol{T^2}) + \mathbf{6.94 \times 10^{-5}}(\boldsymbol{T^3}) + \mathbf{3.82 \times 10^{-7}}(\boldsymbol{T^4})] \quad (5\text{-}3)$$

where T (°C) is the mean water temperature.

5.1.3 Measurement of EPS and Aggregate Stability

After testing each subsample in the flume, the soil remaining was collected for soil organic matter, EPS, and aggregate stability analysis. The collected subsamples were broken apart by hand and allowed to partially dry overnight at 20°C. The following day, a portion of the moist soil was forced through a 2-mm sieve and frozen at -15°C until EPS analysis. The remaining moist soil was air dried and 50 g of 3 – 5 mm aggregates was collected for aggregate stability analysis. The remaining air-dry soil was sieved through a 2-mm sieve and stored at room temperature for organic matter content analysis.

Aggregate stability was measured following the method outlined by Le Bissonnais (1996). The test was performed on 3-5 mm aggregates, dried at 40°C for 24 h. The following fast wetting procedure was carried out: 5 g of aggregates were quickly immersed in deionized water and the excess water removed with a pipette after 10 min. The wetted aggregates were transferred to a sieve (63-μm aperture) immersed in 100% (v/v) ethanol and shaken 20 times (range of 2 cm) by hand. The ethanol was then evaporated in an oven at 40°C prior to aggregate weighing. Dry sieving was performed by hand with a nest of five sieves (2, 1, 0.5, 0.2, 0.1 and 0.063 mm) and all weights retained on each sieve were recorded.

Aggregates were defined as large macroaggregates (>2 mm), macroaggregates (0.2–2 mm), and microaggregates (0.063–0.2 mm), respectively, while the soil component less than 0.063 mm was defined as the silt and clay fraction not associated with aggregates. The water-stable aggregate stability was evaluated according to the following equation (Castro Filho et al., 2002):

$$\mathbf{MWD} = \frac{\sum_{i=1}^{n} \bar{x}_i w_i}{\sum_{i=1}^{n} w_i} \tag{5-4}$$

where MWD is the mean weight diameter (mm), x_i is the mean diameter of each aggregate size, w_i is the weight of each aggregate size, and n is the number of size fractions. The total weight of individual size fractions was also compared.

The EPS extraction procedure used in this study follows methods described by Redmile-Gordon et al. (2014). A 70 g CER/g-SOM ratio (cation exchange resin; Millipore Sigma, Amberlite® HPR1100, Burlington, MA; soil organic matter) was used (Frolund et al., 1996); SOM was estimated using the loss on ignition method (360°C, 2 hours). The moist soil described above was homogenized and added to centrifuge tubes (2.5 g dry weight equivalent). To remove soluble EPS, 25 mL of $CaCl_2$ (4°C, pH 7) was added to the tube and shaken (Eberbach E6010 Benchtop

Reciprocal Shaker, 115V) at 4°C and 280 rpm for 1 h. The mixture was then centrifuged for 10 min at 4500 rpm and 4°C. The produced supernatant was discarded, leaving only the soil pellet.

To analyze bound EPS in the pellet, pre-weighed and pre-washed CER was added to the centrifuge tube together with 25 mL of a phosphate buffered saline (PBS) solution (4°C, pH 7). The CER-pellet mixture was shaken hard by hand, and then placed on the Eberbach shaker at 4°C for 2 hours. Samples were centrifuged as above, and the supernatant was collected and measured spectrophotometrically for carbohydrates and proteins. Proteins were estimated using the modified Lowry assay, corrected for removal of humic substances (Frolund et al., 1996; Redmile-Gordon et al., 2013). Total carbohydrates was measured using the phenolesulphuric acid method (DuBois et al., 1956).

5.1.4 Statistical Analysis

Standard diagnostic tests were conducted to check data for outliers and homoscedasticity; data were transformed as necessary to meet statistical test assumptions. Additionally, Spearman rho correlation coefficients for all measured parameters were examined to measure the strength of relationships between different variables. The Kruskal-Wallis test was used to analyze differences in median soil parameters and erosion rates as a function of OM treatment, while pairwise Wilcoxon rank-sum tests were used to determine significant differences between each treatment type.

Relationships between the soil erodibility coefficient (dependent variable) and measured independent variables were examined using multiple linear regression. For regression analysis, the parameters were first standardized by subtracting the mean and standard deviation so the magnitudes of the regression coefficients could be compared directly to determine the relative influence of each explanatory variable. The best model was chosen based on Akaike's Information Criteria (AIC), Bayesian Information Criteria (BIC), and graphical inspection that the model met required assumptions (independence, normality, and constant variance). Data transformations were used to improve regression diagnostics as needed. The alpha value was set to 0.05 to determine statistical significance.

5.2 Results

5.2.1 Soil Organic Matter, Aggregate Stability, and Extracellular Polymeric Substances

After maturing in a greenhouse for 50 days, OM inputs had a significant impact on soil aggregate stability (Figure 5-2). Treatments with higher OM content had a greater mass of stable macroaggregates. This change in stable macro- vs microaggregates is represented in MWD, which significantly increased with OM content. On average, compared to the control, T0, stable macroaggregate mass increased 5-fold for T1 and nearly 60-fold for T4. MWD and large macroaggregate mass were positively correlated with SOM while microaggregate stability was negatively correlated with SOM (Table 5-1). For extracellular substances, measured EPS carbohydrates were significantly lower in T1 compared to T0 and T4 at day 50 (Figure 5-3). On the other hand, EPS proteins were significantly higher in both T1 and T4 compared to T0 (Figure 5-3).

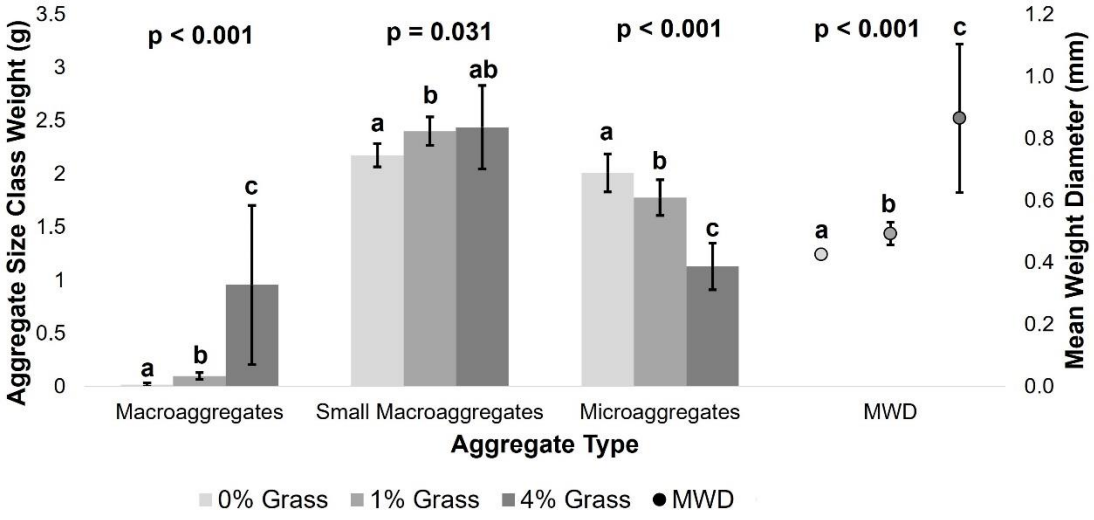

Figure 5-2: Average weight of soil aggregates following fast wetting procedure for each treatment at day 50, separated into three aggregate size classes (macroaggregates, small macroaggregates, and microaggregates). The average mean weight diameters are shown for each treatment as well (circles). The black error bars represent the standard deviation. Letters denote statistically significant differences between each treatment and aggregate size pair (Wilcoxon rank sum test; $p < 0.05$), and the p-value above each measurement denotes the Kruskal-Wallis p-value between all treatments.

Table 5-1: Spearman rho correlation coefficients. Bold numbers indicate a significant correlation (**, $p < 0.05$). K_d = soil erodibility coefficient (cm hr^{-1} Pa^{-1}); SOM = soil organic matter (%); EPS-P = extracellular polymeric substances (EPS) proteins (µg $g\text{-}soil^{-1}$); MWD = mean weight diameter (mm); LargeMacro = stable large macroaggregate mass (g); SmallMacro = stable small macroaggregate mass (g); Micro = stable microaggregate mass (g); VWC = volumetric water content (%); ST = ST = soil temperature (°C); and WT = water temperature (°C).

	k_d	SOM	MWD	LargeMacro	SmallMacro	Micro	EPS-P	EPS-C	VWC
SOM	**-0.73****								
MWD	**-0.71****	**0.90****							
LargeMacro	**-0.74****	**0.88****	**0.93****						
SmallMacro	**-0.56****	**0.53****	**0.47****	**0.42****					
Micro	**0.78****	**-0.90****	**-0.95****	**-0.95****	**-0.48****				
EPS-P	**-0.61****	**0.67****	**0.78****	**0.82****	0.29	**-0.77****			
EPS-C	-0.20	0.05	-0.07	-0.02	-0.19	-0.06	-0.17		
VWC	**-0.49****	**0.72****	**0.66****	**0.64****	0.34	**-0.63****	**0.57****	0.00	
WT-ST	-0.32	0.29	0.31	0.31	0.31	-0.3	0.19	-0.41	0.29

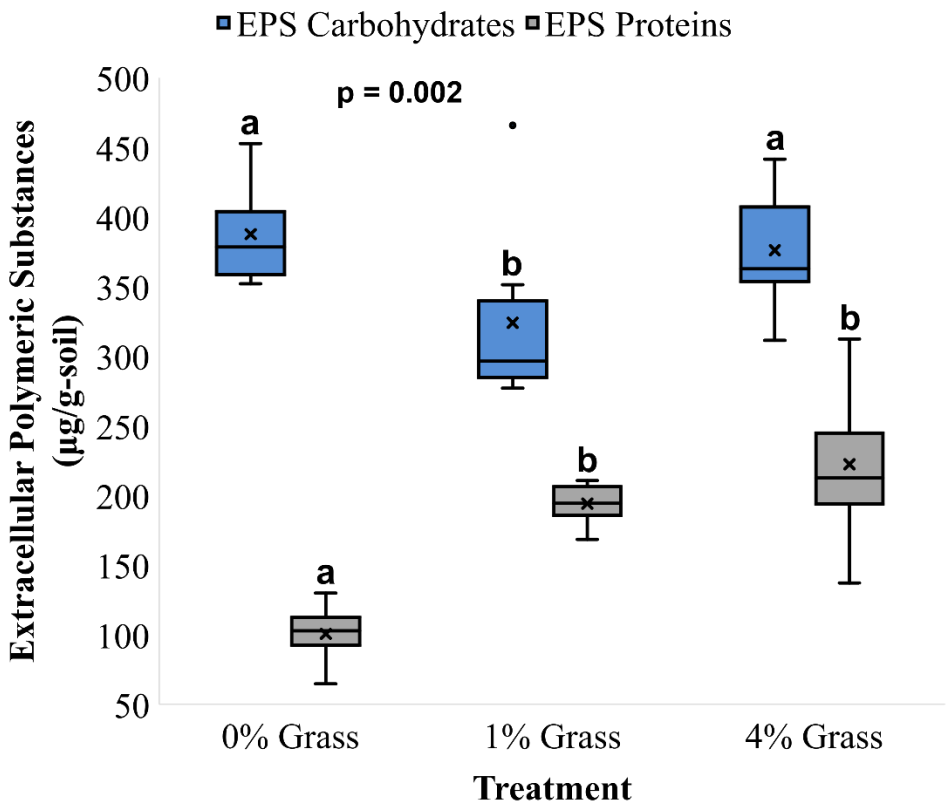

Figure 5-3: Extracellular polymeric substances measured as carbohydrates and proteins for each treatment at day 50. Letters denote statistically significant differences between each treatment pair (Wilcoxon rank sum test; $p < 0.05$), and the p-value on the top left denotes the Kruskal-Wallis p-value. The blue/grey area of the plot spans the interquartile range while "x" and the inner solid black line represents the data mean and median, respectively. Outer dots represent outliers.

5.2.2 Soil Erodibility Coefficient and Structural Equation Modeling

The average soil erodibility coefficient decreased by 25% and 61% for treatments T1 and T4, respectively, compared to T0 (Figure 5-4). However, only T4 was significantly different compared to both T0 and T1. Multiple linear regression analysis was used to identify relationships between soil properties and erosion resistance. Given the high correlation between SOM, EPS-P, and VWC (Table 5-1), only EPS-P, along with EPS-C and WT-ST, were used in the regression analysis and reported in Figure 5-5. Results indicate that k_d is negatively correlated with both EPS-P and EPS-C; WT-ST was not a significant predictor, so that parameter was left out of the result.

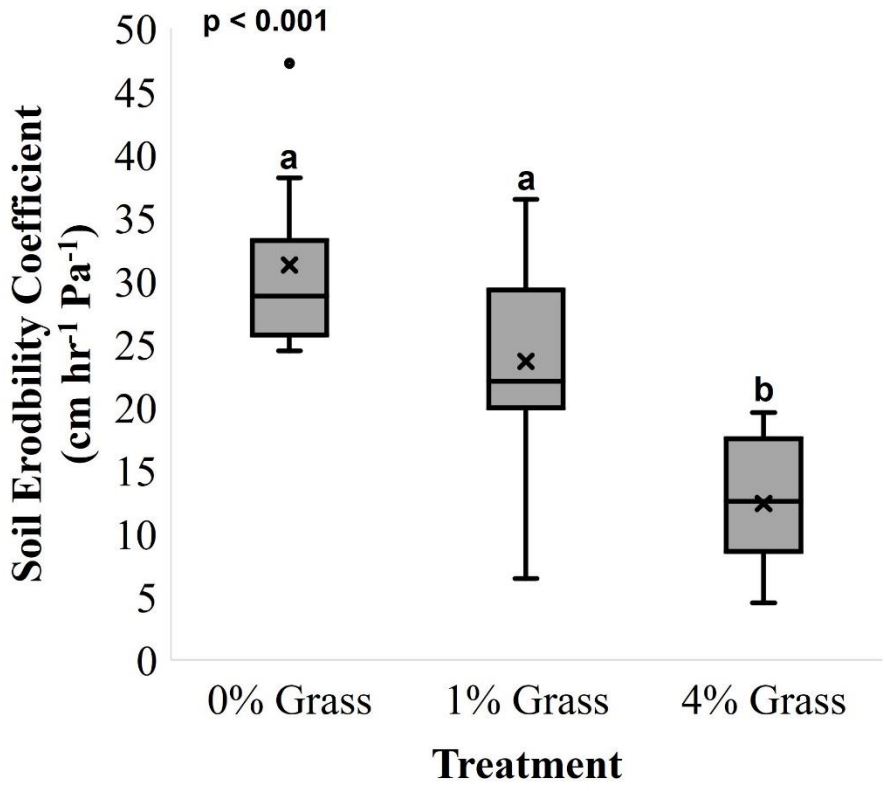

Figure 5-4: Soil erodibility coefficients for each treatment. Letters denote statistically significant differences between each treatment pair (Wilcoxon rank sum test; $p < 0.05$), and the p-value on the top left denotes the Kruskal-Wallis p-value. The grey area of the plot spans the interquartile range while "x" and the inner solid black line represents the data mean and median, respectively. Outer dots represent outliers.

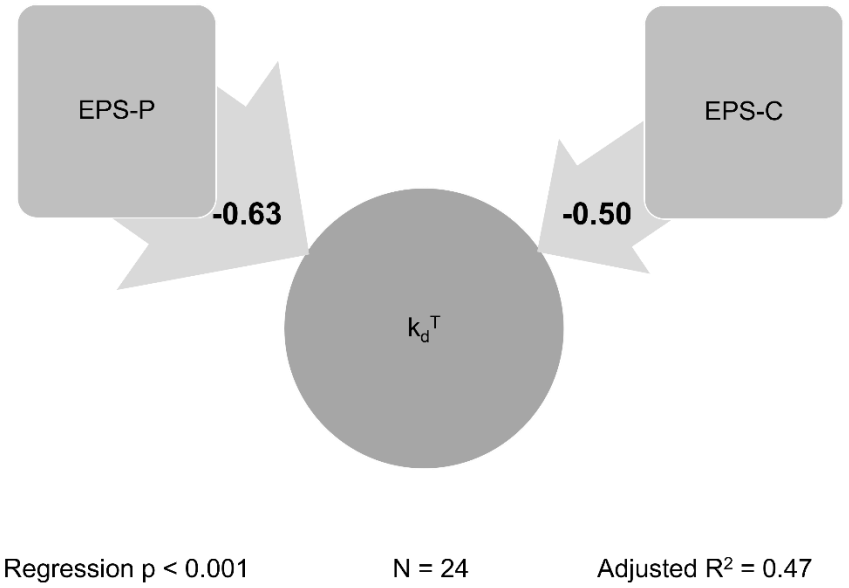

Figure 5-5: Graphical results of multiple linear regression analysis using uncorrelated predictor variables. Numbers within arrows represent the regression coefficient for each predictor variable. Bold numbers indicate that predictor was significant at $p < 0.05$. The corresponding regression p-value, adjusted r-squared, and sample size (N) are shown on the bottom of the graph. The variables were first standardized prior to regression analysis, so the parameter coefficients indicate the relative magnitude of the correlation with k_d. k_d = soil erodibility coefficient (cm hr^{-1} Pa^{-1}), $k_d^T = \ln[k_d]$; EPS-C = extracellular polymeric substances (EPS) carbohydrates (µg g-$soil^{-1}$); and EPS-P = extracellular polymeric substances (EPS) proteins (µg g-$soil^{-1}$).

5.2.3 Soil and Water Conditions During Erosion Testing

Akinola et al. (2019) showed erosion rates increased with increasing water temperature, relative to the soil temperature, while erosion rate was not affected by ST or WT if the two temperatures were equal. Therefore, steps were taken to ensure both ST and WT remained constant at 25°C; however, soil temperatures varied between 18.7°C to 20.7°C. While the difference between WT and ST did not differ significantly between treatments, the variation increased with increasing organic matter additions (Figure 5-6a). VWC in T4 was significantly higher compared to both T0 and T1 (Figure 5-6b).

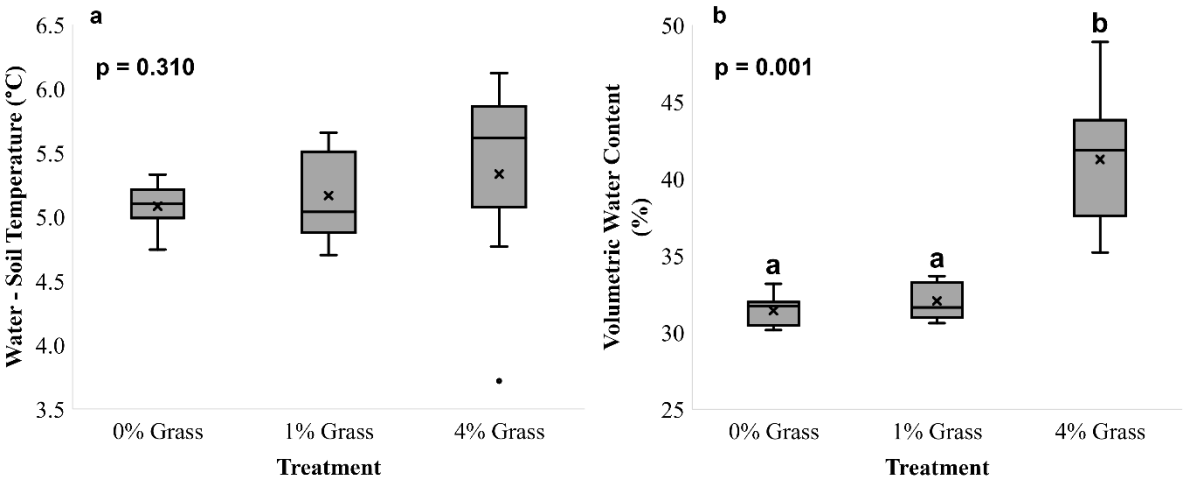

Figure 5-6: The difference between water and soil temperature (a), and volumetric water content (b) for each treatment at day 50. Letters denote statistically significant differences between each treatment pair (Wilcoxon rank sum test; $p < 0.05$), and the p-value on the top left denotes the Kruskal-Wallis p-value. The grey area of the plot spans the interquartile range while "x" and the inner solid black line represents the data mean and median, respectively. Outer dots represent outliers.

5.3 Discussion

5.3.1 Relationship Between OM Inputs, EPS, Soil Aggregate Stability, and the Soil Erodibility Coefficient

When broken down into its elementary mechanisms, soil aggregate breakdown can be caused by 1) soil slaking, the rapid disintegration of an aggregate due to the compression of trapped air during aggregate wetting; 2) differential swelling that causes microcracking in clayey soils; and 3) mechanical breakdown due to impact forces (e.g., raindrop impacts) (Le Bissonnais, 1996). In the present study, the fast-wetting procedure used to measure MWD was a representation of aggregate resistance to soil slaking. Stimulating microbial production of EPS through the addition of labile carbon significantly increased macroaggregate stability and resistance to slaking (Figure 5-2). The production of EPS proteins have largely been overlooked in their role in increasing soil aggregate stability; however, prior work has suggested that the negatively charged amino acids in proteins may make them more important for aggregate structure compared to carbohydrates due to the electrostatic bonds the charged sites create with multivalent cations (Laspidou & Rittmann, 2002).

The significant correlation between EPS-P and MWD in the present study (Table 5-1) supports this claim. Additionally, Redmile-Gordon et al. (2020) found that recent land use changes had a greater impact on soil EPS and aggregate stability compared to prior land uses, with recent inputs of C from perennial grassland contributing the greatest to EPS production and soil stability. The authors found both EPS proteins and carbohydrates were significantly correlated with soil MWD, but EPS proteins had the higher correlation coefficient ($R^2 = 0.30$ for EPS proteins vs 0.15 for EPS carbohydrates). While microbial biomass was not measured directly in the present study, other researchers have clearly demonstrated the role of microorganisms, particularly fungi, on aggregate stability as well (Lucas et al., 2014; Tang et al., 2011). Tang et al. (2011) found significant increases in stable large macroaggregates in soils amended with maize leaves (1 g per 100 g soil) compared to the control at every measurement time over a 40 day period. Lucas et al. (2014) found similar results to Tang and colleagues: vetch clippings and manure soil amendments significantly increased soil macroaggregate stability compared to the unamended control. The authors attributed this increase to the higher fungal:bacterial ratios measured in the vetch and manure treatments due to their relatively high levels of bioavailable organic carbon, as compared to the compost amendment and the control.

The soil used in this experiment was taken from a forested river floodplain, so the soil organic matter content, measured using the loss-on-ignition method, was already relatively high for T0 after the 50-day greenhouse maturation period (5.2% on average) even though no new OM was added. Nevertheless, adding labile OM to the soil significantly increased the measured SOM for T1 (5.5%) and T4 (6.6%) compared to the control following greenhouse maturation. This increase in SOM led to a reduction in the average soil erodibility coefficient of 25% and 61% for T1 and T4, respectively, (Figure 5-4), indicating the importance of labile OM for protecting soil from fluvial forces. The benefit of organic matter on sediment erodibility has been shown for benthic lake and lagoon sediments (Forsberg et al., 2018; Righetti & Lucarelli, 2007). Righetti and Lucarelli (2007) modified Shield's incipient motion curve by adding terms for sediment cohesive and adhesive forces; the authors found that the adhesion coefficient used in their model was strongly correlated with the organic matter content of the benthic sediment. Unlike prior research, the present study demonstrated that the increased soil resistance to fluvial erosion was linked to OM impacts on microbial activity, specifically EPS production. For the fluvial erosion tests, slaking was limited due to prior soil wetting; thus, this procedure can be considered a

representation of internal aggregate cohesion and particle resistance to detachment by flowing water. While EPS proteins appear to provide the backbone of soil stabilization and soil cohesion due to labile OM inputs (Table 5-1), it is shown that EPS carbohydrates are also correlated with increased soil resistance to fluvial erosion (Figure 5-5). Unlike the correlation coefficients, multiple linear regression tests for the significance of each independent variable while holding all other variables constant. As a result, the significant relationship found between EPS-C and k_d in the regression model points to within treatment changes in EPS-C having an impact on soil resistance to fluvial erosion.

The significantly lower EPS carbohydrate concentrations measured in T1 compared to T0 and T4 was surprising (Figure 5-3), but past studies where organic material was added to the soil environment have found similar results. For soil with 10% clay, temporary increases in EPS-C and microbial biomass were found in response to cellulose addition, a major component of grass clippings, by Olagoke et al. (2022). However, after a prolonged incubation (20°C for 80 days), the EPS-C content of the cellulose amended soil was lower than the control soil treatment while EPS-P remained high. In a study conducted by Tang et al. (2011), EPS carbohydrates in amended soil samples steadily decreased after day 20; however, carbohydrates were always significantly higher compared to the control samples. It is important to note that Tang et al. (2011) used a different extraction method compared to this experiment. Redmile-Gordon et al. (2014) found that the extraction method used by Tang and colleagues also co-extracted large amounts of intracellular biomass and extracellular SOC, which may have affected their measurement of EPS carbohydrates. Nevertheless, questions remain on why 1% grass clippings reduced the amount of EPS carbohydrates measured in T1. One possible explanation is related to two concepts: 1) EPS carbohydrates are vulnerable to degradative enzymes (Davies, 1999; Laspidou & Rittmann, 2002) and are regarded as labile carbon sources for bacteria (Goto et al., 2001; Van Duyl et al., 1999); and, 2) the carbon:nitrogen (C:N) of the grass additions. In a 2015 study conducted by Redmile-Gordon et al., soil samples mixed with relatively low C:N ratios (< 20 C:N) resulted in lower EPS-production efficiencies compared to relatively high C:N ratio substrates (100 C:N). In other words, while carbon additions promoted EPS production, the authors theorized that microorganisms shifted carbon investment towards the growth of microbial biomass when inorganic N was in surplus. The C:N ratio of the grass used in the present study, measured using an elemental analyzer-isotope ratio mass spectrometer (IsoPrime Ltd, Cheadle, UK), was 18. As a result, it is speculated

that once the readily available carbon provided by the grass clippings was consumed, the microbial community used EPS carbohydrates for cell maintenance/growth. The lower concentration of EPS-C in T1 could be explained by observations that fresh OM additions to soil tend to increase soil microbial biomass and short-term biomass fluctuations as compared to unamended treatments (Zelenev et al., 2005). This possible change in microbial biomass could have led to increased degradation of the EPS carbohydrate pool in T1 after the initial carbon amendment was depleted.

5.3.2 Volumetric Water Content

The soil samples in this study were placed in a shallow tray of water prior to erosion testing to maintain soil moisture and temperature. Therefore, a higher moisture content of T4 compared to both T1 and T0 (Figure 5-6b) was expected due to the greater mass of grass added at the beginning of the experiment. Avnimelech et al. (2001) note that the water content of flooded soils is positively correlated with organic carbon content. It is also interesting to note that the significant relationship between VWC and k_d was counter to what is typically found in the literature (Grabowski et al., 2011). Specifically, when soil type and other factors are equal, erosion rate generally increases as soil moisture content increases (Grabowski et al., 2011); however, VWC and k_d in Table 5-1 are inversely related. This relationship suggests that OM effects on soil aggregate stability and EPS in this study had a stronger impact on soil erodibility compared to the moisture content. This idea is supported by the significant positive correlation between VWC and SOM (Table 5-1). Similar biostabilization effects for high water content sediments have been described previously (Amos et al., 2004). Had VWC been held constant, the erosion rates of T1 and T4 may have been even lower than measured in this experiment.

5.4 Conclusions

By providing a source of readily available carbon in the soil, microbial production of EPS proteins was stimulated and remained for 50 days while EPS carbohydrates were more variable depending on the initial OM input amount. The lower EPS carbohydrate concentrations from small amounts of initial OM inputs seem to have been due to the stimulation of microbial activity and utilization of EPS carbohydrates in the soil. The significant correlations between EPS proteins, MWD, and k_d found in this study point to the dominant role EPS proteins play in improving soil stabilization and soil resistance to fluvial erosion due to labile OM inputs. Overall, treatments with

added organic matter, T1 and T4, reduced the average soil erodibility coefficient by 25% and 61% and increased the soil mean weight diameter by 16% and over 100% compared to the control treatment, respectively. This research supports the hypothesis that labile organic matter additions to riparian streambank soils, in part through stimulated production of extracellular polymeric substances by soil microorganisms, can significantly improve soil resistance to fluvial erosion and slaking.

Chapter 6. Artificial Roots and Soil Microorganisms Increase Streambank Soil Resistance to Fluvial Erosion

Results from the Chapter 3 mini-JET study revealed some interesting and unexpected relationships between synthetic fibers and soil erodibility. In Chapter 4, it was found that roots extending out of the streambank face increase near-bank turbulent stress but reduce near-bank velocity, and thus wall shear stress, compared to the bare (unvegetated) boundary. Given that both shear stress (e.g., Flanagan & Nearing, 1995; Larsen et al., 2009) and turbulence (e.g., Yang & Nepf, 2018; Zhang et al., 2020) can drive fluvial entrainment, the cumulative impact of exposed roots on streambank erosion rates, using velocity/turbulent stress results alone, is unclear. Chapter 5 showed that adding organic matter to soil can lead to significant reductions in soil erosion rates, in part due to the increased production of the protein component of extracellular polymeric substances. While each of these studies provide insight into the impact of roots and microorganisms on streambank soil erosion, questions remain regarding the relative contribution of different root mechanisms and soil microorganisms on streambank soil resistance to fluvial erosion.

To compare the relative effects of roots binding soil, root boundary layer impacts, and stimulation of microbial EPS production on soil erodibility, three flume walls were constructed to simulate unvegetated streambanks, as well as streambanks with herbaceous and woody roots (Figure 4-1b-d). Additionally, soil treatments were created to represent unamended and organic matter amended soil either without roots (bare soil), with synthetic roots, or with living roots (*Panicum virgatum*). Synthetic fibers in the soil represent the physical binding mechanism of plant roots. Organic matter amendments, in the form of dried and crushed grass clippings, represent the stimulation of soil microorganisms and exudation of "sticky" organic substances through the input of a readily decomposable carbon source. The following hypotheses were addressed: 1) fibers extending out of the streambank face increase soil erosion rates due to fiber effects on the boundary layer; 2) as root length density increases for both live and synthetic fibers, fluvial erosion rates decrease; 3) soil microbes enhance soil resistance to fluvial erosion through production of extracellular polymeric substances; and 4) live roots provide the most reduction in erosion rates due to soil binding, EPS production, and the bonding of aggregates to roots surfaces.

6.1 Methods

6.1.1 Experimental Setup

To quantify the processes that drive soil erosion rates, a factorial combination of four root treatments (no roots (NR), flexible synthetic roots (FSR), rigid synthetic roots (RSR), live roots (LR) from switchgrass (*Panicum virgatum*)) and two soil amendments (unamended and organic matter amended (OM)) were used to represent different root mechanisms (Table 6-1). A randomized complete block design was used for the experimental setup with six replicates of each treatment: 1) NR, control; 2) NR+OM; 3) FSR; 4) FSR+OM; 5) RSR; 6) RSR+OM; 7) LR; and 8) LR+OM). The NR treatment was replicated three times within each block. Silver maple trees (*Acer saccharinum*) were also planted during the greenhouse phase of this experiment; however, these plants did not survive the transplantation and are not considered.

Switchgrass plugs were purchased from Wicklein's Water Gardens and Native Plants (Baltimore MD, USA); plugs were stored and watered in a greenhouse prior to planting. Amended soil samples were mixed with 1 g dried and pulverized grass clippings (<1 mm) per 100 g soil. Based on the carbon content of the grass clippings (40.6%) and surface area of the growth containers 1 g grass per 100 g soil corresponds to 96 g C/m^2. For comparison, a review conducted by Cotrufo & Lavallee (2022) collated prior research and reported that carbon inputs from plant roots (root exudates and root turnover) have been measured as 3 to 400 g C/m^2/year for grasslands and 120 to 960 g C/m^2/year for forests. Flexible synthetic root samples were represented by 0.3 mm polyester thread (Coats and Clark Dual Duty XP®, Charlotte NC, USA), 1.0 mm polyester cords (PandaHall, ShenZhen, China), and 2.0 mm polyester cords (Bohemian Findings, Prince Edward Island, Canada). Braided fishing line (0.38 mm, Pure Fishing, Inc., Spirit Lake, IA) and plastic plant stems (1.0 mm and 2.0 mm, Bloom Room, San Francisco CA, USA) were used for the rigid synthetic root samples.

Table 6-1: Experimental treatments and the root mechanisms they represent.

	No Roots (NR)	Synthetic Roots		Live Roots (LR)
		Flexible (FSR)	Rigid (RSR)	
Unamended soil	Control	Fibers binding soil		Fibers binding soil Aggregates sticking to root surfaces Stimulating EPS production
Amended soil (+OM)	Stimulating EPS production	Fibers binding soil Stimulating EPS production		Fibers binding soil Aggregates sticking to root surfaces Stimulating EPS production

Silt loam soil (16% clay, 27% sand, and 57% silt) was collected from the New River floodplain near Whitethorne, VA (37.192616°, -80.573133°). The soil was passed through a 2-mm sieve, steam sterilized for two hours at 100°C, and then stored in covered 210-L bins. The day before experiment setup, steam sterilization was repeated to ensure limited microbial community colonization of soil. For this experiment, growth containers like those described in Chapter 5, section 5.1.1 (Figure 6-1a) were used. Thin slots of the containers were cut off the sides (Figure 6-1b), effectively dividing the pipe into three equally spaced subsections to allow subdivision of each sample while minimizing soil disturbance. Prior to soil compaction and vegetation planting, SpinOut® (SePRO Corp., Carmel, IN), a root-growth inhibitor, was painted in the pipe interior and at least 2 cm away from the pipe drainage holes. This allowed the roots to grow down and out through the nursery fabric mesh, like natural streambank conditions. All samples were compacted to a bulk density of 0.95 g cm^{-3}.

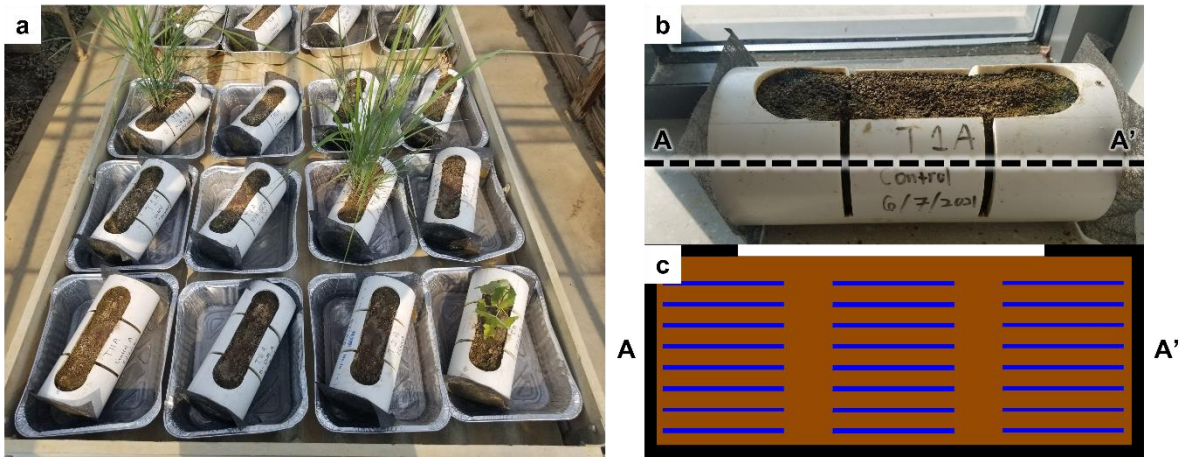

Figure 6-1: a) Greenhouse setup and growth containers for one of six blocks. b) Close up of soil compacted in growth container showing equally spaced sections. c) Schematic of inside of growth pipe (not drawn to scale). Synthetic roots (represented as blue lines) were compacted in random orientations in eight layers within each subsection of the container. Silver maple trees (*Acer saccharinum*) were also planted during the greenhouse phase of this experiment; however, these plants did not survive the transplantation and are not considered.

After weighing out the desired soil mass, nine equal layers of the soil (i.e., soil lifts) were compacted into the pipe for each sample. For OM amended samples, grass clippings were mixed into the soil prior to lift placement and compaction. Following soil compaction, switchgrass plants were removed from the potting soil; the roots were trimmed to ~2 cm in length and rinsed thoroughly with water to remove excess rooting substrate. Switchgrass plugs were then planted by removing the topsoil layer in the center of the pipe in between the two thin slots (Figure 6-1b), placing the plug, and then replacing the soil. All brown shoots were removed following planting and samples were watered immediately. Synthetic root samples were "planted" at root length densities (RLD) between 0.67 to 2.8 cm/cm^3 within each pipe subsection. To do this, following the compaction of one soil layer, $1/8^{th}$ of the total root length needed to reach the desired RLD was placed in each subsection. Fibers were placed at random orientations horizontally along each soil lift within the subsections; care was taken to avoid placing fibers directly underneath the thin slots (Figure 6-1c). Once fibers were placed, another soil layer was compacted on top of the fibers and the process was repeated.

After all treatments were set up, the soil containers were placed in 8.5-cm deep aluminum trays to allow watering by capillary action and allowed to mature in a greenhouse. The containers were arranged in blocks, with one container for each treatment randomly placed within each block. Watering by capillary action was done to reduce the effect of soil wetting/drying cycles on measured soil erosion, particularly in the OM-amended and live rooted samples. Sample trays were never allowed to dry out, and approximately 2 cm of water was always in the tray; therefore, the soil moisture remained consistent across all treatments and blocks throughout the study.

The randomized complete block design was used to account for the spatial and temporal variation of primarily sunlight and temperature in the greenhouse. Block placement in the greenhouse was staggered between June 7th, 2021, and August 28th, 2021. Erosion testing and root sieving for each block required 1-2 weeks, so block staggering was done to ensure that switchgrass samples did not become root-bound during greenhouse maturation. Additionally, degree days, the number of days where the average air temperature was above a specified temperature, were monitored to ensure blocks received similar heating time periods throughout the sample growth period. Each block was in the greenhouse for 31 to 40 degree-days above 30°C prior to erosion testing and subsequent soil analyses. Over the course of the experiment, temperatures in the greenhouse ranged from 30 to 50°C during the day and 17 to 24°C throughout the night. Following the growth period, samples were moved to a temperature-controlled lab and allowed to sit in trays of water overnight at the same depth used in the greenhouse setup. Digital heaters (50-W, Nova Pet Supplies, Guangdong China) were placed in the water trays and used to keep soil temperature constant at 22°C (Akinola et al., 2019). This ensured that all samples were at similar temperatures and moisture contents prior to being tested in the flume.

6.1.2 Erosion Testing Procedure

The flume tank was filled with tap water from the Blacksburg-Christiansburg VPI Water Authority; this water was kept at a constant temperature of 22°C using three 1000-W aquarium heaters (True Temp T-1000, Transworld Aquatic Ent., Inglewood, CA, USA). The actual water temperature, measured directly using the ADP, varied between 22.4°C and 23.7°C for all flume runs. The flume bed slope was held constant at 0.1%.

Immediately prior to erosion testing, a Decagon 5TM soil probe (Decagon Devices, Inc. Pullman, WA, USA) was used to measure volumetric water content (VWC) and soil temperature.

To ensure minimum disturbance of synthetic rooted samples, all VWC and soil temperature measurements were taken between the thin slots on both sides of the growth containers (Figure 6-1b). Immediately prior to erosion testing, each sample was cut into three subsamples using the thin slots as a guide. Each subsample was tested using a different flow rate: 19, 24, or 40 L s^{-1}. The subsample face was completely covered with water during erosion testing.

Subsamples were placed in the flume and pushed flush with the boundary surface. The subsample was covered before running the flume to prevent the application of hydraulic shear on the soil surface as the flow developed in the channel. Erosion testing started once the flow became fully developed (about 90 seconds) and the subsample cover was removed. Erosion testing lasted for 10 minutes, or until all the soil had been eroded away, whichever came first. The distance of the ADP probe head to the soil surface was monitored via the Vectrino software, and the soil core was advanced back to the initial position, flush with the wall, after every millimeter of erosion (Akinola et al., 2019). This process was repeated for all three soil subsamples using a different flow rate. Erosion rate was determined as the total depth of soil eroded during testing divided by the erosion time.

For the erosion testing, soil subsamples were matched with their respective simulated streambank boundary (Table 6-2). Boundary and subsample type were matched to ensure consistent boundary conditions throughout the length of the flume. To quantify the impact of boundary conditions on soil erosion rates, erosion testing was conducted on one of the three no-root samples using each boundary type (Table 6-2). Statistically comparing the ER for the three no-root samples allowed for the influence of boundary type to be measured directly.

Table 6-2: Erosion testing was done using the following simulated wall and subsample combinations. Different walls were used for each subsample depending on the root type to ensure consistent boundary conditions throughout the length of the flume. A no-root sample was run on all three boundaries to determine if the constructed wall influenced measured erosion rates. SW = sand wall, FRW = flexible rooted wall, RRW = rigid rooted wall, NR = no roots (bare soil), OM = organic matter added, FSR = flexible synthetic roots, RSR = rigid synthetic roots, and LR = live roots [switchgrass (*Panicum virgatum*)].

Boundary	Samples Tested				
Sand wall	SW-NR	NR + OM			
Flexible root wall	FRW-NR	FSR	FSR + OM	LR	LR + OM
Rigid root wall	RRW-NR	RSR	RSR + OM		

The velocity time series data from the ADP were processed in R following the procedure outlined in Chapter 5, section 5.1.2. Following data processing for each flume run, the turbulent stress was calculated using turbulent kinetic energy (equation 4.1) and one component of Reynolds stress, τ_{yx} (equation 5.2). Direct measurements of boundary shear stress were not possible in this experiment using the available equipment given the constant erosion of the soil sample and accumulation of sediment in the water column. Turbulent kinetic energy (TKE) and Reynolds stresses are commonly used to predict fluvial entrainment of soil/sediment (Biron et al., 2004; Hopkinson & Wynn-Thompson, 2012; Yang & Nepf, 2018). However, as shown in Chapter 4, the roots protruding out of the streambank result in lower near-bank velocity but higher near-bank turbulence. How these competing effects influence overall soil erosion rates was explored in this chapter.

6.1.3 Extracellular Polymeric Substances and Soil Organic Matter Measurements

After testing each subsample in the flume, if soil remained, about 100 g of soil was broken apart by hand and placed in a clean metal pan. This process was repeated for the remaining two subsamples per sample; all collected soil was placed in the same metal pan. For switchgrass-planted samples, roots were removed by hand from each collected pan sample for 20 minutes; collected roots were preserved in a labeled mason jar filled with 50% ethanol. About 50 g of

collected soil was moved to 50-ml Nalgene® bottles and stored at -18°C for later EPS analysis. The remaining soil was air-dried and sieved through a 2-mm sieve and used for soil organic carbon analysis (SOC; Walkley-Black method; procedure outlined by FAO, 2020).

The EPS extraction procedure used in this study follows methods and procedures described in Chapter 5. Soil organic matter (SOM) for each sample in this experiment was estimated by assuming 58% of SOM is soil organic carbon. After 7 – 8 weeks in the freezer, the frozen soil was thawed at 4°C, homogenized, and added to centrifuge tubes in triplicate at 0.5 g dry weight equivalent. To remove soluble EPS and extract bound EPS, 5 mL of $CaCl_2$ (4°C, pH 7) and phosphate-buffered saline solution (4°C, pH 7) were used, respectively. Bound EPS extractants were collected and measured spectrophotometrically for carbohydrates and proteins. Proteins were estimated using the modified Lowry assay, corrected for removal of humic substances (Frolund et al., 1996; Redmile-Gordon et al., 2013). Total carbohydrates was measured using the phenolesulphuric acid method (DuBois et al., 1956).

Soil not collected for organic carbon or EPS analyses was either discarded or washed to collect any living roots for switchgrass-planted samples. Root diameter, root length density (RLD), and root volume ratio (RVR) were measured using the 2015 WinRhizo™ Tron and 2003 WinRhizo™ Pro systems (Regent Instruments Inc., Québec, Canada). Root diameter classes included: very fine (< 0.5 mm), fine (0.5-2.0 mm) and small (2-5 mm). Given the relatively small pipe volume and the high root growth, RLD and RVR were assumed to be equal for all subsections within one growth pipe.

6.1.4 Statistical Analysis

Initially, following erosion testing, the excess shear stress equation (Moody et al., 2005) was going to be used to calculate the critical shear stress (τ_c) and soil erodibility coefficient (k_d) for each sample. To calculate τ_c and k_d, where τ_c is the stress required to initiate soil motion and k_d is the slope of the regression line, linear regression is conducted on the measured erosion rates vs. the respective turbulent stress. However, this linear model did not provide an adequate fit for 19 out of the 60 samples tested (32%). Given the poor fit for 1/3rd of the data, neither τ_c nor k_d were calculated. Instead, the measured erosion rate at each flume flow rate (19, 24, and 40 L s^{-1}) was used individually in all analyses.

As described in section 5.1.2, a no-root sample was tested using all three boundary conditions (SW, FRW, and RRW) to determine if the wall type influenced measured erosion rates. Thus, the nonparametric Friedman's test and Conover's test (Pereira et al., 2015) were used to analyze the effect of boundary type on the ER of SW-NR, FRW-NR, and RRW-NR treatments (hypothesis 1). Next, Spearman rho correlation coefficients were used to explore relationships between RLD (hypothesis 2) or EPS (hypothesis 3) and soil erosion rates. To investigate the relative impact of root type (flexible synthetic vs. rigid synthetic vs. live), RLD, and EPS on soil resistance to fluvial erosion, boundary effects were factored out. Specifically, the percent change between the ER for a specific sample and the median ER for the NR treatment was calculated within each boundary (EQ 6-2) as

$$\boldsymbol{Percent\ Change} = \frac{\boldsymbol{ER_i - median\left(ER_{NR_j}\right)}}{\boldsymbol{median\left(ER_{NR_j}\right)}} \tag{6-1}$$

where ER is the erosion rate; j = SW, FRW, or RRW; i = NR+OM if j = SW; i = FSR, FSR+OM, LR, or LR+OM if j = FRW; and i = RSR or RSR+OM if j = RRW. Subtracting the median NR within each wall allows for the relative influence of fibers and EPS on soil erosion rates to be analyzed by removing changes in erosion rates caused by the different boundary types.

Finally, the question of changes in erosion rates under different treatment and boundary combinations needed to be considered. To investigate interactions between boundary type (SW vs. FRW vs. RRW; hypothesis 1), root type (FSR vs. RSR vs. LR; hypotheses 2 & 4), soil type (unamended vs. amended; hypothesis 3), and soil erosion rates, all ER data were plotted vs. treatment. The nonparametric Friedman's test and Conover's test (Pereira et al., 2015) were used to statistically analyze these differences.

6.2 Results and Discussion

6.2.1 Influence of Protruding Roots on Soil Erosion Rates (Hypothesis 1)

While the ER of NR samples did not vary significantly at any of the measured flow rates (Figure 6-2a-c), the median erosion rate tended to increase from SW-NR, FRW-NR, and RRW-NR. Specifically, the median erosion rate for RRW-NR was five to ten times higher than SW-NR depending on the flow rate used; the median ER for FRW-NR was two to eight times higher than SW-NR. The generally higher erosion rates for RRW-NR and FRW-NR were expected given the significantly higher near-bank turbulent stress calculated for the RRW and FRW compared to the

SW in Chapter 4 (Figure 4-5). Higher sediment erosion is generally associated with higher turbulent stress produced by sparsely spaced vegetation elements (Nepf, 2012a; Zhang et al., 2020). For example, when using rigid circular rods representing seagrass canopies, Zhang et al. (2020) found that near-bed turbulence increased and net sediment deposition decreased within a sparsely-spaced simulated meadow (260 rods m^{-2}) compared to bare soil. At various intertidal field sites within the Netherlands, van Katwijk et al. (2010) found that meadows with low vegetation cover (< 120 shoots m^{-2}) at relatively muddy sites increased the erosion of fine sediments/OM compared to nearby unvegetated sites.

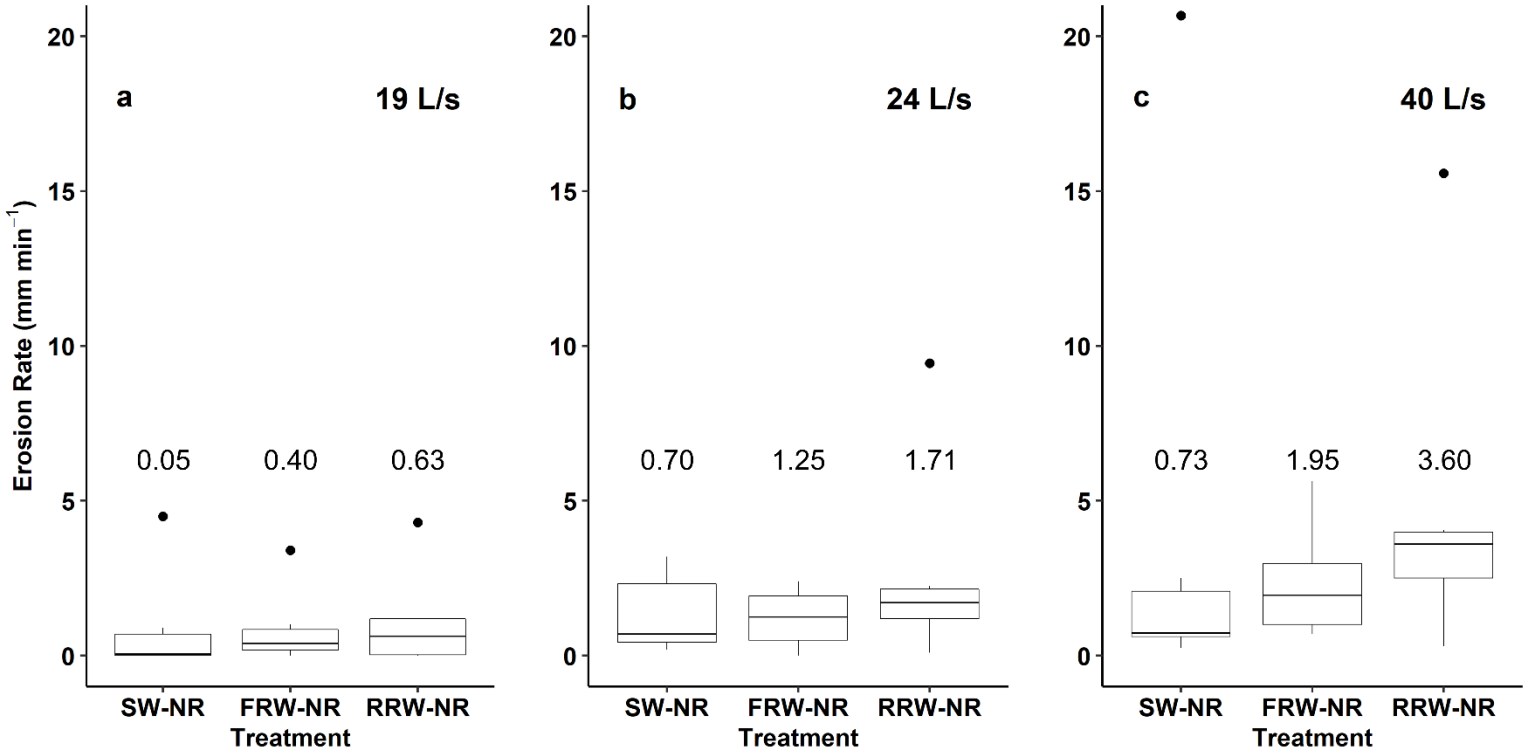

Figure 6-2: Measured erosion rates using flume flow rates of a) 19 L s^{-1}, b) 24 L s^{-1}, and c) 40 L s^{-1} for each no-root (NR) treatment (n = 6). The white area of the plot spans the interquartile range while the inner solid black line represents the median. Numbers above each treatment are the median ER values. Outliers are indicated by filled circles. SW = sand wall; FRW = flexible root wall; RRW = rigid root wall.

Chapter 4 showed that both the FRW and RRW produced significantly higher near-bank turbulent stress compared to the SW (Figure 4-5), suggesting higher near-bank turbulence. On the other hand, both rooted boundaries also had significantly lower near-bank velocities compared to the SW (Figure 4-4), indicating lower wall shear stress. However, the results shown in Figure 6-2 support prior work that has shown that higher near-surface turbulence, rather than lower near-surface velocity, plays an important role in predicting soil erosion/sediment transport potential (Yang & Nepf, 2018). Given the small sample size of the present study and lack of statistically significant treatment effects, further work should be done to confirm these relationships.

6.2.2 Root Length Density Impacts on Fluvial Erosion Rates (Hypothesis 2)

After accounting for the influence of boundary type on sample erosion rates by calculating the percent change, the relative influence of fiber type (live vs. rigid synthetic vs. flexible synthetic), soil microorganisms (EPS production), and their interactions could be compared directly. The percent change was used to explore the impact of RLD on the erosion rates of rooted samples in Figure 6-3a-c. Depending on the flow rate, soil samples with FSR, RSR, and LR reduced median erosion rates by 30-72%, 36-64%, and 95-100%, respectively, compared to the corresponding bare soil treatment. On the other hand, NR+OM, FSR+OM, RSR+OM, and LR+OM treatments reduced median ER by 41-100%, 86-100%, 96-100%, and 95-100%, respectively. The RLD used for the synthetic rooted samples ranged from 0.67 to 1.30 cm cm^{-3} and 1.13 to 2.80 cm cm^{-3} for RSR and FSR, respectively. Living roots exceeded the "planted" RLD for the synthetic root samples, ranging from 2.11 to 8.27 cm cm^{-3} in unamended soils and 3.75 to 13.5 cm cm^{-3} in OM amended soils.

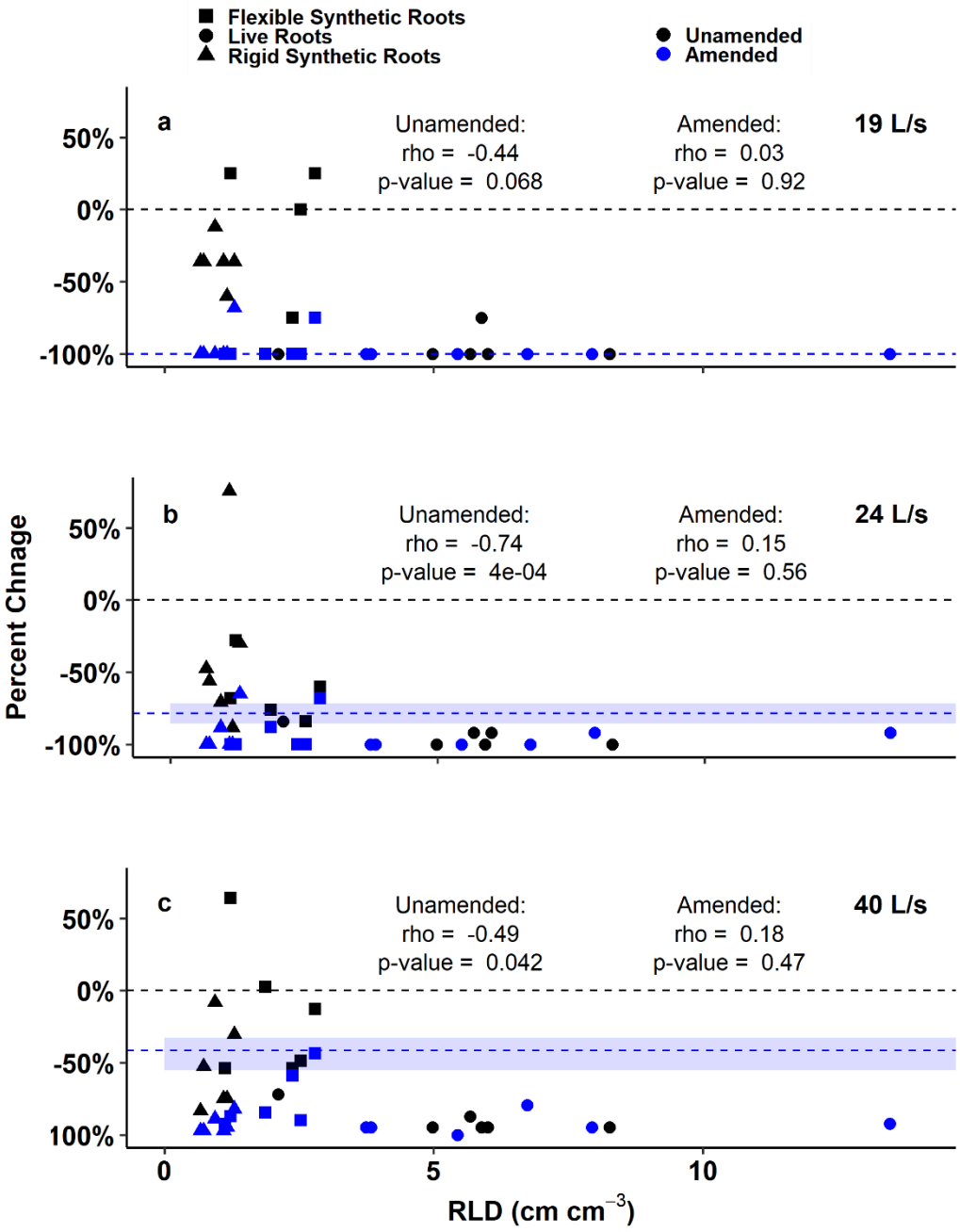

Figure 6-3: Percent change in erosion rate from median no-root soil treatments plotted against root length density (RLD) for the a) 19 L s^{-1} flow rate, b) 24 L s^{-1} flow rate, and c) 40 L s^{-1} flow rate. The Spearman rho correlation coefficients and corresponding p-values are shown for both unamended and amended soil treatments with roots (synthetic and live). The black dashed line at zero represents the median value for no-root soil controls. The blue dashed line and the shaded blue area represent the median and interquartile range for the no roots, organic matter amended treatment (NR+OM; n = 6).

Root length density was significantly correlated with the ER of unamended soil treatments with roots, regardless of flow rate (FSR, RSR, and LR; Figure 6-3a-c). A similar relationship between ER and RLD was not found when OM was added to the soil (Figure 6-3a-c). Therefore, while fiber density alone can aid in stabilizing soil and reducing erosion compared to bare soil, the fibers become less important once soil microorganisms are stimulated through organic matter inputs. This finding is counter to previous findings that show roots, particularly fine roots, (Burylo et al., 2012; De Baets et al., 2007) play the dominant role in increasing soil resistance to fluvial erosion. By stimulating microbial production of EPS, the present study shows that even low RLD samples (0.67 cm cm^{-3} to 2.8 cm cm^{-3}) can have a significant effect on soil erodibility.

Figure 6-3 shows that live roots and organic matter amended treatments appear to require a higher turbulent stress to initiate soil erosion. The median erosion rate was zero for FSR+OM, RSR+OM, or LR+OM until the 40 L s^{-1} flume flow rate was used. Similarly, median erosion was zero for NR+OM and LR until a flow rate above 24 L s^{-1} was used. While critical shear stress could not be calculated directly (see section 6.1.4), preventing erosion until higher applied forces are used is indicative of soil samples with higher critical shear stresses. Therefore, it can be inferred that live roots and organic matter amendments increased soil resistance to fluvial erosion by, in part, increasing the stress required to initiate soil erosion. Chapter 3 and prior studies have also measured higher critical shear stresses in root-permeated soils compared to bare soils (Khanal & Fox, 2017; McNichol et al., 2017).

The reduction in ER compared to bare soil for NR+OM appears to diminish at higher flow rates and higher corresponding turbulent stresses. Specifically, NR+OM had 100%, 79%, and 41% lower median erosion rates at 19 L s^{-1}, 24 L s^{-1}, and 40 L s^{-1}, respectively, compared to bare soil. On the other hand, the presence of FSR and RSR corresponded to reductions in median ER by 36% to 38%, 52% to 72%, and 31% to 64% at 19 L s^{-1}, 24 L s^{-1}, and 40 L s^{-1}, respectively, compared to bare soil. In other words, the benefit provided by fibers alone in the soil did not diminish at higher flow rates. This result highlights potential differences in the mechanisms by which fibers and OM-amended soil increase soil resistance to erosion. While OM amendments and the corresponding EPS production (see Figure 6-4a-c) may lead to a higher critical shear stress, fibers in the soil appear to reduce the total amount of soil eroded over a given time, regardless of the flow rate. In summary, the addition of fibers to soil appear to decrease the soil erodibility

coefficient, or the volume of soil eroded over time. Whether this trend would continue at higher flow rates/turbulent stresses is unclear and is worthy of further study.

6.2.3 EPS Protein Production Drives Reduction in Fluvial Erosion Rates (Hypothesis 3)

Inputs of 1g grass clippings per 100 g soil had significant ($p < 0.001$) but opposite effects on EPS proteins and EPS carbohydrates. Specifically, OM-amended soil contained more EPS proteins (average of all amended samples = 147.2±39.9 µg g-soil^{-1}) compared to unamended soil (70.8±28.5 µg g-soil^{-1}). However, EPS carbohydrates were significantly lower in OM-amended samples (357.5±70.9 µg g-soil^{-1}) compared to unamended samples (409.3±56.8 µg g-soil^{-1}). This increase in EPS proteins was positively correlated with reduced soil erosion rates for OM-amended soils (Figure 6-4a-c) at all flume flow rates. Depending on the flow rate, amended soil treatments reduced the ER by 41% to 100% compared to the bare soil controls. Similar relationships between EPS proteins and soil erosion rates were found in Chapter 5 (Figure 5-5), further emphasizing the quick stabilizing potential of proteinaceous extracellular substances (Moon et al., 2016).

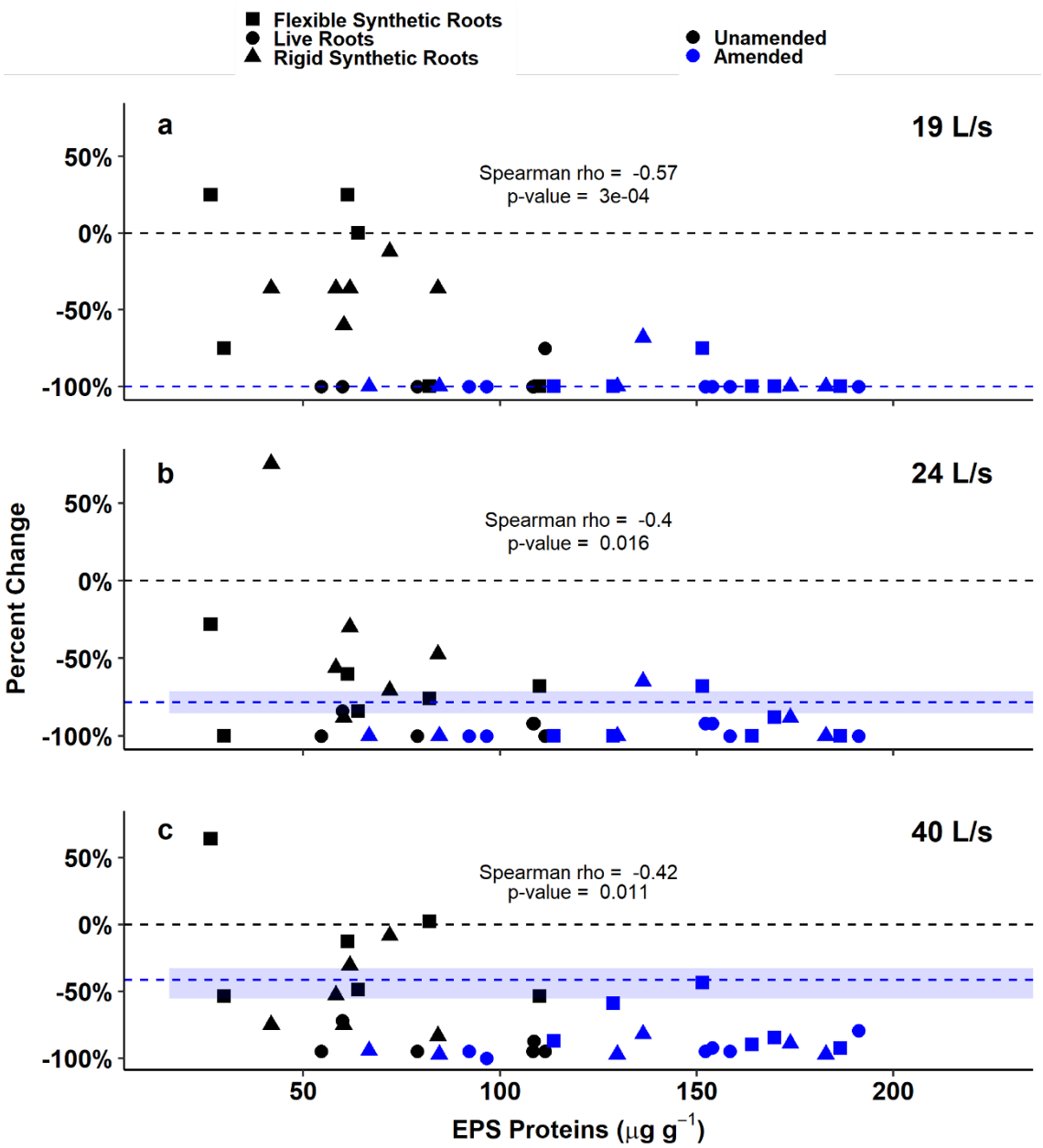

Figure 6-4: Percent change in erosion rate from median no-root soil treatments plotted against the protein component of extracellular polymeric substances (EPS proteins) for the a) 19 L s^{-1} flow rate, b) 24 L s^{-1} flow rate, and c) 40 L s^{-1} flow rate. The Spearman rho correlation coefficients and corresponding p-values are shown for root-permeated treatments (synthetic and live). The black dashed line at zero represents the median value for no-root soil controls. The blue dashed line and the shaded blue area represent the median and interquartile ranges for the no roots, organic matter amended treatment (NR+OM; n = 6).

While EPS proteins were higher in LR compared to the other unamended soil treatments, this difference was not statistically significant. Studies that have looked at the influence of longer term (e.g., >2 years) grassland conversions on extracellular substances found significant increases compared to bare soil (Redmile-Gordon et al., 2020). Wang et al. (2015, 2014) determined that root-biochemical effects explained 7%, 15%, and 14% of the variance in soil detachment for 1-yr, 7-yr, and 24-yr restored natural grasslands, respectively. These results suggest that root biological effects (i.e., EPS production) increase in significance over time as vegetation matures and roots turn over, a process that is not seen in a short-term greenhouse study where root growth is limited and little to no seasonal plant changes like fine root turn over or litter decomposition occurred. In addition, carbon input rates vary with plant species, so this study is limited by considering *Panicum virgatum* alone.

6.2.4 Combined Root and Microbial Effects (Hypotheses 1-4)

Figure 6-5a-c represents how the interactions between boundary type (SW vs. FRW vs. RRW; hypothesis 1), root type (FSR vs. RSR vs. LR; hypotheses 2 & 4), and soil type (unamended vs. amended; hypothesis 3) influence soil erosion rates at each flume flow rate. Synthetic fibers alone never had a significant effect on soil erodibility when compared to the bare soil controls. Even though RSR and FSR tended to reduce erosion rates compared to RRW-NR and FRW-NR, respectively (Figure 6-3a-c), the ER for RSR and FSR tended to be higher than SW-NR at all flow rates used in this study (Figure 6-5a-c). This result highlights two contrasting impacts of roots on soil erosion found in this study. Sparsely spaced roots extending out of the streambank face increased soil erodibility (Figure 6-2); however, roots in the soil provided additional protection against erosive forces when compared to bare soil tested under the same boundary condition.

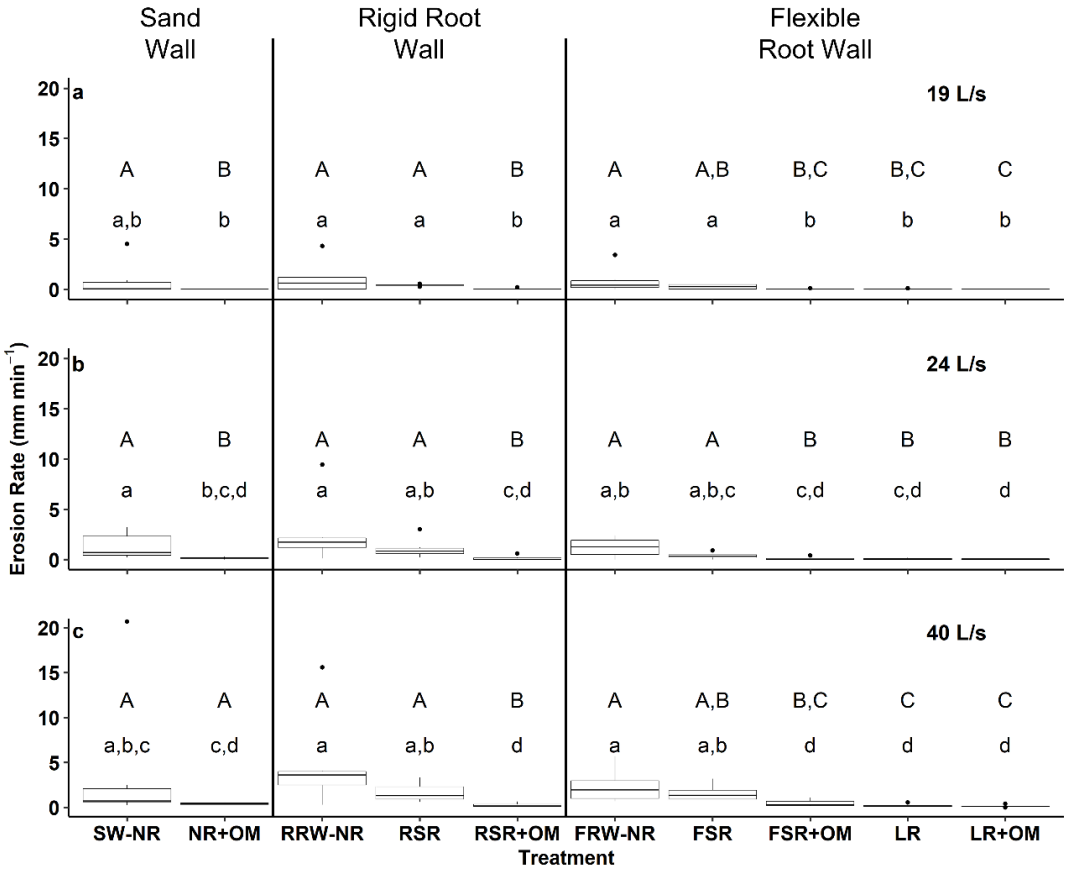

Figure 6-5: Measured erosion rates for each treatment tested at the flume flow rate of a) 19 L s^{-1}, b) 24 L s^{-1}, and c) 40 L s^{-1}. Uppercase letters denote statistically significant differences within each boundary layer type while lowercase letters denote statistically significant differences between all treatments tested at the same flow rate (α <0.1; Conover's test). The white area of the plot spans the interquartile range while the inner solid black line represents the data median. SW = sand wall; FRW = flexible rooted wall; RRW = rigid rooted wall; NR = no-roots; OM = organic matter amended; LR = live roots (*Panicum virgatum*); FSR = flexible synthetic roots; and RSR = rigid synthetic roots.

While 1% OM additions (NR+OM) had a greater impact on soil erosion rates compared to fibers alone, the erosion rate for this treatment was not significantly lower than for SW-NR at a flume flow rate of 40 L s^{-1}. Only LR, LR+OM, FSR+OM, and RSR+OM significantly reduced erosion rates compared FRW-NR and RRW-NR at all flow rates (Figure 6-5a-c). Additionally, excluding the 19 L s^{-1} flow rate, these treatments also had significantly lower ER compared to SW-NR even though the rooted boundaries tended to increase overall erosion rates compared to the unvegetated streambank (Figure 6-2a-c). Therefore, it is through a combination of fibers binding soil and stimulating microbial production of EPS through OM inputs that produce similar reductions in erosion rates compared to living roots. This similar reduction in erosion occurred even though the synthetic rooted treatments had lower RLDs (0.67 to 2.80 cm cm^{-3}) compared to the living roots (2.11 to 13.5 cm cm^{-3}). The lower RLD and differing boundary effects point to a possible synergistic relationship between root fibers and EPS, where EPS production increases the benefit of fiber reinforcement, that has been shown to increase soil stability in past studies (Chen et al., 2022). It is possible that if higher RLDs had been used for the synthetic rooted treatments, even lower erosion rates would have occurred. However, RLD for the synthetic rooted samples were comparable to Wynn et al. (2004) who measured root properties along 25 streambanks in Southwest Virginia, USA. The authors found the total RLD to vary approximately between 0.5 to 3 cm cm^{-3} and 0.5 to 8.5 cm cm^{-3} for forested and herbaceous buffers, respectively, depending on depth.

LR and LR+OM produced identical erosion rates; this similar reduction in ER between LR and LR+OM was likely caused by the high root growth experienced by those treatments. The high root growth likely contributed greatly to reducing erosion rates to zero or near zero for both treatments at all flow rates, possibly overshadowing any additional protection provided by OM inputs. Nevertheless, LR+OM appeared to start eroding at a higher applied turbulent stress compared to LR (Figure 6-3, Figure 6-4, and Figure 6-5), indicating that OM inputs still had an influence on erosion rates even in a high root growth environment.

6.3 Conclusions

This study sought to quantify the root and microbial mechanisms responsible for influencing soil resistance to streambank fluvial erosion. This is the first study to consider how the combination of root binding effects, microbial production of EPS, and root effects on the boundary layer could

influence soil erodibility in a streambank setting. Additionally, while the role of labile organic matter and EPS production in increasing soil cohesion and soil resistance to fluvial erosion has been shown before, the combined effects of artificial fibers plus labile OM have not been explored in this context.

Exposed fibers on constructed streambanks tended to increase the erosion rates of bare soil samples. This result supports that higher near-bank turbulence, rather than lower near-bank velocity, plays an important role in predicting soil erosion/sediment transport potential. Regardless of flow rate, both flexible and rigid synthetic roots tended to increase soil resistance to erosion compared to bare soil. While stimulating microbial production of EPS proteins through labile organic carbon inputs had a greater effect compared to root binding alone, this effect appears to diminish as flow rate (and the corresponding turbulent stress) increases. When stimulated through the incorporation of grass clippings, microbial production of EPS, in combination with synthetic fibers, reduced soil erosion rates comparable to treatments with living roots. This result suggests that an abundance of roots, particularly very fine roots, were not necessary to increase soil resistance to fluvial erosion when soil microbes were also stimulated through organic matter inputs. EPS production was not significantly increased in vegetated samples without additional OM inputs, as compared to unamended soil, indicating vegetated samples did not have sufficient time to increase soil cohesion through the stimulation of microbial activity and/or release of root exudates prior to erosion testing. Over time, as plants grow, turn over, and add labile organic matter to the soil environment, we hypothesize that the role of soil microorganisms and root exudates would increase and reduce erosion rates further.

In conclusion, this study provided evidence that, while sparsely spaced exposed roots may increase soil erosion rates due to impacts on the boundary layer, the net effect of fibers with root length densities as low as 0.7 cm cm^{-3} and organic matter inputs protect soil from fluvial erosion through root binding and microbially stimulated EPS production. EPS production appeared to increase the critical shear stress required to initiate soil erosion, while synthetic fibers alone provided a base reduction in soil erodibility, regardless of the flow rate used. This work highlights how the synergistic relationship between root fibers and soil microbes can have a profound effect on streambank soil erodibility due to fiber reinforcement and EPS production.

Chapter 7. Overall Summary and Conclusions

7.1 Summary and Conclusions

The morphology and migration of stream channels has been a topic of interest for multiple stakeholders. Nevertheless, reducing streambank erosion or predicting channel migration remains an elusive and difficult process due to the complex relationships between streambank soil, vegetation, stream hydrodynamics, and other environmental factors.

Broadly, changes in streambank environments, like the encroachment of invasive species like Japanese knotweed, may alter streambank erosion processes and channel migration. Bank erodibility can have significant impacts on channel morphology, including meander morphology (Bogoni et al., 2017) and channel form (Fernandez et al., 2021). Therefore, effectively mitigating and adapting to global environmental changes is not possible without first understanding the components (e.g., vegetation and organic matter) and/or processes (e.g., EPS production) that are important to cohesive streambank stability. Therefore, the goal of this research was to study how plant root mechanisms and soil microbial processes impact streambank hydrodynamics and soil resistance to fluvial entrainment. Specific objectives included:

1. Measure the impact of synthetic fibers on critical shear stress and the soil erodibility coefficient compared to bare soil and live rooted soil samples (Ch. 3).
2. Quantify the effects of flexible and rigid roots extending out of the streambank face on near-bank velocity and turbulent stress (Ch. 4).
3. Determine the influence of soil microorganisms on soil aggregate stability and soil resistance to fluvial erosion (Ch. 5).
4. Quantify the relative impact of soil microorganisms, plant roots, and the interaction between the two on soil erodibility (Ch. 6).

7.1.1 Chapter 3

In this experiment the critical shear stress, soil erodibility coefficient, and scour hole development were compared on root-permeated soil samples (live and synthetic roots) and on bare soil samples. Samples were allowed to mature in a greenhouse prior to erosion testing using a mini-Jet Erosion Testing (JET) device. Following mini-JET testing, soil erosion was quantified by measuring the final volume of soil loss and calculating critical shear stress (τ_c) and the soil

erodibility coefficient (k_d). Potential explanatory soil and root properties, including percent water stable aggregates (%WSA), root length density (RLD), and extracellular polymeric substances (EPS), were also measured. This study also attempted to highlight the impact of soil microorganisms on erosion resistance; however, EPS results suggested that sterile conditions were not fully achieved as no significant difference in EPS was observed between sterilized and inoculated treatments. Therefore, inoculated soil and sterilized soil results were combined for no-root and synthetic root treatments.

Based on the study results, two overall conclusions were drawn. First, the impact of fibers (both live and synthetic) on k_d indicated that fibers affected the applied hydraulic forces. Samples with relatively low RLDs (below 2 cm cm^{-3}) had a higher k_d compared to the median k_d for no-rooted samples, whereas live rooted samples with RLDs above 2 cm cm^{-3} had a lower k_d. This result is attributed to how densely packed the fibers were, with low RLD samples leading to increased stem-scale turbulence and greater soil loss. Second, the impact of live roots on the soil environment provided additional protection by increasing soil resistance to fluvial erosion (higher τ_c). This increased erosion resistance happened even though %WSA was significantly lower in live rooted treatments compared to the synthetic and no-rooted treatments. Additionally, the presence of roots at densities below 2 cm cm^{-3} did not adversely impact τ_c like they did k_d. These results indicate that root fibers reduce soil loss caused by fluvial erosion through a combined effect on soil aggregate stability and by holding (binding) the soil together through a dense fiber network.

7.1.2 Chapter 4

The goal of this experiment was to compare the effects of root type (herbaceous vs. woody roots) on near-bank velocity and turbulent stress. To achieve this, the velocity, Reynold's stress (τ_{yx}, τ_{zx}, and τ_{yz}), and turbulent kinetic energy (TKE) profiles were developed over three distinct streambank boundary conditions [sand wall (SW – grain roughness), flexible rooted wall (FRW – 5500 roots/m^2), and rigid rooted wall (RRW – 660 roots/m^2)] and examined. Rooted streambanks were modeled after root area ratios measured at the Goodwin Creek Experimental Watershed in Mississippi, USA (Simon & Collison, 2002). Vectrino II acoustic Doppler profiler (ADP) measurements were taken at 12 locations immediately upstream of the circular sample hole, where the flow was still fully developed. Velocity, TKE, and Reynold's stress profiles were developed

using ADP measurements at 6, 10, 20, 30, 40, 50, 70, 90, and 110 mm away from the streambank surface for each boundary condition.

Rooted boundaries significantly reduced near-bank streamwise velocity compared to the sand wall. The RRW produced the lowest near-bank velocity and steepest velocity gradient, but rigid fibers also had the highest measured velocity towards the center of the channel. TKE and τ_{yx} were significantly higher in the rooted boundaries between 6 mm and 50 mm away from the bank surface compared to the sand wall boundary. While higher near-bank turbulent stress suggests higher near-bank turbulence, lower near-bank velocities indicate lower wall shear stresses compared to the bare (unvegetated) boundary. Given that both shear stress (e.g., Flanagan & Nearing, 1995; Larsen et al., 2009) and turbulence (e.g., Yang & Nepf, 2018; Zhang et al., 2020) can drive fluvial entrainment, the cumulative impact of exposed roots on streambank erosion rates, using velocity/turbulent stress results alone, is unclear. The relatively sparse spacing of fibers and the fact that the fibers did not extend far out of the streambank face likely contributed to this result, so different streambank configurations may lead to different results. Lastly, τ_{yx} was the dominant Reynolds stress for all boundary types (one order of magnitude higher than both τ_{zx} and τ_{yz}), indicating that Reynold's stress was generated predominately at the bank surface. Nevertheless, rooted boundaries also increased stress parallel to the bed surface (τ_{zx}) while only the flexible fibers influenced vertical momentum transfer (τ_{yz}) due to the waving motion of the fibers.

7.1.3 Chapter 5

Aggregate stability, EPS, and arbuscular mycorrhizal fungi have all been shown to significantly influence soil resistance to fluvial erosion (Barthès & Roose, 2002; Li et al., 2021; Mardhiah et al., 2016; Wynn & Mostaghimi, 2006); however, to the authors' knowledge, no work had been done directly linking the effect of increasing microbial production of EPS, stimulated by amending the soil with labile OM, with increasing soil resistance to fluvial streambank erosion. Therefore, the goal of this experiment was to determine if soils amended with OM would be more stable and resistant to fluvial erosion via an increase in EPS. To quantify the impact of OM inputs on soil aggregate stability, EPS, and streambank fluvial erosion rates, increasing amounts of dried and crushed (< 1 mm) cool season grass clippings were mixed at rates of 0, 1, and 4 g of clippings per 100 g of sieved soil (treatments T0, T1, and T4, respectively). Based on the carbon content of the grass clippings (40.6%) and surface area of the growth containers, T0, T1, and T4 corresponded

to 0, 96 g C/m^2, and 384 g C/m^2, respectively. For comparison, a review conducted by Cotrufo & Lavallee (2022) collated prior research and reported that carbon inputs from plant roots (root exudates and root turnover) have been measured as 3 to 400 g/m^2/year for grasslands and 120 to 960 g C/m^2/year for forests. A total of eight samples were created per treatment (24 samples in total). Following mixing of soil and OM inputs, soil samples were compacted in the growth containers to a bulk density of 0.95 g/cm^3 and allowed to mature in a closed greenhouse for 50 days prior to erosion testing and soil sampling. Following erosion testing, the soil remaining was collected for soil organic matter, EPS carbohydrate, EPS protein, and aggregate stability analysis.

By providing a source of readily available carbon in the soil, microbial production of EPS proteins was stimulated and remained for 50 days while EPS carbohydrates were more variable depending on the initial OM input amount. The lower EPS carbohydrate concentrations from small amounts of initial OM inputs seem to have been due to the stimulation of microbial activity and utilization of EPS carbohydrates in the soil. The significant correlations between EPS proteins, MWD, and k_d found in this study point to the dominant role EPS proteins play in improving soil stabilization and soil resistance to fluvial erosion due to labile OM inputs. Overall, treatments with added organic matter, T1 and T4, reduced the average soil erodibility coefficient by 25% and 61% and increased the soil mean weight diameter by 16% and over 100% compared to the control treatment, respectively. This research supports the hypothesis that labile organic matter additions to riparian streambank soils, in part through stimulated production of extracellular polymeric substances by soil microorganisms, can significantly improve soil resistance to fluvial erosion and slaking.

7.1.4 Chapter 6

Given the complex relationships between roots, microbes, and fluvial entrainment of soils, the goal of this experiment was to quantify the root and microbial mechanisms that influence soil erodibility. To do this, three flume walls were constructed to simulate unvegetated streambanks, as well as streambanks with herbaceous and woody roots. Additionally, three root treatments (bare soil, synthetic fibers, and living roots), and two soil types (soil amended with organic matter and unamended soil), were considered. Synthetic fibers represented the physical binding mechanism of plant roots without the biological interactions. Organic matter amendments, in the form of dried

and crushed grass clippings, represented the stimulation of soil microorganisms and exudation of "sticky" organic substances through the input of a readily degradable carbon source.

Exposed fibers on constructed streambanks tended to increase the erosion rates of bare soil samples. This result supports that higher near-bank turbulence, rather than lower near-bank velocity, plays an important role in predicting soil erosion/sediment transport potential. Regardless of flow rate, both flexible and rigid synthetic roots tended to increase soil resistance to erosion compared to bare soil. While stimulating microbial production of EPS proteins through labile organic carbon inputs had a greater effect compared to root binding alone, this effect appears to diminish as flow rate (and the corresponding turbulent stress) increases. When stimulated through the incorporation of grass clippings, microbial production of EPS, in combination with synthetic fibers, reduced soil erosion rates comparable to treatments with living roots. This result suggests that an abundance of roots, particularly very fine roots, were not necessary to increase soil resistance to fluvial erosion when soil microbes were also stimulated through organic matter inputs. EPS production was not significantly increased in vegetated samples without additional OM inputs, indicating vegetated samples did not have sufficient time to stimulate microbial activity prior to erosion testing. Over time, as plants grow, turn over, and add labile organic matter into the soil environment, it is hypothesized that the role of soil microorganisms would increase and reduce erosion rates further. In conclusion, this study provided evidence that, while sparsely spaced exposed roots may increase soil erosion rates due to impacts on the boundary layer, the net effect of fibers with root length densities as low as 0.7 cm cm^{-3} and organic matter inputs protect soil from fluvial erosion through root binding and microbially stimulated EPS production. EPS production appeared to increase the critical shear stress required to initiate soil erosion, while synthetic fibers alone provided a base reduction in soil erodibility, regardless of the flow rate used.

7.2 Research Contributions

This study is the first to consider how the combination of root physical effects, root/microbial biological effects, and root effects on the hydrodynamic boundary layer could influence streambank soil erodibility. Chapters 3 through 5 studied these mechanisms individually, while Chapter 6 explored how the interaction between each mechanism influenced net soil erosion rates. While sparsely spaced exposed roots may increase soil erosion rates due to impacts on the boundary layer, overall results highlight how the synergistic relationship between root fibers and

soil microbes can have a profound effect on streambank soil erodibility due to fiber reinforcement and EPS production.

7.3 Study Limitations

This research made use of a mini-JET device and a model streambank in a flume for erosion testing. Additionally, samples matured in a greenhouse setting under a completely randomized block design prior to experimentation. These study conditions had limitations which are presented here:

1. The foundation ring used for the mini-JET device initially disturbed the soil prior to erosion testing. This was particularly true for the synthetic fiber soil samples; the fibers near the foundation ring had to be cut prior to JET placement to minimize initial disturbance at the testing location. Nevertheless, this disturbance possibly influenced the study results and was one of the primary reasons a flume study was considered for all future experiments.
2. The model streambanks used in Chapters 4-6 were based off of one study conducted by Simon & Collison (2002). Different boundary configurations for exposed roots may have influenced the calculated turbulent stress and/or soil erosion rate results. Future research should consider how different root densities, root lengths, and root diameters could change the results presented here.
3. The maximum turbulent stress developed during the flume erosion testing was limited. The limited range in applied force makes it difficult to assess if the experimental results would be the same for higher applied stresses in the field. Future work should cover a wider range of potential stresses.
4. The short growth time for greenhouse soil samples limits the applicability of these results. How early after labile organic matter inputs do microbes start to influence erosion rates? How long after OM input do the benefits start to decrease? These are questions that cannot be answered by the present dissertation and should be explored further in future research.

7.4 Future Research Opportunities

While experimental measurements are limited, the story of Japanese knotweed potentially exacerbating streambank erosion rates compared to native vegetation or unvegetated streambanks (Colleran et al., 2020; Matte et al., 2021) highlights the importance of understanding how

vegetation and their roots influence streambank erodibility. What about Japanese knotweed or other invasive species like U.S. privet (*Ligustrum vulgare*) and Amur honeysuckle (*Lonicera maackii*) make them influential, or not influential, on streambank erosion compared to native vegetation? Do the plant root systems vary significantly enough to amplify or reduce erosion rates? How do they contribute to microbial production of extracellular polymeric substances, and in turn how does that influence soil erodibility? Japanese knotweed presents an interesting case study to consider further. The roots of knotweed have been described as "underground stems" lacking root hairs (Colleran et al., 2020). The roots are also typically large (5 – 100 mm), have shallow rooting depths, and practitioners have found that removing newly established knotweeds was fastest by hand (Child & Wade, 2000; Colleran et al., 2020). The results presented in this study highlight potential Japanese knotweed root properties/mechanisms that could enhance streambank soil erodibility. For instance, it is hypothesized the knotweed roots amplify soil erosion by 1) the lack of roots/root hairs physically binding soil particles together; 2) the lack of roots that to biologically interact with soil microorganisms; and 3) increasing near-bank turbulent stress and amplify the dislodgement of the surrounding soil due to roots becoming exposed on the streambank face. As a result, the potential of Japanese knotweed to amply erosional processes highlight the need to further study how plants with different root structures and functions influence streambank erosion. Following these experiments, the effect of certain vegetation on stream migration can be understood and mitigated if necessary.

On a local scale, the recognition that organic matter inputs influence soil microbes and drive soil structure and soil resistance to fluvial erosion is of particular importance for riparian vegetation management and stream restoration practices. Fresh plant material (i.e., surface residue, sloughed roots, or root exudates) are known to initiate aggregate development by forming the center of new aggregates through the production of microbially-derived substances like EPS (Six et al., 2004). Prior studies have measured significantly higher total SOC content in woody plant-dominated riparian areas/upland environments compared to areas dominated by herbaceous vegetation (de Rebello et al., 2019; Paul et al., 2008). However, higher root densities in grass-dominated environments may lead to greater fractions of SOC that are directly associated with initial aggregate formation/stabilization (Paul et al., 2008). The differences in SOC as a function of vegetation type underscores the need to further study the pools of SOC (e.g., total SOC vs. SOC occluded within soil aggregates) that drive streambank soil resistance to fluvial erosion. What are

the differences between SOC fractions in forested vs herbaceous riparian areas? How do SOC fractions influence soil structure/stability? Are those fractions correlated with streambank erosion rates? Ultimately, answering questions such as these could increase our understanding of how/why cohesive streambank soils erode and make it possible to design nature-based solutions that increase channel resilience to degradation.

In geotechnical engineering, fiber-reinforced soil has been accepted since 1969 (Vidal, 1969) and used for a variety of applications including road pavement construction and building foundation design (Gowthaman et al., 2018). Recent work in the geotechnical field has also considered the combination of fiber-reinforced soil and biopolymer (organic byproducts secreted by plants/microorganisms such as EPS) mixtures to improve soil strength for design applications (Chen et al., 2022). In other fields like stream restoration design, soil fill is commonly used to rebuild a streambank and protect it from erosion until vegetation grows. The mat acts as a protective barrier that limits soil raindrop impact and hydraulic forces from interacting with the underlying soil and causing erosion. While mats are commonly used as a protective barrier that limits erosion of fill material, incorporating fibers and organic matter together with the soil fill to increase soil resistance to erosion prior to fill placement has not been explored. While plant roots naturally provide both fibers and "sticky" EPS to soils, the present research as shown that these materials could be incorporated into fill soils during construction to rapidly increase soil erosion resistance following levee construction and/or stream restoration projects. Therefore, the feasibility and applicability of incorporating fibers/soil microbes to design projects should be explored further in pilot-scale and field-scale research projects.

References

Abernethy, B., & Rutherfurd, I. (2001). The distribution and strength of riparian tree roots in relation to riverbank reinforcement. *Hydrological Processes*, *15*(1), 63–79. https://doi.org/10.1002/hyp.152

Abiven, S., Menasseri, S., & Chenu, C. (2009). The effects of organic inputs over time on soil aggregate stability - A literature analysis. *Soil Biology and Biochemistry*, *41*(1), 1–12. https://doi.org/10.1016/j.soilbio.2008.09.015

Akinola, Akinrotimi I., Wynn-Thompson, T., Olgun, C. G., Mostaghimi, S., & Eick, M. J. (2019). Fluvial Erosion Rate of Cohesive Streambanks Is Directly Related to the Difference in Soil and Water Temperatures. *Journal of Environment Quality*, *48*(6), 1741. https://doi.org/10.2134/jeq2018.10.0385

Akinola, Akinrotimi Idowu. (2018). Temporal and Thermal Effects on Fluvial Erosion of Cohesive Streambank Soils. In *Dissertation*. Virginia Polytechnic Institute and State University.

Akinola, Akinrotimi Idowu, Wynn-Thompson, T., Olgun, C. G., Cuceoglu, F., & Mostaghimi, S. (2018). Influence of Sample Holding Time on the Fluvial Erosion of Remolded Cohesive Soils. *Journal of Hydraulic Engineering*, *144*(8), 04018049. https://doi.org/10.1061/(ASCE)HY.1943-7900.0001504

Al-Madhhachi, A. T., Hanson, G. J., Fox, G. A., Tyagi, A. K., & Bulut, R. (2013a). Deriving Parameters of a Fundamental Detachment Model for Cohesive Soils from Flume and Jet Erosion Tests. *Transactions of the ASABE*, *56*(2), 489–504. https://doi.org/10.1016/j.envsoft.2006.06.007

Al-Madhhachi, A. T., Hanson, G. J., Fox, G. A., Tyagi, A. K., & Bulut, R. (2013b). Measuring Soil Erodibility Using a Laboratory "Mini" Jet. *Transactions of the Asabe*, *56*(3), 901–910. https://doi.org/10.13031/trans.56.9742

Amos, C. L., Bergamasco, A., Umgiesser, G., Cappucci, S., Cloutier, D., DeNat, L., Flindt, M., Bonardi, M., & Cristante, S. (2004). The stability of tidal flats in Venice Lagoon—the results of in-situ measurements using two benthic, annular flumes. *Journal of Marine Science*, *51*, 211–241. https://doi.org/10.1016/j.jmarsys.2004.05.013

Anderson, R. J., Bledsoe, B. P., & Hession, W. C. (2004). WIDTH OF STREAMS AND RIVERS IN RESPONSE TO VEGETATION, BANK MATERIAL, AND OTHER FACTORS. *Journal of the American Water Resources Association*, *40*(5), 1159–1172. https://doi.org/10.1111/j.1752-1688.2004.tb01576.x

Annabi, M., Houot, S., Francou, C., Poitrenaud, M., & Bissonnais, Y. Le. (2007). Soil Aggregate Stability Improvement with Urban Composts of Different Maturities. *Soil Science Society of America Journal*, *71*(2), 413–423. https://doi.org/10.2136/sssaj2006.0161

Annabi, M., Le Bissonnais, Y., Le Villio-Poitrenaud, M., & Houot, S. (2011). Improvement of soil aggregate stability by repeated applications of organic amendments to a cultivated silty loam soil. *Agriculture, Ecosystems and Environment*, *144*(1), 382–389. https://doi.org/10.1016/j.agee.2011.07.005

Avnimelech, Y., Ritvo, G., Meijer, L. E., & Kochba, M. (2001). Water content, organic carbon

and dry bulk density in flooded sediments. *Aquacultural Engineering*, *25*, 25–33.

Badri, D. V., & Vivanco, J. M. (2009). Regulation and function of root exudates. *Plant, Cell & Environment*, *32*(6), 666–681. https://doi.org/10.1111/j.1365-3040.2009.01926.x

Badri, D. V., Zolla, G., Bakker, M. G., Manter, D. K., & Vivanco, J. M. (2013). Potential impact of soil microbiomes on the leaf metabolome and on herbivore feeding behavior. *New Phytologist*, *198*(1), 264–273. https://doi.org/10.1111/nph.12124

Barthès, B., & Roose, E. (2002). Aggregate stability as an indicator of soil susceptibility to runoff and erosion; validation at several levels. *CATENA*, *47*(2), 133–149. https://doi.org/10.1016/S0341-8162(01)00180-1

Barto, E. K., Alt, F., Oelmann, Y., Wilcke, W., & Rillig, M. C. (2010). Contributions of biotic and abiotic factors to soil aggregation across a land use gradient. *Soil Biology and Biochemistry*. https://doi.org/10.1016/j.soilbio.2010.09.008

Biron, P. M., Robson, C., Lapointe, M. F., & Gaskin, S. J. (2004). Comparing different methods of bed shear stress estimates in simple and complex flow fields. *Earth Surface Processes and Landforms*, *29*(11), 1403–1415. https://doi.org/10.1002/esp.1111

Black, K. S., Tolhurst, T. J., Paterson, D. M., & Hagerthey, S. E. (2002). Working with Natural Cohesive Sediments. *J. Hydraul. Eng.*, *128*(1), 2–8.

Blaisdell, F. W., Anderson, C. L., & Hebaus, G. G. (1981). Ultimate Dimensions of Local Scour. *J. Hydraul. Eng.*, *107*, 327–337.

Bogoni, M., Putti, M., & Lanzoni, S. (2017). Modeling meander morphodynamics over self-formed heterogeneous floodplains. *Water Resources Research*, *53*(6), 5137–5157. https://doi.org/10.1002/2017WR020726

Brand, A., Noss, C., Dinkel, C., & Holzner, M. (2016). High-resolution measurements of turbulent flow close to the sediment-water interface using a bistatic acoustic profiler. *Journal of Atmospheric and Oceanic Technology*, *33*(4), 769–788. https://doi.org/10.1175/JTECH-D-15-0152.1

Burylo, M., Rey, F., Mathys, N., & Dutoit, T. (2012). Plant root traits affecting the resistance of soils to concentrated flow erosion. *Earth Surface Processes and Landforms*, *37*(14), 1463–1470. https://doi.org/10.1002/esp.3248

Busscher, H. J., & Weerkamp, A. H. (1987). Specific and non-specific interactions in bacterial adhesion to solid substrata. *FEMS Microbiology Letters*, *46*(2), 165–173. https://doi.org/10.1111/j.1574-6968.1987.tb02457.x

Castro Filho, C., Ëo, A. L., De, M., Guimara Äes, F., & Fonseca, I. C. B. (2002). Aggregate stability under different soil management systems in a red latosol in the state of Parana, Brazil. *Soil & Tillage Research*, *65*, 45–51. https://doi.org/doi.org/10.1016/S0167-1987(01)00275-6

Chang, W.-S., van de Mortel, M., Nielsen, L., Nino de Guzman, G., Li, X., & Halverson, L. J. (2007). Alginate production by Pseudomonas putida creates a hydrated microenvironment and contributes to biofilm architecture and stress tolerance under water-limiting conditions. *Journal of Bacteriology*, *189*(22), 8290–8299. https://doi.org/10.1128/JB.00727-07

Chaparro, J. M., Badri, D. V, Bakker, M. G., Sugiyama, A., Manter, D. K., & Vivanco, J. M.

(2013). Root exudation of phytochemicals in Arabidopsis follows specific patterns that are developmentally programmed and correlate with soil microbial functions. *PloS One*, *8*(2), e55731. https://doi.org/10.1371/journal.pone.0055731

Characklis, W. G., & Wilderer, P. A. (1989). Glossary. In W. G. Characklis & P. A. Wilderer (Eds.), *Structure and function of biofilms.* (pp. 369–371). Wiley.

Chen, C., Wei, K., Gu, J., Huang, X., Dai, X., & Liu, Q. (2022). Combined Effect of Biopolymer and Fiber Inclusions on Unconfined Compressive Strength of Soft Soil. *Polymers*, *14*(4), 1–14.

Cheng, W., & Kuzyakov, Y. (2005). Root effects on soil organic matter decomposition. In R. W. Zobel & S. F. Wright (Eds.), *Roots and Soil Management: Interactions between Roots and the Soil* (pp. 119–143). Agronomy Monograph No. 48. American Society of Agronomy, Crop Science Society of America, Soil Science Society of America,.

Child, L., & Wade, M. (2000). *The Japanese knotweed manual: the management and control of an invasive alien weed*. Packard Publishing Limited.

Coles, S. M. (1979). Benthic microalgal populations on intertidal sediments and their role as precursors to salt marsh development. In R. . Jeffries & A. . Davies (Eds.), *Ecological Processes in Coastal Environments: The First European Symposium of the British Ecological Society* (pp. 25–42). Blackwell Scientific.

Colleran, B., Lacy, S. N., & Retamal, M. R. (2020). Invasive Japanese knotweed (Reynoutria japonica Houtt.) and related knotweeds as catalysts for streambank erosion. *River Research and Applications*, 1962–1969. https://doi.org/10.1002/rra.3725

Comte, S., Guibaud, G., & Baudu, M. (2006a). Relations between extraction protocols for activated sludge extracellular polymeric substances (EPS) and complexation properties of Pb and Cd with EPS: Part II. Consequences of EPS extraction methods on Pb2+ and Cd2+ complexation. *Enzyme and Microbial Technology*, *38*(1–2), 246–252. https://doi.org/10.1016/J.ENZMICTEC.2005.06.023

Comte, S., Guibaud, G., & Baudu, M. (2006b). Relations between extraction protocols for activated sludge extracellular polymeric substances (EPS) and EPS complexation properties: Part I. Comparison of the efficiency of eight EPS extraction methods. *Enzyme and Microbial Technology*, *38*(1–2), 237–245. https://doi.org/10.1016/J.ENZMICTEC.2005.06.016

Coppin, N. J., & Richards, I. G. (1990). *Use of Vegetation in Civil Engineering*. Construction Industry Research and Information Association.

Costa, O. Y. A., Raaijmakers, J. M., & Kuramae, E. E. (2018). Microbial Extracellular Polymeric Substances: Ecological Function and Impact on Soil Aggregation. *Frontiers in Microbiology*, *9*, 1636. https://doi.org/10.3389/fmicb.2018.01636

Cotrufo, M. F., & Lavallee, J. M. (2022). Soil organic matter formation, persistence, and functioning: A synthesis of current understanding to inform its conservation and regeneration. In *Advances in Agronomy* (1st ed., Vol. 172). Elsevier Inc. https://doi.org/10.1016/bs.agron.2021.11.002

Craig, R. G. A., Loadman, C., Clement, B., Rusello, P. J., & Siegel, E. (2011). Characterization and testing of a new bistatic profiling acoustic Doppler velocimeter: The Vectrino-II. *2011*

IEEE/OES/CWTM 10th Working Conference on Current, Waves and Turbulence Measurement, CWTM 2011, 246–252. https://doi.org/10.1109/CWTM.2011.5759559

Curran, J. C., & Hession, W. C. (2013). Vegetative impacts on hydraulics and sediment processes across the fluvial system. *Journal of Hydrology*, *505*, 364–376. https://doi.org/10.1016/J.JHYDROL.2013.10.013

D'Abzac, P., Bordas, F., Van Hullebusch, E., Lens, P. N. L., & Guibaud, G. (2010). Extraction of extracellular polymeric substances (EPS) from anaerobic granular sludges: Comparison of chemical and physical extraction protocols. *Applied Microbiology and Biotechnology*, *85*, 1589–1599. https://doi.org/10.1007/s00253-009-2288-x

Dade, W. Brian, Davis, J. D., Nichols, P. D., Nowell, A. R. M., Thistle, D., Trexler, M. B., White, D. C., & Davis, J. D. (1990). Effects of bacterial exopolymer adhesion on the entrainment of sand. *Geomicrobiology Journal*, *8*(1), 1–16. https://doi.org/10.1080/01490459009377874

Dade, W.B., Self, R. L., Pellerin, N. B., Moffet, A., Jumars, P. A., & Nowell, A. R. M. (1996). THE EFFECTS OF BACTERIA ON THE FLOW BEHAVIOR OF CLAY-SEAWATER SUSPENSIONS. *Journal of Sedimentary Research*, *66*(1), 39–42. https://doi.org/https://doi.org/10.1306/D42682A7-2B26-11D7-8648000102C1865D

Daly, E. R., Fox, G. A., Al-Madhhachi, A. T., & Miller, R. B. (2013). A Scour Depth Approach for Deriving Erodibility Parameters from Jet Erosion Tests. *Transactions of the ASABE*, *56*(6), 1343–1351. https://doi.org/10.13031/trans.56.10350

Davies-Colley, R. J. (1997). Stream channels are narrower in pasture than in forest. *New Zealand Journal of Marine and Freshwater Research*, *31*(5), 599–608. https://doi.org/10.1080/00288330.1997.9516792

Davies, D. G. (1999). Regulation of matrix polymer in biofilm formation and dispersion. In J Wingender, T. R. Neu, & H. C. Flemming (Eds.), *Microbial extracellular polymeric substances: characterization, structure and function* (pp. 93–112). Springer.

De Baets, S., Poesen, J., Gyssels, G., & Knapen, A. (2006). Effects of grass roots on the erodibility of topsoils during concentrated flow. *Geomorphology*, *76*(1–2), 54–67. https://doi.org/10.1016/j.geomorph.2005.10.002

De Baets, S., Poesen, J., Knapen, A., & Galindo, P. (2007). Impact of root architecture on the erosion-reducing potential of roots during concentrated flow. *Earth Surface Processes and Landforms*, *32*, 1323–1345. https://doi.org/10.1002/esp.1470

De Baets, Sarah, Denbigh, T. D. G., Smyth, K. M., Eldridge, B. M., Weldon, L., Higgins, B., Matyjaszkiewicz, A., Meersmans, J., Larson, E. R., Chenchiah, I. V., Liverpool, T. B., Quine, T. A., & Grierson, C. S. (2020). Micro-scale interactions between Arabidopsis root hairs and soil particles influence soil erosion. *Communications Biology*, *3*(1), 1–11. https://doi.org/10.1038/s42003-020-0886-4

De Boer, P. L. (1981). Mechanical effects of micro-organisms on intertidal bedform migration. *Sedimentology*, *28*(1), 129–132. https://doi.org/10.1111/j.1365-3091.1981.tb01670.x

de Rebello, T. R., Bortolozo, F. R., & Parron, L. M. (2019). Organic matter content in riparian areas of soil composed of woody vegetation and grass and its effects on pesticide adsorption. *International Journal of Recycling of Organic Waste in Agriculture*, *8*(1), 67–72.

https://doi.org/10.1007/s40093-018-0229-3

Dingman, S. L. (2001). *Physical Hydrology* (2nd ed.). Prentice Hall.

Docker, B. B., & Hubble, T. C. T. (2008). Quantifying root-reinforcement of river bank soils by four Australian tree species. *Geomorphology*, *100*(3–4), 401–418. https://doi.org/10.1016/j.geomorph.2008.01.009

Droppo, I.G., Lau, Y. L., & Mitchell, C. (2001). The effect of depositional history on contaminated bed sediment stability. *Science of The Total Environment*, *266*(1–3), 7–13. https://doi.org/10.1016/S0048-9697(00)00748-8

Droppo, Ian G. (2009). Biofilm structure and bed stability of five contrasting freshwater sediments. *Marine and Freshwater Research*, *60*, 690–699. https://doi.org/10.1071/MF08019

DuBois, M., Gilles, K. A., Hamilton, J. K., Rebers, P. A., & Smith, F. (1956). Colorimetric Method for Determination of Sugars and Related Substances. *Analytical Chemistry*, *28*(3), 350–356. https://doi.org/10.1021/ac60111a017

Dunn, I. S. (1959). Tractive resistance of cohesive channels. *Proc. Journal of the Soil Mechanics and Foundation Division, ASCE*, *85*(SM3), 1–24.

Fang, H., Cheng, W., Fazeli, M., & Dey, S. (2017). Bedforms and Flow Resistance of Cohesive Beds with and without Biofilm Coating. *Journal of Hydraulic Engineering*, *143*(8), 06017010. https://doi.org/10.1061/(ASCE)HY.1943-7900.0001313

Fang, H., Fazeli, M., Cheng, W., & Dey, S. (2016). Transport of biofilm-coated sediment particles. *Journal of Hydraulic Research*, *54*(6), 631–645. https://doi.org/10.1080/00221686.2016.1212938

Fang, H., Fazeli, M., Cheng, W., Huang, L., & Hu, H. (2015). Biostabilization and transport of cohesive sediment deposits in the Three Gorges Reservoir. *PLoS ONE*. https://doi.org/10.1371/journal.pone.0142673

Fang, H., Shang, Q., Chen, M., & He, G. (2014). Changes in the critical erosion velocity for sediment colonized by biofilm. *Sedimentology*, *61*(3), 648–659. https://doi.org/10.1111/sed.12065

Fang, H. W., Lai, H. J., Cheng, W., Huang, L., & He, G. J. (2017). Modeling sediment transport with an integrated view of the biofilm effects. *Water Resources Research*, *53*, 7536–7557. https://doi.org/10.1002/2017WR020628

FAO. (2020). *Standard operating procedure for soil organic carbon Walkley-Black method*. http://www.fao.org/publications/card/en/c/CA7471EN/

Fernandez, R. L., McLelland, S., Parsons, D. R., & Bodewes, B. (2021). Riparian vegetation life stages control the impact of flood sequencing on braided river morphodynamics. *Earth Surface Processes and Landforms*, 1–15. https://doi.org/10.1002/esp.5177

Flanagan, D. C., & Nearing, M. A. (1995). *USDA-Water Erosion Prediction Project: Hillslope Profile and Watershed Model Documentation* (Issue NSERL Rep. 10). https://doi.org/https://www.ars.usda.gov/midwest-area/west-lafayette-in/national-soil-erosion-research/docs/wepp/wepp-model-documentation/

Flemming, H.-C., Neu, T. R., & Wozniak, D. J. (2007). The EPS matrix: the "house of

biofilm cells". *Journal of Bacteriology*, *189*(22), 7945–7947. https://doi.org/10.1128/JB.00858-07

Flemming, H.-C., & Wingender, J. (2010). The biofilm matrix. *Nature Reviews Microbiology*, *8*(9), 623–633. https://doi.org/10.1038/nrmicro2415

Forsberg, P. L., Skinnebach, K. H., Becker, M., Ernstsen, V. B., Kroon, A., & Andersen, T. J. (2018). The influence of aggregation on cohesive sediment erosion and settling. *Continental Shelf Research*, *171*, 52–62. https://doi.org/10.1016/J.CSR.2018.10.005

Frolund, B., Palmgren, R., Keiding, K., & Nielsen, P. H. (1996). Extraction of extracellular polymers from activated sludge using a cation exchange resin. *Water Research*, *30*(8), 1749–1758. https://doi.org/10.1016/0043-1354(95)00323-1

Garcia-Aragon, J., Droppo, I. G., Krishnappan, B. G., Trapp, B., & Jaskot, C. (2011). Erosion characteristics and floc strength of Athabasca River cohesive sediments: towards managing sediment-related issues. *Journal of Soils and Sediments*, *11*(4), 679–689. https://doi.org/10.1007/s11368-011-0345-4

Gerbersdorf, S. U., & Wieprecht, S. (2015). Biostabilization of cohesive sediments: revisiting the role of abiotic conditions, physiology and diversity of microbes, polymeric secretion, and biofilm architecture. *Geobiology*, *13*(1), 68–97. https://doi.org/10.1111/gbi.12115

Gerbersdorf, S U, Jancke, T., Westrich, B., & Paterson, D. M. (2008). Microbial stabilization of riverine sediments by extracellular polymeric substances. *Geobiology*, *6*, 57–69. https://doi.org/10.1111/j.1472-4669.2007.00120.x

Gerbersdorf, Sabine Ulrike, Jancke, T., & Westrich, B. (2005). Physico-chemical and biological sediment properties determining erosion resistance of contaminated riverine sediments – Temporal and vertical pattern at the Lauffen reservoir/River Neckar, Germany. *Limnologica*, *35*(3), 132–144. https://doi.org/10.1016/J.LIMNO.2005.05.001

Gerbersdorf, Sabine Ulrike, Westrich, B., & Paterson, D. M. (2009). Microbial extracellular polymeric substances (EPS) in fresh water sediments. *Microbial Ecology*. https://doi.org/10.1007/s00248-009-9498-8

Goring, D. G., & Nikora, V. I. (2002). Despiking Acoustic Doppler Velocimeter Data. *Journal of Hydraulic Engineering*, *128*(1), 117–126. https://doi.org/10.1061/ASCE0733-94292002128:1117

Goto, N., Mitamura, O., & Terai, H. (2001). Biodegradation of photosynthetically produced extracellular organic carbon from intertidal benthic algae. *Journal of Experimental Marine BIology and Ecology*, *257*, 73–86.

Gowthaman, S., Nakashima, K., & Kawasaki, S. (2018). A State-of-the-Art Review on Soil Reinforcement Technology Using Natural Plant Fiber Materials : Past Findings, Present Trends and Future Directions. *Materials*, *11*(4), 1–23. https://doi.org/10.3390/ma11040553

Grabowski, R. C., Droppo, I. G., & Wharton, G. (2011). Erodibility of cohesive sediment: The importance of sediment properties. *Earth-Science Reviews*, *105*(3–4), 101–120. https://doi.org/10.1016/j.earscirev.2011.01.008

Graf, F., & Frei, M. (2013). Soil aggregate stability related to soil density, root length, and mycorrhiza using site-specific Alnus incana and Melanogaster variegatus s.l. *Ecological*

Engineering, *57*, 314–323. https://doi.org/10.1016/J.ECOLENG.2013.04.037

Gray, D. H. (1973). *Effects of forest clear-cutting on the stability of natural slopes: results of field studies* (p. 119). https://deepblue.lib.umich.edu/handle/2027.42/5207

Gray, D. H., & Leiser, A. T. (1982). *Biotechnical Slope Protection and Erosion Control*. Van Nostrand Reinhold, Co.

Gyssels, G., & Poesen, J. (2003). The importance of plant root characteristics in controlling concentrated flow erosion rates. *Earth Surface Processes and Landforms*, *28*(4), 371–384. https://doi.org/10.1002/esp.447

Gyssels, G., Poesen, J., Bochet, E., & Li, Y. (2005). Impact of plant roots on the resistance of soils to erosion by water: a review. *Progress in Physical Geography*, *29*(2), 189–217. https://doi.org/10.1191/0309133305pp443ra

Gyssels, G., Poesen, J., Liu, G., Van Dessel, W., Knapen, A., & De Baets, S. (2006). Effects of cereal roots on detachment rates of single- and double-drilled topsoils during concentrated flow. *European Journal of Soil Science*, *57*(3), 381–391. https://doi.org/10.1111/j.1365-2389.2005.00749.x

Hanson, G. J. (1990a). Surface Erodibility of Earthen Channels at High Stresses Part I - Open Channel Testing. *Transactions of the ASAE*, *33*(1), 0127–0131. https://doi.org/10.13031/2013.31305

Hanson, G. J. (1990b). Surface Erodibility of Earthen Channels at High Stresses Part II - Developing an In Situ Testing Device. *Transactions of the American Society of Agricultural Engineers*, *33*(1), 127–131. https://doi.org/10.13031/2013.31305

Hanson, G. J. (1991). Development of a Jet Index To Characterize Erosion Resistance of Soils in Earthen Spillways. *Transactions of the ASAE*, *34*(5), 2015–2020. https://doi.org/10.13031/2013.31831

Hanson, G. J., & Cook, K. R. (1997). Development of Excess Shear Stress Parameters for Circular Jet Testing. *ASAE Paper No. 97- 2227*, *American Society of Agricultural Engineers, St. Joseph, Michigan.*

Hanson, G. J., & Cook, K. R. (2004). Apparatus, test procedures, and analytical methods to measure soil erodibility in situ. *Applied Engineering in Agriculture*, *20*(4), 455–462. https://doi.org/10.13031/2013.16492

Hanson, G. J., & Cook, K. R. (1999). Procedure to estimate soil erodibility for water management purposes. *ASAE Paper No. 992133. Proc. Mini-Conf. Advance in Water Quality Modeling*, 51–56.

Hanson, G. J., Robinson, K. M., & Cook, K. R. (2002). Scour Below an Overfall: Part II. Prediction. *Transactions of the ASAE*, *45*(1), 957–964. https://doi.org/10.13031/2013.9948

Hanson, G. J., & Simon, A. (2001). Erodibility of cohesive streambeds in the loess area of the Midwestern USA. *Hydrological Processes*, *15*(1), 23–38. https://doi.org/10.1002/hyp.149

Haynes, R. J., & Beare, M. H. (1997). Influence of six crop species on aggregate stability and some labile organic matter fractions. *Soil Biology and Biochemistry*, *29*(11–12), 1647–1653. https://doi.org/10.1016/S0038-0717(97)00078-3

Heinzen, R. T. (1976). *Erodibility Criteria for Soil*. University of CA, Davis.

Hill, A. V. (1910). The possible effects of the aggregation of the molecules of haemoglobin on its dissociation curves. *Journal of Physiology*, *40*, iv–vii.

Holland, A. F., Zingmark, R. G., & Dean, J. M. (1974). Quantitative evidence concerning the stabilization of sediments by marine benthic diatoms. *Marine Biology*, *27*(3), 191–196. https://doi.org/10.1007/BF00391943

Hollick, M. (1976). Towards a routine test for the assessment of the critical tractive forces of cohesive soils. *Transactions of the ASAE*, *19*(6), 1076–1081.

Hoomehr, S., Akinola, A. I., Wynn-Thompson, T., Garnand, W., & Eick, M. J. (2018). Water Temperature, pH, and Road Salt Impacts on the Fluvial Erosion of Cohesive Streambanks. *Water*, *10*(302), 1–16. https://doi.org/10.3390/w10030302

Hopkinson, L., & Wynn-Thompson, T. (2012). Streambank shear stress estimates using turbulent kinetic energy. *Journal of Hydraulic Research*, *50*(3), 320–323. https://doi.org/10.1080/00221686.2012.684771

Hopkinson, L., & Wynn, T. (2009). Vegetation impacts on near bank flow. *Ecohydrology*, *2*(4), 404–418. https://doi.org/10.1002/eco.87

Ielpi, A., Lapotre, M. G. A., Gibling, M. R., & Boyce, C. K. (2022). The impact of vegetation on meandering rivers. *Nature Reviews Earth & Environment*, *January*, 1–14. https://doi.org/10.1038/s43017-021-00249-6

Ikard, S. J. (2016). *Phase-space Threshold Algorithm for Time Series Data*. Researchgate. https://doi.org/10.13140/RG.2.1.1831.4325

Ikeda, S., Parker, G., & Sawai, K. (1981). Bend Theory of River Meanders. Part 1. Linear Development. *Journal of Fluid Mechanics*, *112*, 363–377. https://doi.org/10.1017/S0022112081000451

Jones, F. E., & Harris, G. L. (1992). ITS-90 density of water formulation for volumetric standards calibration. In *J. Res. Natl. Inst. Stand. Technol.* (Vol. 97, Issue 3, pp. 335–340). https://doi.org/10.6028/jres.097.013

Kay, B. D. (1990). Rates of Change of Soil Structure Under Different Cropping Systems. In Stewart B.A. (Ed.), *Advances in Soil Science* (12th ed., pp. 1–52). Springer, New York, NY. https://doi.org/10.1007/978-1-4612-3316-9_1

Kemper, W., & Rosenau, R. (1986). Aggregate stability and size distribution. In A. Klute (Ed.), *Methods of Soil Analysis* (2nd ed., pp. 425–442). ASA (Agronomy Monograph 9).

Khanal, A., & Fox, G. A. (2017). Detachment characteristics of root-permeated soils from laboratory jet erosion tests. *Ecological Engineering*, *100*, 335–343. https://doi.org/10.1016/j.ecoleng.2016.10.081

Khanal, A., Fox, G. A., & Al-Madhhachi, A. T. (2016). Variability of Erodibility Parameters from Laboratory Mini Jet Erosion Tests. *J. Hydraul. Eng.*, *21*(10), 1–17. https://doi.org/10.1061/(ASCE)HE.1943-5584.0001404.

Koca, K., Noss, C., Anlanger, C., Brand, A., & Lorke, A. (2017). Performance of the Vectrino Profiler at the sediment–water interface. *Journal of Hydraulic Research*, *55*(4), 573–581.

https://doi.org/10.1080/00221686.2016.1275049

Kramer, J., & Weaver, J. E. (1936). *Relative Efficiency of Roots and Tops of Plants in Protecting the Soil from Erosion*. The University of Nebraska.

Larsen, L. G., Harvey, J. W., & Crimaldi, J. P. (2009). Predicting bed shear stress and its role in sediment dynamics and restoration potential of the Everglades and other vegetated flow systems. *Ecological Engineering*, *35*(12), 1773–1785. https://doi.org/10.1016/j.ecoleng.2009.09.002

Laspidou, C. S., & Rittmann, B. E. (2002). A unified theory for extracellular polymeric substances, soluble microbial products, and active and inert biomass. *Water Research*, *36*, 2711–2720. https://doi.org/10.1155/2017/3760238

Lawler, D. M. (1992). Process dominance in bank erosion systems. In P. A. Carling & G. E. Petts (Eds.), *Lowland floodplain rivers: Geomorphological perspectives* (pp. 117–143). John Wiley & Sons Ltd.

Lawler, D. M. (1995). The impact of scale on the processes of channel-side sediment supply: a conceptual model. *Effects of Scale on Interpretation and Mangement of Sediment and Water Quality*, *226*, 175–184.

Lawler, D. M., Thorne, C. R., & Hooke, J. M. (1997). Bank erosion and instability. In C. R. Thorne, R. D. Hey, & M. D. Newson (Eds.), *Applied Fluvial Geomorphology for River Engineering and Management* (pp. 138–172). John Wiley & Sons.

Lawson, S. E., McGlathery, K. J., & Wiberg, P. L. (2012). Enhancement of sediment suspension and nutrient flux by benthic macrophytes at low biomass. *Marine Ecology Progress Series*, *448*, 259–270. https://doi.org/10.3354/meps09579

Le Bissonnais, Y. (1996). Aggregate stability and assessment of soil crustability and erodibility: I. Theory and methodology. *European Journal of Soil Science*, *47*, 425–437. https://doi.org/10.1111/j.1365-2389.1996.tb01843.x

Li, H., Liu, G., Gu, J., Chen, H., Shi, H., Abd Elbasit, M. A. M., & Hu, F. (2021). Response of soil aggregate disintegration to the different content of organic carbon and its fractions during splash erosion. *Hydrological Processes*, *January*. https://doi.org/10.1002/hyp.14060

Li, Q., Liu, G. B., Zhang, Z., Tuo, D. F., Bai, R., & Qiao, F. (2017). Relative contribution of root physical enlacing and biochemistrical exudates to soil erosion resistance in the Loess soil. *Catena*, *153*, 61–65. https://doi.org/10.1016/j.catena.2017.01.037

Li, Y., Zhu, X.-M., & Tian, J.-Y. (1991). Effectiveness of plant roots to increase the anti-scourability of soil on the Loess Plateau. *Chinese Science Bulletin*, *36*(24), 2077–2082.

Liu, C., Shan, Y., & Nepf, H. (2021). Impact of Stem Size on Turbulence and Sediment Resuspension Under Unidirectional Flow. *Water Resources Research*, 1–11. https://doi.org/10.1029/2020WR028620

Liu, D., Valyrakis, M., & Williams, R. (2017). Flow Hydrodynamics across Open Channel Flows with Riparian Zones: Implications for Riverbank Stability. *Water*, *9*(9), 720. https://doi.org/10.3390/w9090720

Liu, H., & Fang, H. H. P. (2002). Extraction of extracellular polymeric substances (EPS) of

sludges. *Journal of Biotechnology*, *95*(3), 249–256. https://doi.org/10.1016/S0168-1656(02)00025-1

Liu, Y., & Fang, H. H. P. (2003). Influences of Extracellular Polymeric Substances (EPS) on Flocculation, Settling, and Dewatering of Activated Sludge. *Critical Reviews in Environmental Science and Technology*, *33*(3), 237–273. https://doi.org/10.1080/10643380390814479

Lu, J., Dijkstra, F. A., Wang, P., & Cheng, W. (2019). Roots of non-woody perennials accelerated long-term soil organic matter decomposition through biological and physical mechanisms. *Soil Biology and Biochemistry*, *134*, 42–53. https://doi.org/10.1016/J.SOILBIO.2019.03.015

Lucas, S. T., D'Angelo, E. M., & Williams, M. A. (2014). Improving soil structure by promoting fungal abundance with organic soil amendments. *Applied Soil Ecology*, *75*, 13–23. https://doi.org/10.1016/j.apsoil.2013.10.002

Mahalder, B., Schwartz, J., Palomino, A., Zirkle, J., Mahalder, B., Schwartz, J. S., Palomino, A. M., & Zirkle, J. (2018). Estimating Erodibility Parameters for Streambanks with Cohesive Soils Using the Mini Jet Test Device: A Comparison of Field and Computational Methods. *Water*, *10*(3), 304. https://doi.org/10.3390/w10030304

Malarkey, J., Baas, J. H., Hope, J. A., Aspden, R. J., Parsons, D. R., Peakall, J., Paterson, D. M., Schindler, R. J., Ye, L., Lichtman, I. D., Bass, S. J., Davies, A. G., Manning, A. J., & Thorne, P. D. (2015). The pervasive role of biological cohesion in bedform development. *Nature Communications*, *6*(6257), 1–6. https://doi.org/10.1038/ncomms7257

Mamo, M., & Bubenzer, G. D. (2001a). Detachment Rate, Soil Erodibility, and Soil Strength As Influenced By Living Plant Roots Part I: Laboratory Study. *American Society of Agricultural Engineers*, *44*(5), 1167–1174. https://doi.org/10.13031/2013.6445

Mamo, M., & Bubenzer, G. D. (2001b). Detachment rate, soil erodibility, and soil strength as influenced by living plant roots part II: Field study. *Transactions of the Asae*, *44*(5), 1175–1181. https://doi.org/10.13031/2013.6445

Mardhiah, U., Caruso, T., Gurnell, A., & Rillig, M. C. (2016). Arbuscular mycorrhizal fungal hyphae reduce soil erosion by surface water flow in a greenhouse experiment. *Applied Soil Ecology*, *99*, 137–140. https://doi.org/10.1016/j.apsoil.2015.11.027

Marschner, P., & Rumberger, A. (2004). Rapid changes in the rhizosphere bacterial community structure during re-colonization of sterilized soil. *Biology and Fertility of Soils*. https://doi.org/10.1007/s00374-004-0736-4

Martin, J. P., Martin, W. P., Page, J. B., Raney, W. A., & de Ment, J. D. (1955). Soil Aggregation. *Advances in Agronomy*, *7*, 1–37. https://doi.org/10.1016/S0065-2113(08)60333-8

Martin, V., Fisher, T. S. R., Millar, R. G., & Quick, M. C. (2002). ADV Data Analysis for Turbulent Flows: Low Correlation Problem. *Hydraulic Measurements and Experimental Methods*, 770–779. https://doi.org/10.1061/40655(2002)101

Matte, R., Boivin, M., & Lavoie, C. (2021). Japanese knotweed increases soil erosion on riverbanks. *River Research and Applications*, 1–12. https://doi.org/10.1002/rra.3918

McBride, M., Hession, W. C., Rizzo, D. M., & Thompson, D. M. (2007). The influence of riparian vegetation on near-bank turbulence: a flume experiment. *Earth Surface Processes and*

Landforms, *32*(13), 2019–2037. https://doi.org/10.1002/esp.1513

McNichol, B., Kassa, K., Fox, G., Miller, R., & Guertault, L. (2017). Erodibility Parameters Derived from Jet and Flume Erosion Tests on Root-Permeated Soils. *Journal of Contemporary Water Research & Education*, *160*(1), 119–131. https://doi.org/10.1111/j.1936-704x.2017.03244.x

Miller, R. B., Fox, G. A., Penn, C. J., Wilson, S., Parnell, A., Purvis, R. A., & Criswell, K. (2014). Estimating sediment and phosphorus loads from streambanks with and without riparian protection. *Agriculture, Ecosystems and Environment*, *189*, 70–81. https://doi.org/10.1016/j.agee.2014.03.016

Mirtskhulava, E. (1966). Erosional Stability Of Cohesive Soils. *Journal of Hydraulic Research*, *4*(1), 37–50. https://doi.org/10.1080/00221686609500091

Moody, J. A., Dungan Smith, J., & Ragan, B. W. (2005). Critical shear stress for erosion of cohesive soils subjected to temperatures typical of wildfires. *Journal of Geophysical Research: Earth Surface*, *110*(1), 1–13. https://doi.org/10.1029/2004JF000141

Moon, J., Ma, L., Xia, K., & Williams, M. A. (2016). Plant-Microbial and mineral contributions to amino acid and protein organic matter accumulation during 4000 years of pedogenesis. *Soil Biology & Biochemistry*, *100*, 42–50. https://doi.org/10.1016/j.soilbio.2016.05.011

Moore, W. L., & Masch, F. D. (1962). Experiments on the scour resistance of cohesive sediments. *Journal of Geophysical Research*, *67*(4), 1437–1446.

More, T. T., Yadav, J. S. S., Yan, S., Tyagi, R. D., & Surampalli, R. Y. (2014). Extracellular polymeric substances of bacteria and their potential environmental applications. *Journal of Environmental Management*, *144*, 1–25. https://doi.org/10.1016/J.JENVMAN.2014.05.010

Nelson, K. C., & Palmer, M. A. (2007). Stream Temperature Surges Under Urbanization and Climate Change: Data, Models, and Responses. *Journal of the American Water Resources Association (JAWRA)*, *43*(2), 440–452. https://doi.org/10.1111/j.1752-1688.2007.00034.x

Nepf, H., & Ghisalberti, M. (2008). Flow and transport in channels with submerged vegetation. *Acta Geophysica*, *56*(3), 753–777. https://doi.org/10.2478/s11600-008-0017-y

Nepf, H. M. (1999). Drag, turbulence, and diffusion in flow through emergent vegetation. *Water Resources Research*, *35*(2), 479–489. https://doi.org/10.1029/1998WR900069

Nepf, Heidi M. (2012a). Flow and transport in regions with aquatic vegetation. *Annual Review of Fluid Mechanics*, *44*, 123–142. https://doi.org/10.1146/annurev-fluid-120710-101048

Nepf, Heidi M. (2012b). Hydrodynamics of vegetated channels. *Journal of Hydraulic Research*, *50*(3), 262–279. https://doi.org/10.1080/00221686.2012.696559

Oades, J. M. (1984). Soil organic matter and structural stability: mechanisms and implications for management. *Plant and Soil*, *76*(1–3), 319–337. https://doi.org/10.1007/BF02205590

Odgaard, J. (1989). River-Meander Model I: Development. *J. Hydraul. Eng*, *115*(11), 1433–1450.

Olagoke, F. K., Bettermann, A., Thi, P., Nguyen, B., Redmile, M., & Doreen, G. (2022). Importance of substrate quality and clay content on microbial extracellular polymeric substances production and aggregate stability in soils. *Biology and Fertility of Soils*, 435–457. https://doi.org/10.1007/s00374-022-01632-1

Osman, A. M., & Thorne, C. R. (1988). Riverbank Stability Analysis. I: Theory. *Journal of Hydraulic Engineering*, *114*(2), 134–150. https://doi.org/10.1061/(asce)0733-9429(1988)114:2(134)

Pallardy, S. G., & Kozlowski, T. T. (2007). *Physiology of woody plants*. Elsevier Science & Technology.

Parks, O. W. (2012). *Effect of Water Temperature on Cohesive Streambank Erosion* [Virginia Polytechnic Institute and State University]. http://hdl.handle.net/10919/49663

Parsons, D. R., Schindler, R. J., Hope, J. A., Malarkey, J., Baas, J. H., Peakall, J., Manning, A. J., Ye, L., Simmons, S., Paterson, D. M., Aspden, R. J., Bass, S. J., Davies, A. G., Lichtman, I. D., & Thorne, P. D. (2016). The role of biophysical cohesion on subaqueous bed form size. *Geophys. Res. Lett.*, *43*, 1566–1573. https://doi.org/10.1002/2016GL067667

Partheniades, E. (1965). Erosion and Deposition of Cohesive Soils. *Pochvoznanie i Agrokhimiya*, *91*(1), 105–139. https://doi.org/10.1017/S000748530002229X

Partheniades, E. (2009). *Cohesive sediments in open channels*. Butterworth-Heinemann.

Paul, S., Veldkamp, E., & Flessa, H. (2008). Soil organic carbon in density fractions of tropical soils under forest - pasture - secondary forest land use changes. *European Journal of Soil Science*, *59*(2), 359–371. https://doi.org/10.1111/j.1365-2389.2007.01010.x

Pereira, D. G., Afonso, A., & Medeiros, F. M. (2015). Overview of Friedman's Test and Post-hoc Analysis. *Communications in Statistics - Simulation and Computation*, *44*(10), 2636–2653. https://doi.org/10.1080/03610918.2014.931971

Piotrowski, J. S., Denich, T., Klironomos, J. N., Graham, J. M., & Rillig, M. C. (2004). The effects of arbuscular mycorrhizas on soil aggregation depend on the interaction between plant and fungal species. *New Phytologist*, *164*(2), 365–373. https://doi.org/10.1111/j.1469-8137.2004.01181.x

Pizzuto, J. (2009). An empirical model of event scale cohesive bank profile evolution. *Earth Surface Processes and Landforms*, *34*, 1234–1244. https://doi.org/10.1002/esp.1808

Pizzuto, J. E., & Meckelnburg, T. S. (1989). Evaluation of a Linear Bank Erosion Equation. *Water Resources Research*, *25*(5), 1005–1013. https://doi.org/10.1029/WR025i005p01005

Poesen, J., & Savat, J. (1981). Detachment and transportation of loose sediments by raindrop splash: Part II detachability and transport ability measurements. *Catena*, *8*(1), 19–41.

Pollen-Bankhead, N., & Simon, A. (2010). Hydrologic and hydraulic effects of riparian root networks on streambank stability: Is mechanical root-reinforcement the whole story? *Geomorphology*, *116*(3–4), 353–362. https://doi.org/10.1016/j.geomorph.2009.11.013

Pollen, N., Simon, A., & Collison, A. (2004). Advances in Assessing the Mechanical and Hydrologic Effects of Riparian Vegetation on Streambank Stability. In S. Bennett & A. Simon (Eds.), *Riparian Vegetation and Fluvial Geomorphology*, *Water Science and Applications* (pp. 125–139). AGU. http://naldc.nal.usda.gov/download/4031/PDF

Purvis, R. A., & Fox, G. A. (2016). Streambank sediment loading rates at the watershed scale and the benefit of riparian protection. *Earth Surface Processes and Landforms*, *41*(10), 1327–1336. https://doi.org/10.1002/esp.3901

R Core Team. (2021). *R:* A language and environment for statistical computing. R Foundation for Statistical Computing, Vienna, Austria. https://www.R-project.org/.

Redmile-Gordon, M. A., Armenise, E., White, R. P., Hirsch, P. R., & Goulding, K. W. T. (2013). A comparison of two colorimetric assays, based upon Lowry and Bradford techniques, to estimate total protein in soil extracts. *Soil Biology and Biochemistry*, *67*, 166–173. https://doi.org/10.1016/j.soilbio.2013.08.017

Redmile-Gordon, M. A., Brookes, P. C., Evershed, R. P., Goulding, K. W. T., & Hirsch, P. R. (2014). Measuring the soil-microbial interface: Extraction of extracellular polymeric substances (EPS) from soil biofilms. *Soil Biology and Biochemistry*, *72*, 163–171. https://doi.org/10.1016/j.soilbio.2014.01.025

Redmile-Gordon, M. A., Evershed, R. P., Hirsch, P. R., White, R. P., & Goulding, K. W. T. (2015). Soil organic matter and the extracellular microbial matrix show contrasting responses to C and N availability. *Soil Biology and Biochemistry*, *88*, 257–267. https://doi.org/10.1016/j.soilbio.2015.05.025

Redmile-Gordon, M., Gregory, A. S., White, R. P., & Watts, C. W. (2020). Soil organic carbon, extracellular polymeric substances (EPS), and soil structural stability as affected by previous and current land-use. *Geoderma*, *363*(January), 114143. https://doi.org/10.1016/j.geoderma.2019.114143

Reid, J. B., & Goss, M. J. (1980). Changes in the aggregate stability of a sandy loam effected by growing roots of perennial ryegrass (Lolium perenne). *Journal of the Science of Food and Agriculture*, *31*(3), 325–328. https://doi.org/10.1002/jsfa.2740310320

Reid, J. B., & Goss, M. J. (1981). Effect of Living Roots of Different Plant Species on the Aggregate Stability of Two Arable Soils. *Journal of Soil Science*, *32*(4), 521–541. https://doi.org/10.1111/j.1365-2389.1981.tb01727.x

Rice, R. M., Crobett, E. S., & Bailey, R. G. (1969). Soil Slips Related to Vegetation, Topography, and Soil in Southern California. *Water Resources Research*, *5*(3), 647–659. https://doi.org/10.1029/WR005i003p00647

Righetti, M., & Lucarelli, C. (2007). May the Shields theory be extended to cohesive and adhesive benthic sediments? *Journal of Geophysical Research: Oceans*, *112*(5), 1–14. https://doi.org/10.1029/2006JC003669

Rinaldi, M., & Darby, S. E. (2007). Modelling river-bank-erosion processes and mass failure mechanisms: progress towards fully coupled simulations. *Developments in Earth Surface Processes*, *11*(February), 213–239. https://doi.org/10.1016/S0928-2025(07)11126-3

Rood, S. B., Bigelow, S. G., Polzin, M. L., Gill, K. M., & Coburn, C. A. (2015). Biological bank protection: Trees are more effective than grasses at resisting erosion from major river floods. *Ecohydrology*. https://doi.org/10.1002/eco.1544

Rose, C. W., Williams, J. R., Sander, G. C., & Barry, D. A. (1983). A Mathematical Model of Soil Erosion and Deposition Processes: I. Theory for a Plane Land Element. *Soil Science Society of America Journal*, *47*(5), 991–995. https://doi.org/10.2136/sssaj1983.03615995004700050030x

Ross, D. S., Wemple, B. C., Willson, L. J., & Balling, C. M. (2019). Impact of an Extreme Storm

Event on River Corridor Bank Erosion and Phosphorus Mobilization in a Mountainous Watershed in the Northeastern United States. *JGR Biogeosciences*, *124*, 18–32. https://doi.org/10.1029/2018JG004497

Sen, P. K. (1968). Estimates of the Regression Coefficient Based on Kendall's Tau. *Journal of the American Statistical Association*, *63*(324), 1379–1389. https://www.jstor.org/stable/pdf/2285891.pdf?refreqid=excelsior%3Ade4a6fc7a961fe262d28796b527fc2a7

Shaler, N. S. (1892). *The origin and nature of soils. U.S. Geological Survey 12th Annual Report*.

Shang, Q., Fang, H., ZHAO, H., He, G., & Cui, Z. (2014). Biofilm effects on size gradation, drag coefficient and settling velocity of sediment particles. *International Journal of Sediment Research*, *29*(4), 471–480. https://doi.org/10.1016/S1001-6279(14)60060-3

Sheng, G.-P., Yu, H.-Q., & Li, X.-Y. (2010). Extracellular polymeric substances (EPS) of microbial aggregates in biological wastewater treatment systems: A review. *Biotechnology Advances*, *28*(6), 882–894. https://doi.org/10.1016/J.BIOTECHADV.2010.08.001

Shukla, S., Sivakugan, N., & Das, B. (2009). Fundamental concepts of soil reinforcement — an overview. *International Journal of Geotechnical Engineering*, *3*(3), 329–342. https://doi.org/10.3328/IJGE.2009.03.03.329-342

Siegel, A. F. (1982). Robust regression using repeated medians. *Biometrika*, *69*(1), 242–244. https://www.jstor.org/stable/pdf/2335877.pdf?refreqid=excelsior%3Ac21be9055d6d93cfc88b4c3c4a5581bc

Simon, A., & Collison, A. J. C. (2002). Quantifying the mechanical and hydrologic effects of riparian vegetation on streambank stability. *Earth Surface Processes and Landforms*, *27*(5), 527–546. https://doi.org/10.1002/esp.325

Simon, A., Thomas, R. E., & Klimetz, L. (2010). Comparison and Experiences With Field Techniques To Measure Critical Shear Stress and Erodibility of Cohesive Deposits. *2nd Joint Federal Interagency Conference, Las Vegas*.

Six, J., Bossuyt, H., Degryze, S., & Denef, K. (2004). A history of research on the link between (micro)aggregates, soil biota, and soil organic matter dynamics. *Soil and Tillage Research*, *79*(1), 7–31. https://doi.org/10.1016/j.still.2004.03.008

Smith, D. G. (1976). Effect of vegetation on lateral migration of anastomosed channels of a glacier meltwater river. *Bulletin of the Geological Society of America*, *87*(6), 857–860. https://doi.org/10.1130/0016-7606(1976)87<857:EOVOLM>2.0.CO;2

Smith, D. J., Wynn-Thompson, T. M., Williams, M. A., & Seiler, J. R. (2021). Do Roots Bind Soil? Comparing the Physical and Biological Role of Plant Roots in Fluvial Streambank Erosion: A Mini-JET Study. *Geomorphology*, *375*, 1–9. https://doi.org/10.1016/j.geomorph.2020.107523

Stal, L. J. (2003). Microphytobenthos, their Extracellular Polymeric Substances, and the Morphogenesis of Intertidal Sediments. *Geomicrobiology Journal*, *20*(5), 463–478. https://doi.org/10.1080/713851126

Stein, O. R., Julien, P. Y., & Alonso, C. V. (1993). Mechanics of jet scour downstream of a headcut. *J. Hydraulic Research*, *31*(6), 732–738.

Stein, O. R., & Nett, D. D. (1997). *Impinging Jet Calibration of Excess Shear Sediment Detachment Parameters*. *40*(6), 1573–1580.

Strom, K. B., & Papanicolaou, A. N. (2007). ADV Measurements around a Cluster Microform in a Shallow Mountain Stream. *Journal of Hydraulic Engineering*, *133*(12), 1379–1389. https://doi.org/10.1061/(asce)0733-9429(2007)133:12(1379)

Sutherland, T. F., Grant, J., & Amos, C. L. (1998). The effect of carbohydrate production by the diatom Nitzschia curvilineata on the erodibility of sediment. *Limnology and Oceanography*, *43*(1), 65–72. https://doi.org/10.4319/lo.1998.43.1.0065

Tang, J., Mo, Y., Zhang, J., & Zhang, R. (2011). Influence of biological aggregating agents associated with microbial population on soil aggregate stability. *Applied Soil Ecology*, *47*(3), 153–159. https://doi.org/10.1016/j.apsoil.2011.01.001

Teasdale, S. L., Wu, X., Ye, L., & Hackney, C. R. (2018). The identification and extraction of extracellular polymeric substances (EPS) from sediments. *Geomorphological Techniques*, 1–14.

Tengbeh, G. T. (1993). The effect of grass roots on shear strength variations with moisture content. *Soil Technology*, *6*(3), 287–295. https://doi.org/10.1016/0933-3630(93)90017-9

Theil, H. (1992). A Rank-Invariant Method of Linear and Polynomial Regression Analysis. In B. Raj & J. Koerts (Eds.), *Henri Theil's Contributions to Economics and Econometrics. Advanced Studies in Theoretical and Applied Econometrics* (pp. 345–381). Springer, Dordrecht. https://doi.org/10.1007/978-94-011-2546-8_20

Thom, M., Schmidt, H., Gerbersdorf, S. U., & Wieprecht, S. (2015). Seasonal biostabilization and erosion behavior of fluvial biofilms under different hydrodynamic and light conditions. *International Journal of Sediment Research*, *30*(4), 273–284. https://doi.org/10.1016/j.ijsrc.2015.03.015

Thorne, C. R. (1990). Effects of vegetation on riverbank erosion and stability. In J. B. Thornes (Ed.), *Vegetation and Erosion: Processes and Environments* (pp. 125–144). John Wiley & Sons.

Thorne, C. R., Hey, R. D., & Newson, M. D. (1997). *Applied Fluvial Geomorphology for River Engineering and Management*. John Wiley & Sons.

Thorne, S. D., & Furbish, D. J. (1995). Influences of coarse bank roughness on flow within a sharply curved river bend. *Geomorphology*, *12*(3), 241–257. https://doi.org/10.1016/0169-555X(95)00007-R

Tisdall, J. M., & Oades, J. M. (1982). Organic matter and water-stable aggregates in soils. *European Journal of Soil Science*, *33*(2), 141–163. https://doi.org/10.1111/j.1365-2389.1982.tb01755.x

Turkelboom, F., Poesen, J., Ohler, I., Van Keer, K., Ongprasert, S., & Vlassak, K. (1997). Assessment of tillage erosion rates on steep slopes in northern Thailand. *CATENA*, *29*(1), 29–44. https://doi.org/10.1016/S0341-8162(96)00063-X

Underwood, G J C, Paterson, D. A., & Parkes, R. J. (1995). The measurement of microbial carbohydrate exopolymers from intertidal sediments. *Limnol. Oceanogr*, *40*(7), 1243–1253.

Underwood, Graham J C, & Paterson, D. M. (2003). The Importance of Extracellular Carbohydrate Production by Marine Epipelic Diatoms. *Advances in Botanical Research*, *40*, 184–240. https://doi.org/https://doi.org/10.1016/S0065-2296(05)40005-1

Utley, B. C., & Wynn, T. M. (2008). Cohesive Soil Erosion: Theory and Practice. *World Environmental and Water Resources Congress 2008*, 1–10. https://doi.org/10.1061/40976(316)289

Valyrakis, M., Liu, D., Turker, U., & Yagci, O. (2021). The role of increasing riverbank vegetation density on flow dynamics across an asymmetrical channel. *Environmental Fluid Mechanics*, *21*(3), 643–666. https://doi.org/10.1007/s10652-021-09791-9

Van De Lageweg, W. I., Mclelland, S. J., & Parsons, D. R. (2018). Quantifying biostabilisation effects of biofilm-secreted and extracted extracellular polymeric substances (EPSs) on sandy substrate. *Earth Surf. Dynam*, *6*, 203–215. https://doi.org/10.5194/esurf-6-203-2018

Van Duyl, F. C., De Winder, B., Kop, A. J., & Wollenzien, U. (1999). Tidal coupling between carbohydrate concentrations and bacterial activities in diatom-inhabited intertidal mudflats. *Marine Ecology Progress Series*, *191*, 19–32. https://doi.org/10.3354/meps191019

van Katwijk, M. M., Bos, A. R., Hermus, D. C. R., & Suykerbuyk, W. (2010). Sediment modification by seagrass beds: Muddification and sandification induced by plant cover and environmental conditions. *Estuarine, Coastal and Shelf Science*, *89*(2), 175–181. https://doi.org/10.1016/j.ecss.2010.06.008

Vidal, H. (1966). *La terre Armée. Annales de l'Institut Technique de Batiment et de Travaux Publics, France*.

Vidal, H. (1969). The principle of reinforced earth. *Highway Research Record 282*, 1–16.

Vu, B., Chen, M., Crawford, R. J., & Ivanova, E. P. (2009). Bacterial extracellular polysaccharides involved in biofilm formation. *Molecules (Basel, Switzerland)*, *14*(7), 2535–2554. https://doi.org/10.3390/molecules14072535

Wahl, T. L. (2002). Discussion of '"Despiking Acoustic Doppler Velocimeter Data"' by Derek G. Goring and Vladimir I. Nikora. *International Journal of Steel Structures*, *128*(1), 117–126. https://doi.org/10.1007/s13296-013-2015-4

Wang, B., Zhang, G.-H., Shi, Y.-Y., Li, Z.-W., & Shan, Z.-J. (2015). Effects of Near Soil Surface Characteristics on the Soil Detachment Process in a Chronological Series of Vegetation Restoration. *Soil Science Society of America Journal*, *79*, 1213–1222. https://doi.org/10.2136/sssaj2015.03.0120

Wang, B., Zhang, G.-H., Zhang, X. C., Li, Z.-W., Su, Z.-L., Yi, T., & Shi, Y.-Y. (2014). Effects of Near Soil Surface Characteristics on Soil Detachment by Overland Flow in a Natural Succession Grassland. *Soil Science Society of America Journal*, *78*(2), 589–597. https://doi.org/10.2136/sssaj2013.09.0392

Watnick, P., & Kolter, R. (2000). Biofilm, city of microbes. *Journal of Bacteriology*, *182*(10), 2675–2679. https://doi.org/10.1128/jb.182.10.2675-2679.2000

Weaver, J. E., & Noll, W. (1935). Comparison of Runoff and Erosion in Prairie, Pasture, and Cultivated Land. In *The University of Nebraska, Conservation and Survey Division* (Issue 11). The University of Nebraska.

Wertz, S., Czarnes, S., Bartoli, F., Renault, P., Commeaux, C., Guillaumaud, N., & Clays-Josserand, A. (2007). Early-stage bacterial colonization between a sterilized remoulded soil clod and natural soil aggregates of the same soil. *Soil Biology and Biochemistry*, *39*(12), 3127–3137. https://doi.org/10.1016/J.SOILBIO.2007.07.005

Wingender, Jost, Neu, T. R., & Flemming, H.-C. (Eds.). (1999). *Microbial Extracellular Polymeric Substances.: characterization, structure and function* (1st ed.). Springer. https://doi.org/10.1007/978-3-642-60147-7

Wynn, T. (2006). Streambank retreat: a primer. *AWRA Hydrology & Watershed Management Technical Committee*, *4*(1), 1–14. http://www.remarkableriparian.org/pdfs/pubs/streambank retreat.pdf

Wynn, T. M., Burger, J., Dillaha, T., & Heatwole, C. (2004). *The Effects of Vegetation on Stream Bank Erosion*. *0300*(04).

Wynn, T., & Mostaghimi, S. (2006). The Effects of Vegetation and Soil Type on Streambank Erosion, Southwestern Virginia, USA. *Journal of the American Water Resources Association*, *42*(1), 69–82.

Wynn, Theresa. (2004). The Effects of Vegetation on Stream Bank Erosion [Virginia Tech]. In *Dissertation: Vol. Ph.D.* https://doi.org/10.13031/2013.16423

Wynn, Theresa, Mostaghimi, S., Harpold, A., Henderson, M., & Henry, L.-A. (2004). Variation in Root Density Along Stream Banks. *Journal of Environmental Quality*, *33*, 400–411. https://doi.org/10.2134/jeq2004.2030

Xiao, R., & Zheng, Y. (2016). Overview of microalgal extracellular polymeric substances (EPS) and their applications. *Biotechnology Advances*, *34*(7), 1225–1244. https://doi.org/10.1016/J.BIOTECHADV.2016.08.004

Yang, J. Q., & Nepf, H. M. (2018). A Turbulence-Based Bed-Load Transport Model for Bare and Vegetated Channels. *Geophysical Research Letters*, *45*(19), 10,428-10,436. https://doi.org/10.1029/2018GL079319

Yang, K., Cao, S., & Knight, D. W. (2007). Flow Patterns in Compound Channels with Vegetated Floodplains. *Journal of Hydraulic Engineering*, *133*(2), 148–159. https://doi.org/10.1061/(ASCE)0733-9429(2007)133:2(148)

Zelenev, V. V., Van Bruggen, A. H. C., & Semenov, A. M. (2005). Short-term wavelike dynamics of bacterial populations in response to nutrient input from fresh plant residues. *Microbial Ecology*, *49*(1), 83–93. https://doi.org/10.1007/s00248-003-1054-3

Zhang, G., Tang, K., Ren, Z., & Zhang, X. C. (2013). Impact of Grass Root Mass Density on Soil Detachment Capacity by Concentrated Flow on Steep Slopes. *ASABE*, *56*(3), 927–934.

Zhang, J., Lei, J., Huai, W., & Nepf, H. (2020). Turbulence and Particle Deposition under Steady flow along a Submerged Seagrass Meadow. *Journal of Geophysical Research: Oceans*, *125*, 0–34. https://doi.org/http://dx.doi.org/10.1029/2019jc015985

Zreik, D. A., Germaine, J. T., & Ladd, C. C. (1998). Erosional and Mechanical Strengths of Deposited Cohesive Sediments. *J. Hydr. Engr.*, *124*(11), 1076–1085.

Appendix A: Chapter 3 Experimental Data

Table A-1: Chapter 3 mini-JET experimental data

Treatment	Block	Water Stable Aggregates	τ_c (Pa)	k_d ($cm^3\ N^{-1}\ s^{-1}$)	Runtime (min)	SHV (cm^3)	EPS ($\mu g\ g^{-1}$)	Very Fine RLD ($cm\ cm^{-3}$)	Fine RLD ($cm\ cm^{-3}$)	Small RLD ($cm\ cm^{-3}$)	Total RLD ($cm\ cm^{-3}$)
LR-I	A	78%	2.01	72.1	43.5	38.3	40.9	1.29	0.29	0.067	1.65
LR-I	B	76%	2.25	66.4	45.3	43.3	41.1	1.22	0.17	0.066	1.46
LR-I	C	75%	2.15	155.4	48.3	44.7	38.2	1.00	0.19	0.048	1.23
LR-I	D	76%	1.64	76.0	51.8	51.0	34.5	1.26	0.17	0.057	1.48
LR-I	E	67%	1.32	28.0	54.0	30.0	33.0	1.94	0.15	0.002	2.09
LR-I	F	70%	1.74	32.0	48.0	35.0	42.9	3.67	0.35	0.098	4.11
LR-I	G	70%	1.60	71.5	42.8	49.3	35.0	1.07	0.30	0.088	1.46
LR-I	H	74%	4.41	50.9	46.8	32.0	31.2	2.16	0.32	0.064	2.54
LR-I	I	70%	1.86	67.1	60.3	69.0	41.5	1.17	0.16	0.028	1.37
LR-I	J	70%	1.68	84.4	52.8	60.0	40.7	0.51	0.13	0.019	0.67
LR-I	K	79%	2.67	82.6	48.3	50.0	38.4	1.44	0.28	0.068	1.79
LR-I	L	71%	2.74	28.9	53.8	15.0	27.3	2.65	0.40	0.114	3.16
SR-I	A	81%	1.69	56.9	49.5	58.0	33.0	0.78	0.1	0.012	0.892
SR-I	B	83%	1.59	118.1	48.8	58.7	32.4	0.78	0.1	0.012	0.892
SR-I	C	82%	3.07	76.8	44.5	10.0	26.2	0.78	0.1	0.012	0.892
SR-I	D	80%	1.24	25.4	52.5	43.0	24.5	0.78	0.1	0.012	0.892
SR-I	E	83%	1.40	134.8	49.0	57.0	25.5	0.78	0.1	0.012	0.892
SR-I	F	84%	1.42	144.7	49.0	52.0	26.0	0.78	0.1	0.012	0.892
SR-I	G	81%	1.46	95.1	49.3	64.0	29.2	0.78	0.1	0.012	0.892
SR-I	H	82%	1.93	111.7	57.8	47.3	33.6	0.78	0.1	0.012	0.892
SR-I	I	78%	1.92	162.9	47.3	50.0	34.4	0.78	0.1	0.012	0.892
SR-I	J	56%	1.66	103.5	52.0	55.7	35.8	0.78	0.1	0.012	0.892
SR-I	K	83%	2.00	95.4	45.3	66.7	36.9	0.78	0.1	0.012	0.892
SR-I	L	85%	1.38	143.9	43.0	61.7	33.0	0.78	0.1	0.012	0.892
SR-S	A	82%	1.94	171.8	51.0	68.0	39.5	0.78	0.1	0.012	0.892
SR-S	B	82%	1.48	87.9	49.3	58.0	39.1	0.78	0.1	0.012	0.892
SR-S	C	82%	1.59	155.5	45.5	47.7	34.8	0.78	0.1	0.012	0.892

Table A1, continued: Chapter 3 mini-JET experimental data

Treatment	Block	Water Stable Aggregates	τ_c (Pa)	k_d ($cm^3\ N^{-1}\ s^{-1}$)	Runtime (min)	SHV (cm^3)	EPS ($\mu g\ g^{-1}$)	Very Fine RLD ($cm\ cm^{-3}$)	Fine RLD ($cm\ cm^{-3}$)	Small RLD ($cm\ cm^{-3}$)	Total RLD ($cm\ cm^{-3}$)
SR-S	D	82%	1.72	99.7	55.0	72.0	25.4	0.78	0.1	0.012	0.892
SR-S	E	83%	1.45	77.2	48.5	50.0	29.3	0.78	0.1	0.012	0.892
SR-S	F	81%	2.16	50.5	60.5	68.0	28.7	0.78	0.1	0.012	0.892
SR-S	G	78%	1.46	100.9	49.8	61.0	32.3	0.78	0.1	0.012	0.892
SR-S	H	82%	1.34	149.6	48.5	65.3	32.6	0.78	0.1	0.012	0.892
SR-S	I	76%	1.61	104.1	62.5	50.0	41.4	0.78	0.1	0.012	0.892
SR-S	J	78%	1.75	50.8	66.3	70.7	29.6	0.78	0.1	0.012	0.892
SR-S	K	83%	1.96	82.8	47.5	52.7	32.5	0.78	0.1	0.012	0.892
SR-S	L	82%	1.43	33.6	55.3	51.7	35.0	0.78	0.1	0.012	0.892
NR-I	A	81%	1.84	25.6	57.0	74.0	32.8	0	0	0	0
NR-I	B	79%	1.90	35.2	61.0	64.0	37.4	0	0	0	0
NR-I	C	82%	1.66	50.0	52.0	51.0	29.7	0	0	0	0
NR-I	D	82%	1.34	79.8	46.5	61.0	NM	0	0	0	0
NR-I	E	80%	1.50	115.4	51.3	55.0	26.2	0	0	0	0
NR-I	F	83%	0.90	16.2	50.0	46.0	30.3	0	0	0	0
NR-I	G	81%	1.42	104.1	37.8	46.7	26.2	0	0	0	0
NR-I	H	83%	1.64	30.0	60.5	63.7	33.3	0	0	0	0
NR-I	I	79%	1.85	67.7	47.0	62.0	37.9	0	0	0	0
NR-I	J	59%	1.56	70.1	43.0	59.0	26.2	0	0	0	0
NR-I	K	82%	1.41	49.5	51.3	59.7	30.3	0	0	0	0
NR-I	L	82%	1.57	40.2	45.5	40.7	33.7	0	0	0	0
NR-S	A	82%	1.62	68.4	64.3	71.0	NM	0	0	0	0
NR-S	B	84%	1.62	41.5	51.3	63.0	33.7	0	0	0	0
NR-S	C	83%	1.86	57.8	47.8	61.3	32.9	0	0	0	0
NR-S	D	84%	1.46	37.5	52.0	48.0	28.7	0	0	0	0
NR-S	E	82%	1.56	71.0	49.8	52.0	28.6	0	0	0	0
NR-S	F	83%	2.91	32.5	61.0	32.0	30.9	0	0	0	0
NR-S	G	84%	1.61	46.5	47.0	55.0	29.9	0	0	0	0
NR-S	H	82%	1.43	20.3	63.8	58.3	33.5	0	0	0	0
NR-S	I	75%	1.77	17.5	70.8	74.0	38.1	0	0	0	0

Table A1, continued: Chapter 3 mini-JET experimental data

Treatment	Block	Water Stable Aggregates	τ_c (Pa)	k_d ($cm^3 N^{-1} s^{-1}$)	Runtime (min)	SHV (cm^3)	EPS ($\mu g\ g^{-1}$)	Very Fine RLD ($cm\ cm^{-3}$)	Fine RLD ($cm\ cm^{-3}$)	Small RLD ($cm\ cm^{-3}$)	Total RLD ($cm\ cm^{-3}$)
NR-S	J	79%	1.87	24.0	78.8	82.3	31.7	0	0	0	0
NR-S	K	82%	1.53	67.9	50.8	51.0	31.3	0	0	0	0
NR-S	L	85%	1.72	118.1	47.0	57.3	35.0	0	0	0	0

Appendix B: Chapter 4 Experimental Data

All data files, R-code, and corresponding data tables for Chapter 5 can be downloaded online for free from Smith, D. J., & Wynn-Thompson, T. M. (2022). Flume Experiment Testing the Impact of Artificial Streambank Roots on Velocity, Reynold's Shear Stress, and Turbulent Kinetic Energy using an Acoustic Doppler Profiler ver 1. Environmental Data Initiative. https://doi.org/10.6073/pasta/cf6f71949066c546177bb3136a7ec74b

Appendix C: Chapter 5 Experimental Data

All data files, R-code, and corresponding data tables for Chapter 4 can be downloaded online for free from Smith, D. J., Snead, M., & Wynn-Thompson, T. M. (2021). Flume Erosion Testing of Unamended and Organic Matter Amended Soil Samples Using an Acoustic Doppler Profiler, 2021 ver 3. Environmental Data Initiative. https://doi.org/10.6073/pasta/6464eb390308f2fadc46e7e7b139803c

Appendix D: Chapter 6 Experimental Data

All data files, R-code, and corresponding data tables for Chapter 6 can be downloaded online for free from Smith, D. J., & Wynn-Thompson, T. M. (2022). Flume Erosion Testing Data of Root-Permeated and Organic Matter Amended Soil Samples Using Three Streambank Boundary Conditions. ver 1. Environmental Data Initiative. https://doi.org/10.6073/pasta/ddc596a162d294a28d572a3119362c16